Winter 12-15-2018

A Mouse Model of Börjeson-Forssman-Lehmann Syndrome reveals a potential link with Autism Spectrum Disorder

Cheng Cheng
Washington University in St. Louis

WASHINGTON UNIVERSITY IN ST. LOUIS

Division of Biology and Biomedical Sciences
Developmental, Regenerative and Stem Cell Biology

Dissertation Examination Committee:
Azad Bonni, Chair
Joseph Dougherty
Harrison Gabel
Jason Yi
Andrew Yoo

A Mouse Model of Börjeson-Forssman-Lehmann Syndrome reveals a potential link with Autism Spectrum Disorder

By
Cheng Cheng

A dissertation presented to
The Graduate School
of Washington University in
partial fulfillment of the
requirements for the degree
of Doctor of Philosophy

Dec. 2018
St. Louis, Missouri

Table of Contents

List of Figures and Tables

Figures:

Chapter 1

Chapter 2

Chapter 3

Appendix

Tables:

Chapter 1

Acknowledgments

I would like to thank my thesis mentor, Dr. Azad Bonni for his support and guidance during graduate career. As a great scientist, He always provides great insights for my study. As a graduate student mentor, his office door is always open to me whenever I have questions and have lost direction on the project. He not only patiently guided me through the setbacks from individual experiments, but also discussed with me about big picture and future directions on the project. He provided me with resources and collaboration when needed. I am thankful for his support and guidance throughout my graduate school career. His dedication and passion for science has taught me what it takes to become a successful scientist.

Thank you to my thesis committee, Dr. Andrew Yoo, Dr. Joe Daugherty, Dr. Jason Yi and Dr. Harrison Gabel for their constructive feedbacks and support that really helped to shape the thesis work.

I would like to thank all the members of the Bonni lab who have helped me both in science and in life during the past five years. I have learned so much from each one of them. Thank you especially to my cohorts who joined the lab at the same time, Shahriyar Majidi for being my "first-turn-to" friend when I have questions or feel upset in lab; Naveen Reddy for being sarcastic, yet very helpful when comes to engineering or computer problems; Kelly Hill for many philosophical conversations about life when we were in lab late at night; Sarah Smith for being so positive and strong all the time, which also gave me strength; my mentors Tomoko Yamada, Yoshiho Ikeuchi and Ju Huang during my first years in the lab, and all other members of Bonni lab.

Outside of the lab, a collection of friends has provided encouragement and support that I am grateful for. I especially would like to thank Yinjiao, Yangqing, Xitong, Xueying, Qihao, Yajing and Mengxi.

To my parents, Ling and Ming, I cannot thank you enough for the freedom and support you selflessly provide. Thanks for teaching me the core values of love, honesty, open-

mindedness and caring, and giving me the opportunities to pursue higher education abroad. I would also like to thank my biological father, Bingbing, for the love, guidance and support; and my little sister, Chen Cheng for always being a source of happiness in the family.

Finally, I would like to thank my husband, Ziran for the unending encouragement, joy and love; and to the most important achievement during my graduate work, my dearest daughter, Shinyi, thanks for the happiness and motivation you bring into my life each and every single day.

Cheng Cheng

Washington University in St. Louis

December 2018

ABSTRACT OF THE DISSERTATION

A Mouse Model of Börjeson-Forssman-Lehmann Syndrome reveals a potential link with Autism Spectrum Disorder

By

Cheng Cheng

Doctor of Philosophy in Biology and Biomedical Sciences

Developmental, Regenerative and Stem Cell Biology

Washington University in St. Louis, 2018

Dr. Azad Bonni, Chair

Intellectual disability (ID) is a prevalent neurodevelopmental disorder that affects 1% to 3% of the general population. ID is characterized by developmental deficiencies in cognitive function and adaptive behaviors. Lacking effective treatments, ID currently presents an immense burden to affected families and the economy. Therefore, there is an urgent need to elucidate the pathogenesis of ID. Human genetic studies have associated ID with a number of gene mutations. ID can be divided into two major groups: a non-syndromic form, characterized by intellectual impairment manifesting alone, and a syndromic form, characterized by both cognitive deficiencies and other anomalies, including biochemical disorders, skeletal abnormalities, facial dysmorphisms and neurological disorders. However, scientists have limited their studies to relatively few syndromic forms of ID, such as Rett, Angelman and Fragile X syndrome. In addition to these commonly studied syndromes, Börjeson-Forssman-Lehman syndrome (BFLS)

was identified over five decades ago as a cause of X-linked ID and characterized as a syndromic form of moderately to severely impaired cognitive function associated with early developmental delay, truncal obesity, small genitalia, facial dysmorphism and seizures. Whether BFLS patients display other neurological manifestations besides cognitive impairment and seizures remains unexplored. In particular, whereas some genetic forms of ID are accompanied by manifestations of autism spectrum disorders (ASD), whether BFLS also features symptoms and signs of ASD is unknown. Forty years after the first description of BFLS, mutations in the gene encoding plant homeofinger protein 6 (PHF6) were discovered to be causative for BFLS. These mutations are distributed throughout the entire gene in distinct domains of PHF6, and are composed of missense, nonsense, truncation, duplication and frameshift. Accumulating evidence suggests that PHF6 plays a role in transcriptional regulation. PHF6 contains nuclear localization sequences and PHD domains and can interact with transcriptional elongation complex, PAF1 to regulate cortical neural migration. Furthermore, other studies also suggest that PHF6 may regulate transcription through association with the nucleosome remodeling complex NuRD and upstream binding factor UBF1. The discovery of PHF6 interactors and their functions during neural development have raised additional interesting questions in understanding BFLS pathogenesis. How does PHF6 regulation of gene expression at the genome-wide level impact BFLS pathogenesis? How do specific PHF6 mutations trigger the pathogenesis of BFLS? Within this thesis, I provide detailed characterization of a mouse containing a patient-specific mutation of PHF6 as a novel BFLS model. Mice with the patient-specific PHF6 C99F mutation display deficits in cognitive function, emotionality and social behaviors, and are more susceptible to seizures, suggesting that PHF6 C99F mice feature phenotypes relevant to BFLS. In electrophysiological studies in acute slices, the intrinsic excitability of entorhinal cortical layer II stellate neurons is increased, providing mechanistic basis for susceptibility of BFLS mice to seizures. Genome-wide RNA-Seq analyses of the cerebral cortex show that PHF6 promotes the expression of neurogenesis genes and concomitantly suppresses the expression of synaptic genes, suggesting that PHF6 promotes an immature state of neurons. Strikingly, bioinformatics analyses

reveal that PHF6-regulated genes are overrepresented by ASD relevant gene signatures including modules that are misregulated in single gene causes of ASD. Consistent with these findings, we have identified an ASD patient with an underlying PHF6 missense mutation. Collectively, our findings in the novel BFLS mouse model broaden our understanding of the clinical features of BFLS patients and elucidate cellular and molecular underpinnings of BFLS pathogenesis.

Chapter 1: Pathogenesis of Börjeson-Forssman-Lehmann Syndrome: Insights from PHF6 function

From

Arezu Jahani-Asl*, Cheng Cheng*, Chi Zhang, Azad Bonni

*Co-first authors

Jahani-Asl, A*., Cheng, C*., Zhang, C. and Bonni, A. (2016). Pathogenesis of Börjeson-Forssman-Lehmann syndrome: Insights from PHF6 function. Neurobiol. Dis *96*, 227-235. *equal contribution

Abstract

Intellectual disability encompasses a large set of neurodevelopmental disorders of cognition that are highly prevalent. Intellectual disability is more common in males than females, and accordingly mutations in over 100 X-linked genes that cause intellectual disability have been identified. However, whereas a few X-linked intellectual disability proteins have been intensively studied, the molecular mechanisms underlying the majority of X-linked intellectual disability disorders remains poorly understood. A substantial fraction of X-linked intellectual disability genes encode nuclear proteins, suggesting that elucidating their functions in the regulation of transcription may provide novel insights into the pathogenesis of intellectual disability. In this regard, recent studies have begun to elucidate the mechanisms by which mutations of the gene encoding PHF6 contribute to the pathogenesis of the X-linked intellectual disability disorder Börjeson-Forssman-Lehmann syndrome (BFLS). Mutations of the PHD-containing protein PHF6 were identified over a decade ago as the cause of BFLS. However, until recently the function of PHF6 in brain development remained unknown. Recent studies have revealed that PHF6 plays a critical role in the migration of neurons in the mouse cerebral cortex *in vivo*. Remarkably, PHF6 physically associates with the PAF1 transcriptional elongation complex and thereby drives neuronal migration in the cerebral cortex. Other studies have identified an interaction of PHF6 with the NuRD chromatin remodeling complex and nucleolar transcription factor UBF. Interestingly, PHF6 mRNA has been identified as the target of the microRNA miR-128 in the cerebral cortex, providing new insights into how PHF6 function in neuronal migration is regulated. Importantly, deregulation of PHF6 function in neuronal migration triggers the formation of white matter heterotopias that harbor neuronal hyperexcitability, which may be relevant to the pathogenesis of intellectual disability and seizures in BFLS. Collectively, these studies are beginning to provide insights into the molecular pathogenesis of BFLS and pave the way for future studies that will significantly improve our understanding of X-linked intellectual disability.

X-linked Intellectual disability is a prevalent neurodevelopmental disorder

X-linked intellectual disability (XLID) affects 1 to 3 percent of the population (Bhasin et al., 2006; van Bokhoven and Kramer, 2010; Larson et al., 2001). Clinically, XLID is characterized by a deficit in intellectual function with an intelligence quotient (IQ) of less than 70 before the age of 18 and impairment of adaptive behaviors leading to deficient communication and social interactions (van Bokhoven and Kramer, 2010). Based on IQ score, intellectual disability may be classified as IQ: profound (IQ<20), severe (IQ 20-34), moderate (IQ 35-49) and mild (IQ 50-69) (Ropers, 2010). XLID affects more males than females (Ropers, 2010). XLID has been grouped into syndromic and nonsyndromic forms. Nonsyndromic XLID is characterized by intellectual disability in the absence of other symptoms or signs, whereas syndromic XLID patients display intellectual disability together with other developmental abnormalities (Kleine-Kohlbrecher et al., 2010). Gene deletions, duplications, inversions and point mutations on the X chromosome have been associated with XLID. Thus far, mutations in over 100 genes on the X chromosome have been associated with intellectual disability. These mutations affect proteins with functions in transcription, translation, signal transduction and cell cycle regulation (Kleine-Kohlbrecher et al., 2010).

Characterization of XLID-associated proteins has opened up new fields of study in brain development and disease. The X-linked fragile X and Rett syndromes represent two major examples of XLID syndromes that have spawned major lines of research at the intersection of development and cognitive disorders of the brain. Characterized by intellectual disability, autistic features, developmental delay, hyperactivity and attention deficit behavior (Coffee et al., 2008; Huber et al., 2002; Leigh & Hagerman, 2013), fragile X syndrome is caused by expansion of CGG nucleotide repeats in the 5' untranslated region of the *Fmr1* gene, leading to its transcriptional silencing (Verkerk et al., 1991; Yu et al., 1991). A large number of studies have elucidated functions for the *Fmr1*-encoded protein, FMRP in protein translation and synaptic plasticity (for review, see Leigh & Hagerman, 2013). In the mutant mice lacking FMRP, long-

term depression triggered by metabotropic glutamate receptors activation is enhanced (Bhakar et al., 2012; Huber et al., 2002). In the cerebral cortex, FMRP knockout mice have increased dendritic spine number with more immature long shaped spines but fewer spines with mature mushroom shape (Irwin et al., 2000). Thus, FMRP regulates both synaptic development and plasticity. At a molecular level, FMRP operates as an RNA-binding protein to control mRNA stability (Zalfa et al., 2007). FMRP may enter the nucleus and assemble with targeted RNAs into mRNP and undergo export to dendrites and regulate local protein synthesis (Eberhart et al., 1996). In fragile X syndrome patients, loss of FMRP function causes deregulation of localized mRNA synthesis, leading to defects in synapse function (Comery et al., 1997; Jin and Warren, 2000).

Rett syndrome patients have normal psychomotor development for the first 6 months after birth but subsequently fail to attain psychomotor milestones and eventually lose language and hand skills (Samaco and Neul, 2011). Mutations in methyl CpG binding protein 2 (MeCP2) cause Rett syndrome (Amir et al., 1999). MeCP2 knockout mice behave normally before weaning age (Guy et al., 2001), but by week eight these mice have unstable gait and reduced spontaneous movement followed by hindlimb clasping (Guy et al., 2001). Induced pluripotent stem cell (iPSC)-derived neurons from patients with Rett syndrome have reduced spine density, soma size and glutamatergic synapses (Marchetto et al., 2010), mimicking neuropathological findings on the brains of Rett syndrome patients (Kaufmann and Moser, 2000; Reiss et al., 1993; Samaco and Neul, 2011). MeCP2 binds to methylated cytosine within CpG motifs and has been implicated in the regulation of transcription (Nan et al., 1997). MeCP2 may silence transcription by recruiting co-repressors including histone deacetylases (Hdacs) (Nan et al., 1998; Skene et al., 2010). Remarkably, MeCP2 binds to methylated CA motifs within long genes (> 100 kb) to repress transcription, and upon MeCP2 depletion long gene expression is increased (Gabel et al., 2015). Although MeCP2 accumulates in post-mitotic neurons, MeCP2 may also play a role in glial cells and mutations of MeCP2 in glial cells may cause non-cell autonomous defects in neurons (Ballas et al., 2009).

Studies of FMRP and MeCP2 illustrate that significant advances in our understanding of neural development and pathogenesis of intellectual disability can be achieved from systematic studies of individual XLID proteins. Therefore, characterization of PHF6 is likely to yield novel insights into our understanding of brain development and intellectual disability.

Börjeson-Forssman-Lehmann syndrome (BFLS)

The Börjeson-Forssman-Lehmann syndrome (BFLS) was first described as an X-linked intellectual disability syndrome by Mats Börjeson and colleagues in 1962 (Börjeson et al., 1962). Since then, additional cases of BFLS patients have been identified. A summary of the clinical features of BFLS is presented in Table 1. BFLS patients typically have normal birth weight, head circumference and delivery (Lower et al., 2002). However, the main clinical features of BFLS become apparent with age and show considerable variation among different patients (de Winter et al., 2009; Lower et al., 2002). Developmental delay usually appears before the first birthday. All BFLS patients have intellectual disability, ranging from mild to severe, as well as small genitalia and short stature (Gécz et al., 2006; Lower et al., 2002). Approximately 75% of the patients have obesity emerging in late childhood; BFLS patients display microcephaly or macrocephaly at a frequency of 6% and 15% respectively; Epileptic seizures have been observed in approximately 8% patients (Carter et al., 2009; Di Donato et al., 2014; Mangelsdorf et al., 2009; Zweier et al., 2013). Other features of the syndrome include tapered fingers and broad foreshortened toes. Adult BFLS patients display some coarsening of facial features with prominence of the supraorbital ridges and deep-set eyes (Gécz et al., 2006; Lower et al., 2002). Other abnormalities observed uncommonly in BFLS patients include mild polyneuropathy, hearing impairment, cleft lip and hypopituitarism (Gécz et al., 2006). Female carriers of BFLS may have learning problems and show physical manifestations including shortened toes, thickened fleshy ear lobes, pronounced supraorbital ridges and deep-set eyes (Gécz et al., 2006; Lower et al., 2002).

Molecular genetics studies have led to the identification of multiple mutations in the *PHF6* gene on the X chromosome in BFLS patients (Berland et al., 2011; Carter et al., 2009; Lower et al., 2002; Turner et al., 2004). Most *PHF6* mutations in BFLS are missense or lead to truncation of PHF6 protein. Five *PHF6* mutations in BFLS are recurrent including c.2T>C/p.M1T, c134G>A/p.C45Y, c769A>G/p.R257G, c.999-1001delTGA/p.D333del and c1024C>T/p.R342X, found in 21% of patients. The truncation mutation c.1024C>T/p.R342X is

found in five different BFLS families (Chao et al., 2010; Crawford et al., 2006; Lower et al., 2002, 2004). The majority of *PHF6* mutations occur in exon 2, which encodes the N-terminus of PHF6 protein. A fundamental question that remains to be addressed is how PHF6 mutations lead to BFLS.

Mechanisms of PHF6 function

The *PHF6* gene is comprised of 11 exons that is transcribed into a 4.5 kb mRNA and translated into a 41 kDa protein with 365 amino acids. Two major isoforms of PHF6 mRNA, depending on whether intron 10 is spliced out, give the same protein product (Gécz et al., 2006). PHF6 protein is highly conserved in vertebrates. Structurally, PHF6 protein contains two plant homeodomain (PHD)-like zinc fingers, two nuclear localization sequences and a nucleolar localization sequence (Liu et al., 2014a), suggesting that PHF6 may play a role in the regulation of transcription. PHD zinc fingers are structurally conserved modules that interact with chromatin or mediate protein-protein interactions (Sanchez and Zhou, 2011). The Cys_4-His-Cys_3 motifs within the PHD domain of PHF6 coordinate two Zn^{2+} ions and stabilize PHF6 protein structure (Liu et al., 2014a). The evolutionary conserved PHF6 cysteine residues C45, C99 and C305 are targeted by missense mutations in BFLS. PHD fingers also recognize specific histone modifications (Aasland et al., 1995; Sanchez & Zhou, 2011; Wysocka et al., 2006), and regulate the function of epigenome readers in transcription via molecular recruitment of multi-protein complexes. However, unlike other PHD domain proteins, PHF6 contains two imperfect PHD domains (Liu et al., 2014a). Therefore, it is unclear whether the PHD domains in PHF6 function similarly as other PHD domains to recognize specific chromatin marks or participate in recruitment of other proteins.

Employing an unbiased computation-assisted proteomics approach, Zhang et al. discovered that PHF6 associates with subunits of the PAF1 transcription elongation complex including PAF1, LEO1, CTR9, and CDC73 (Zhang et al., 2013). The interaction of PHF6 with the PAF1 complex plays a critical role in PHF6 function in neuronal migration in the cerebral cortex. Knockdown of PAF1 mimics the PHF6 knockdown-induced phenotype of impaired neuronal migration in the mouse cerebral cortex (Zhang et al., 2013). Both PHF6 and the PAF1 complex induce expression of the gene encoding Neuroglycan C, which in turn mediates the ability of PHF6 and PAF1 complex to promote neuronal migration (Zhang et al., 2013). Knockdown of Neuroglycan C phenocopies the effect of PHF6 knockdown and PAF1

knockdown on neuronal migration, and expression of Neuroglycan C in PHF6-depleted progenitors rescues the defects in neuron migration (Zhang et al., 2013).

The PAF1 complex occupies the promoter and gene body of actively transcribed genes and associates with RNA polymerase II (PolII) to promote transcriptional elongation and transcription-coupled histone modifications (Chen et al., 2009; Krogan et al., 2002; Marton & Desiderio, 2008; Rondon et al., 2004; Squazzo et al., 2002). The C-terminal domain (CTD) phosphorylation of PolII is thought to mediate PAF1 recruitment to PolII. The PAF1 complex may directly stimulate RNA PolII transcription or act synergistically with other factors to promote transcriptional elongation (Jaehning et al., 2010). During transcriptional elongation, the PAF1 complex may recruit the histone methyltransferase Set2 to induce trimethylation of H3K36 and the ATPase Chd1 to remodel chromatin structure (Tomson and Arndt, 2013). In yeast, the PAF1 complex also promotes H2B K123 monoubiquitylation by recruiting the ubiquitin-ligase Rad6-Bre1. The H2B moniubiquitination facilitates dimethylation and trimethylation of H3K4 and H3K79 by the histone methyltransferases Set1 and Dot1 (Tomson & Arndt, 2013; Wood et al., 2003). Recent studies have shown that PAF1 may also regulate promoter-proximal pausing of PolII (Chen et al., 2015). PAF1 regulates PolII pausing approximately 50 nucleotides downstream of the transcription start site (TSS) where significant PolII occupancy is found. Upon PAF1 knockdown, PolII is released to the gene body (Chen et al., 2015). Together, these studies indicate the PAF1 complex regulates multiple aspects of transcription. By interacting with the PAF1 complex, PHF6 is thus poised to influence transcription.

PHF6 also interacts with the nucleosome remodeling and deacetylation (NuRD) chromatin remodeling complex (Todd and Picketts, 2012). The NuRD complex is composed of the histone deacetylase Hdac1 or Hdac2 and ATPase Chd3 or Chd4, with combinatorial assembly of other subunits, including histone-binding protein RbAp46 and RbAp48, scaffold protein Mta1/2, DNA-binding protein Mbd3, and GATA zinc finger domain-containing protein 2A Gatad2a and Gatad2b (Zhang et al., 1998, 1999). The NuRD complex has been widely studied in cancer and embryonic stem (ES) cells (Lai and Wade, 2011). In acute promyelocytic

leukemia (APL), the NuRD complex alters DNA methylation levels leading to gene repression. Upon removing the NuRD subunit Mbd3 in leukemia cells, DNA methylation levels at the RARb2 gene are significantly reduced (Morey et al., 2008). In addition, depletion of Mbd3 allows reprogramming of somatic cells to induced pluripotent stem (iPS) cells (Rais et al., 2013). The Mbd3-NuRD complex is thought to be recruited to the OSKM (Oct4, Sox2, Klf4, and Myc) target genes and inhibit robust reprogramming. Upon Mbd3 depletion, OSKM proteins interact with other pluoripotency-inducing chromatin regulators to drive efficient reprogramming (Rais et al., 2013). Recently, two *de novo* mutations in the NuRD subunit Gatad2a have been described in patients with severe intellectual disability (Willemsen et al., 2013), suggesting that the NuRD complex plays a critical role in brain development.

The NuRD complex is highly expressed in the developing brain. Recent studies by Yamada, Yang et al. have identified a novel function for the NuRD complex in neuronal connectivity in the brain (Yamada et al., 2014). The NuRD complex decommissions a subset of gene promoters by removing H3K9/14 acetylation marks and thereby represses the expression of developmentally regulated genes to trigger granule neuron parallel fiber/Purkinje cell synaptic connectivity in the mammalian brain. Upon depletion of Chd4, the core ATPase subunit of the NuRD complex, these developmental genes are derepressed, leading to defects in granule neuron presynaptic bouton formation (Yamada et al., 2014). Whether the interaction of PHF6 with the NuRD complex influences gene expression and establishment of neuronal connectivity remains unexplored.

PHF6 also interacts with the nucleolar transcription factor upstream binding factor (UBF) in cells (Wang et al., 2013). UBF recruits RNA polymerase I to rDNA promoter regions. Upon PHF6 depletion, HeLa cells arrest at the G2/M phase of the cell cycle and have increased levels of UBF and ribosomal RNA synthesis. PHF6 interacts with UBF and is recruited to rDNA promoters to repress rDNA expression. Knockdown of PHF6 derepresses the rDNA promoter, leading to increased ribosomal RNA levels (Wang et al., 2013). However, the mechanism of rDNA repression by the PHF6-UBF interaction localized to the rDNA promoter remains unclear.

In situ RNA hybridization and expression analyses have shown that PHF6 is highly expressed in the developing central nervous system (CNS) and declines along the course of development (Voss et al., 2007). These observations suggest that PHF6 expression is tightly regulated during brain development. Recent studies by Franzoni et al provide insights into the mechanisms underlying the regulation of PHF6 expression (Franzoni et al., 2015). Downregulation of *PHF6* expression is correlated with an increase in the expression levels of miR-128, suggesting that miR-128 may regulate PHF6 expression during brain development. Consistent with this interpretation, expression of miR-128 in cortical neurons triggers the downregulation of PHF6, an effect that is mediated by miR-128 binding sites within the 3'UTR of PHF6 mRNA (Franzoni et al., 2015). A prediction of these results is that miR-128 might influence neuronal migration in the cerebral cortex. Consistent with this prediction, expression of miR-128 by *in utero* electroporation in the mouse brain arrests the migration of cortical neurons in layers III and IV-VI (Franzoni et al., 2015), which phenocopies the migration defects observed upon PHF6 knockdown (Zhang et al., 2013). Importantly, expression of PHF6 reverses the miR-128-induced migration defects (Franzoni et al., 2015), suggesting that PHF6 operates downstream of miR-128 in the regulation of cortical migration. Whether miR-128 regulation of PHF6 expression influences other aspects of brain development remains to be explored.

PHF6 in BFLS Pathogenesis

Identification of a critical role for PHF6 in radial neuronal migration in the cerebral cortex raises the important question of whether deregulation of PHF6 function in migration contributes to BFLS pathogenesis. Proper migration and positioning of neurons is a prerequisite for correct neuronal connectivity (Ayala et al., 2007; Morgan-Smith et al., 2014; Nadarajah & Parnavelas, 2002). Radially migrating neurons in the cerebral cortex are born in the ventricular zone (VZ) and sub-ventricular zone (SVZ), migrate along the radial glia scaffold to reach the cortical plate (Ayala et al., 2007; Kriegstein & Noctor, 2004; Vaillend et al., 2008). The oldest neurons reside in the deep layer of the cortical plate, and newly generated neurons pass the deep layers to reside in more superficial layers (Greig et al., 2013). Upon PHF6 knockdown, neurons arrest in the intermediate zone, and the ectopic cells have neuronal hyperexcitability (Zhang et al., 2013). Introduction of an RNAi-resistant form of wild type-PHF6 into PHF6 knockdown mice rescues the migration defects, suggesting that the RNAi-induced phenotype is the result of specific knockdown of PHF6 rather than off target effects (Zhang et al., 2013). *In vivo* structure-function analyses of PHF6 demonstrate that BFLS patient-specific mutations impair the ability of PHF6 to promote neuronal migration (Zhang et al., 2013). Strikingly, neuropathological studies performed in the first identified BFLS patient have revealed defects of neuronal migration in the cortical plate including coarse gyri, cortical dysplasia with indistinct lamination and heterotopic neurons observed in the subcortical white matter (Brun et al., 1974).

PHF6 knockdown in the mouse cerebral cortex also triggers the formation of white matter heterotopias with aberrant neuronal activity (Zhang et al., 2013). Importantly, electrophysiological recordings reveal significant hyperexcitability of heterotopic neurons. Whole-cell patch clamp recordings reveal an aberrant pattern of activity in heterotopic neurons in PHF6 knockdown animals (Zhang et al., 2013). The membrane potential of heterotopic neurons oscillates, leading to frequent firing of action potentials. Further, knockdown of Neuroglycan C, a PHF6 target gene, also leads to formation of heterotopias that harbor neuronal hyperexcitability (Zhang et al., 2013). Heterotopias have been postulated to contribute to seizure

susceptibility (Ackman et al., 2009). Heterotopias may serve as loci that initiate seizure activity. Studies in both genetically induced animal models and depth electrode recordings from patients have suggested that heterotopic loci may function to generate epilepsy (Aghakhani et al., 2005; Kothare et al., 1998, Manent et al., 2009). Together, these data suggest that inhibition of the PHF6 pathway triggers the formation of heterotopias in which neurons are hyperexcitable. These findings may be relevant to reduced seizure threshold in BFLS patients.

Although recent studies of PHF6 function have focused on its role in the regulation of neuronal migration and positioning in the cerebral cortex, it is likely that PHF6 has additional functions in the developing brain owing to its expression pattern (Voss et al., 2007; Zhang et al., 2013). PHF6 is expressed throughout the cerebral cortex and although levels of PHF6 drop with maturation, PHF6 is poised to regulate other aspects of neuronal development beyond neuronal positioning. In addition, PHF6 may have developmental roles outside of the cerebral cortex that may be relevant to BFLS pathogenesis.

Perspectives

Recent studies have advanced our understanding of the underlying molecular mechanisms of PHF6 function and its relevance to BFLS pathogenesis. These studies suggest that PHF6 is required for proper neuronal migration and that deregulation of PHF6 function in neuronal positioning contributes to the pathogenesis of BFLS. Analyses of PHF6 signaling in cells, primary neurons, and in the developing mouse brain suggest a role for PHF6 in transcription. Although progress has been made, further research is required to gain a better understanding of PHF6 functions in brain development and pathogenic mechanisms underlying BFLS.

The finding that migration arrest in the PHF6 knockdown animals leads to the formation of heterotopias has important implications in the pathogenesis of BFLS. Clinically, heterotopia formation is associated with epileptic activity in the brain, which has been documented in BFLS patients (Robinson et al., 1983). Additionally, heterotopic neurons are hyperexcitable (Ackman et al., 2009). In neuropathological studies, in addition to evidence of whiter matter heterotopias, the cerebral cortex displays cortical dysplasia with indistinct or absent lamination (Brun et al., 1974). Whether cortical dysplasia due to impairment of PHF6 function is relevant to BFLS requires further study.

The identification of a novel transcriptional PHF6/PAF1 pathway in the developing brain has opened new avenues for the study of the molecular mechanisms that underlie XLID, and has also brought new insights into the regulation of transcription. The association of PHF6 with the PAF1 complex suggests an important role for PHF6 in the regulation of transcriptional elongation during neuronal development. Intriguingly, nascent transcriptional initiation is wide-spread across the genome, and the transition from transcriptional initiation to elongation represents a critical step of gene regulation (Guenther et al., 2007; Krumm et al., 1995; Muse et al., 2007; Nechaev & Adelman, 2012). Previous studies have revealed that the PAF1 complex cooperates with DSIF and the elongation factor SII/TFIIS, and thereby promotes elongation of PolII along the gene body (Chen et al., 2009; Zhu et al., 2005). In view of the findings that PHF6

may function to negatively or positively regulate gene expression (Todd & Picketts, 2012; Wang et al., 2013; Zhang et al., 2013) and PAF1's critical role in gene pausing (Chen et al., 2015), it would be interesting to investigate whether PHF6 regulates gene pausing, pause release, or both. The PAF1 complex appears to be critical for histone modifications including H3K4 tri-methylation (H3K4me3) or histone H2B (ubH2B) ubiquitination (Krogan et al., 2003; Wood et al., 2003). Whether PHF6 promotes modifications of histones via interactions with the PAF1 complex remains an open question.

The identification of Neuroglycan C as a target gene of PHF6 and the PAF1 complex provides new insights in neuronal migration and intellectual disability (Zhang et al., 2013). The Neuroglycan C gene, a member of the neuregulin family, encodes a transmembrane chondroitin sulfate glycoprotein, which has been implicated in the regulation of cortical radial migration (Anton et al., 1997; Brandt et al., 2007; Kinugasa et al., 2004; Rio et al., 1997). The Neuroglycan C gene might represent a locus associated with schizophrenia, a neuropsychiatric disorder in which impaired neuronal migration may play a pathogenic role (Impagnatiello et al., 1998; Lee et al., 2011; So et al., 2010; Tomita et al., 2011). These observations raise the possibility that mutations of PHF6 may contribute to the pathogenesis of neuropsychiatric disorders beyond intellectual disability. It will be also interesting to determine whether deregulation of Neuroglycan C might play a role in intellectual disability and epilepsy.

Beyond the role of the PHF6-PAF1 interaction in neuronal positioning, it will be important to characterize the significance of the PHF6 interaction with the NuRD complex in brain development. Recently, two *de novo* mutations in the NuRD subunit Gatad2a have been reported in patients with severe intellectual disability (Willemsen et al., 2013). The NuRD complex represses transcription of developmentally regulated genes and thereby drives synaptogenesis in the mammalian brain (Yamada et al., 2014). Whether the NuRD complex regulates neuronal migration in the cerebral cortex remains unclear. In granule neurons of the cerebellum, the NuRD complex removes H3K9/14 acetylation marks at a subset of genes during development to drive synaptogenesis (Yamada et al., 2014). However, how the NuRD complex

and PHF6 might regulate the epigenetic landscape of the genome in the cerebral cortex remains unknown.

Identification of the PHF6/UBF interaction in HeLa cells suggests that PHF6 may function in the nucleolus to regulate rDNA transcription (Wang et al., 2013). The nucleolus is a prominent subnuclear domain implicated in ribosomal RNA (rRNA) transcription, which accounts for up to 80% of RNA synthesis in eukaryotic cells (Nemeth and Langst, 2011). Transcription of rDNA is essential during the cell cycle (Roussel et al., 1996); however, its importance in post-mitotic neurons remains to be elucidated. Recently, intellectual disability-linked proteins including FMRP and the RNA methyltransferase NSUN2 have been shown to be transported to nucleoli (Khan et al., 2012; Nemeth and Langst, 2011). Whether PHF6 may harbor regulatory roles in the nucleolus has been unexplored.

Future studies of PHF6 should focus on elucidation of the biochemical functions of PHF6 including the role of its PHD domains. In addition, it will be important to explore whether PHF6 harbors additional biological functions in brain development including neural progenitor proliferation, differentiation, synaptic development and circuit integration, and determine whether deregulation of such functions contributes to the pathogenesis of BFLS.

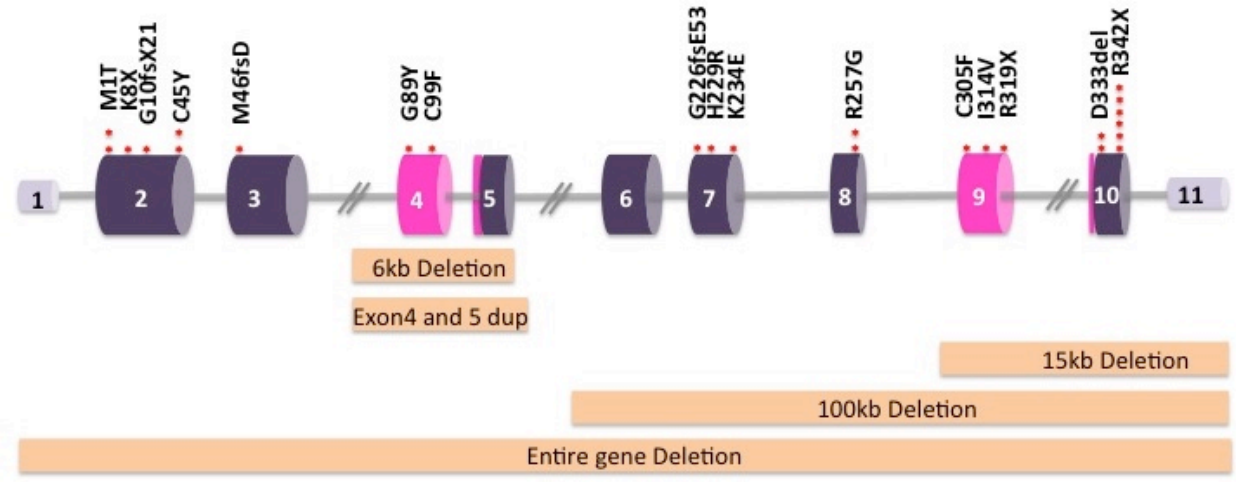

Figure 1. *PHF6* gene with patient mutations. The small blocks in light purple represent the 3' and 5' UTR of *PHF6* gene. The blocks in dark purple represent the coding exons with PHD domains shown in pink. Point mutations in BFLS are shown as red dots. Five large domain deletions in BFLS are also shown.

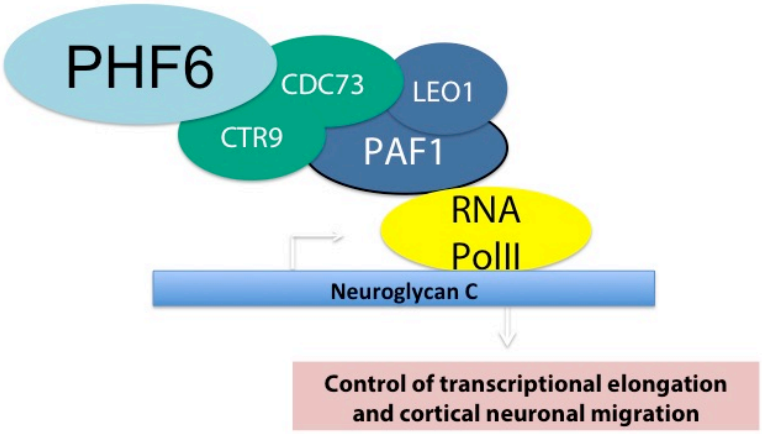

Figure 2. A proposed model for PHF6-PAF1 complex in regulation of neuronal migration during cortical development. During critical period of neuronal migration, PHF6 interacts with PAF1 transcriptional elongation complex to regulate downstream targets including Neuroglycan C to regulate neuronal migration and positioning.

Table1. Summary of PHF6 mutations in BFLS patients in different individuals from different families.

F/ M	Nucleotide	Amino Acid	Mutation	Reported clinical features	Ref
M	c. 2T>C	p.M1T	Missense	Classical features of BFLS with no detailed clinical records.	(Lower et al., 2002)
M	c. 2T>C	p.M1T	Missense	Classical features of BFLS. Born at term after uneventful pregnancy, delayed early milestones, walked at age 4, began saying a few words at age 5, height of 140cm (<3rd centile), weight of 45kg (5th centile), and occipital-frontal head circumference of 53.3cm (10th-25th centile) at age 15, short stature, triangular face, hyperplastic supraorbital digits, deep-set eyes, large ears, gynecomastia, lower abdominal obesity, and small penis and testes with no evidence of pubertal change.	(Crawford et al., 2006)
M	c.134G>A	p.C45Y (familial)	Missense	Classical features of BFLS with no detailed clinical records.	(Lower et al., 2002)
M	c.134G>A	p.C45Y (de novo)	Missense	Classical features of BFLS with no detailed clinical records.	(Lower et al., 2002)
M	c.266G>T	p.G89Y	Missense	Classical features of BFLS. At age 22, height 173cm, weight 108kg, head circumference 61cm. Moderate intellectual disability; delayed development, good tempered with occasional	(Mangelsdorf et al., 2009)

				aggressive attacks, no epileptic seizures. Brother has similar symptoms with severe intellectual disability, Female carrier in the family has shown mild intellectual disability.	
M	c.296G>T	p.C99F	Missense	Classical features of BFLS. Female carrier has mild clinical features of BFLS including obesity, large ears, amenorrhea, hypothyroidism, epilepsy, and learning difficulties.	(Lower et al., 2002)
M, F	c.686A>G	p.H229R	Missense	Classical features of BFLS with no detailed clinical records.	(Lower et al., 2002)
M	c.700A>G	p.K234E	Missense	Classical features of BFLS with no detailed clinical records.	(Lower et al., 2002)
M	c.769A>G	p.R257G	Missense	Classical features of BFLS with no detailed clinical records.	(Lower et al., 2002)
M	c.769A>G	p.R257G	Missense	Classical features of BFLS. Severe intellectual disability, self-injurious behavior, stooped hyposcoliotic posture, central obesity, marked gynecomastia, hypogonadism, and hand and feet anomalies. Hodgkin's lymphoma	(Vallée et al., 2004) (Carter et al., 2009)

M	c.940A>G	p.I314V	Missense	Classical features of BFLS. Psychomotor developmental delay, language delay, mild intellectual disability (IQ of 61) and lack of inhibition in sexual contacts. At age 18, height 171.5 cm, head circumference 55.7cm, moderate obesity, marked gynecomastia, limbs showing hypermobility.	(Crawford et al., 2006)
M	c.22A>T	p.K8X	Nonsense	Classical features of BFLS.	(Lower et al., 2002)
F	c.955C>T	p.R319X	Nonsense	Classical features of BFLS. Head circumference 34cm (-0.5SD), delayed walking at age 2.5. During first years, frontotemporal alopecia, nystagmus, strabismus, small teeth, hypoplastic labia minora and clitoris. At age 6, head circumference of 49cm (-1.63SD), moderate to severe intellectual disability, lack of swallowing coordination, sociable and happy, facial dimorphism, and tapering fingers. Normal MRI.	(Zweier et al., 2013b)
M	c.1024C>T (original	p.R342X	Nonsense	Classical features of BFLS.	(Gécz et al., 2006; Lower et al., 2004)

	family)			Developmental delay, upslanting palpebral fissures, large ears, a high palate, hypotonia, cryptorchidism, and an inguinal hernia. At age 15, talk sentances consisting of three or four words, short stature and obesity, large ears, protruding cheeks,. Female carrier is clumsy when running/jumping, but has normal cognitive function. Big hands, ears and feet, with some sensory impairment in the legs. Normal MRI.	
M	c.1024C>T	p.R342X	Nonsense	Delayed developmental milestones, height on 25th centile, weight over 97th centile, head circumference over 98th centile, narrow bitemporal diameter, upslanting eyes, prominent supraorbiral ridges, hypotelorism, long ears/earlobes, a prominent chin, obese, marked gynecomastia, a hypoplastic scrotum with retractile testes, cubitus valgus, tapered fingers. Female carrier is obese, has deep-set eyes, prominent supraorbital ridges, large ear lobes, tapered fingers, broad feet and short toes.	(Lower et al., 2002)

M	c.1024C>T	p.R342X	Nonsense	Classical features of BFLS.	(Lower et al., 2002)
M	c.1024C>T	p.R342X	Nonsense	Classical features of BFLS.	(Crawford et al., 2006)
M	c.1024C>T	p.R342X	Nonsense	Classical features of BFLS.	(Crawford et al., 2006)
M	c.1024C>T	p.R342X	Nonsense	Classical features of BFLS and T cell acute lymphoblastic leukemia at age 9	(Chao et al., 2010)
F	c.27dupA	p.G10fsX21	Frameshift	Classical features of BFLS. Poor coordination, delayed speech, normal IQ of 87, high level of thyroid stimulating hormone, low level of thyroxin at age 7-8; at age 14, height 180cm, weight 115 kg, shallow forehead, fleshy earlobes, deep set eyes, broad feet, hammertoes, no menstruation at age 14, tactile defensive and emotionally labile, poor spatial awareness, and startles to noise.	(Crawford et al., 2006)
M	IVS2-8A>G	M46fsD exon3	Frameshift	Classical features of BFLS with mild to moderate intellectual disability, and global developmental delay.	(Vallée et al., 2004)
F	c.677delG	p.G226fsE53	Frameshift	Classical features of BFLS Diagnosed with Coffin Siris Syndrome in early infancy. At 9 years old,	(Wieczorek et al., 2013; Zweier et al., 2013b)

				height 1.7SD, weight 30kg, head circumference 54cm (1.4SD). Mild intellectual disability, shy and intolerance for being alone, sleeping difficulties, mild clinodactyly, short toes, and facial dysmorphism.	
F	c.914G>T	p. C305F	Missense	Classical features of BFLS, previously diagnosed with Coffin Siris Syndrome, unstable gait on stairs, head circumference of-1.0SD at age 11, aggressive behavior, susceptibility to urinary tract infections, frequent constipation, facial dysmorphism, and tapered fingers.	(Wieczorek et al., 2013; Zweier et al., 2013b)
F		Dosage gain of exon 4, 5	Duplication	Classical features of BFLS, delayed milestones, unstable gait, delayed speech, conductive hearing loss, potential retinal dystrophy, and seizures at age 20. At age 22, head circumference 56.5(1.4 SD), facial dysmorphism, tapering fingers. Behavioral problems including short attention span, hyperactivity, compulsive behavior, sleeping difficulties, and lack of emotional detachment.	(Zweier et al., 2013b)
F		Dosage gain of exon 4,	Duplication	Classical features of BFLS.	(Zweier et al., 2013b)

		5		Head circumference of 34cm (1.4 SD) at birth; At age 3-4 month, several single seizures, delayed walking and language, sociable behavior, constipation, and neurogenic bladder. At age 32, head circumference 54cm (-0.3 SD).	
F	6kb deletion	Affecting exon 4, 5	Deletion	Classical features of BFLS with moderate intellectual disability. Head circumference 53cm (2.2SD), linear skin hyperpigmentation, sociable behavior, and facial dimorphism.	(Zweier et al., 2013b)
F	100kb deletion	Deletion of last 5 coding exons	Deletion	Classical features of BFLS. Delayed developmental milestone, feeding difficulties, muscular hypotonia, single horseshoe kidney, obstructive uropathy, recurrent pyelonephritis, and multiple febrile seizures.	(Di Donato et al., 2014)
F	15kb deletion	Deletion of last 3 exons	Deletion	Classical features of BFLS with mild intellectual disability. At age 7, mild hearing loss, and recurrent middle ear infections; At age 16, head circumference 56.6cm (75^{th} centile), slightly widened ventricles and	(Berland et al., 2011)

				increased white matter signal abnormality on MRI.	
M	c.999-1001 delTGA	p.D333del	Deletion	Classical features of BFLS with delayed milestones.	(Baumstark et al., 2003)
M	c.999-1001 delTGA	p.D333del	Deletion	First patient description. Delayed milestones, severe mental deficiency with IQ of 20, seizures, hyperactive and aggressive behaviors, large ears, short stature, small genitalia, and small pituitary gland. Coarse gyri, widened ventricular system, cortical dysplasia with indistinct lamination, and heterotopias.	(Börjeson et al., 1962; Gécz et al., 2006)
F	Entire gene deleted		Deletion	Classical features of BFLS. Head circumference 35.5 (0.5SD) at birth, delayed motor milestones and facial dysmorphism. Sleeping difficulties, compulsive eating behavior, muscular hypotonia, ectopic left kidney, strabismus, hyperopia, bilateral sensorineural hearing loss, enlarged ventricles on MRI.	(Zweier et al., 2013)
F	270kb deletion		Deletion	Classical features of BFLS. Mild muscular hypotonia, mild speech delay, narrow external auditory canal, mild learning disability; IQ	(Di Donato et al., 2014)

				within borderline to normal range.	

Table1. Summary of PHF6 mutations in BFLS patients in different individuals from different families. Classical features of BFLS includes mild to severe mental retardation, hypogonadism, hypometabolism, obesity with marked gynecomastia, facial dysmorphism, narrow palpebral fissure, large and fleshy ears, tapered fingers.

Acknowledgments

We thank the members of the Bonni laboratory for critical reading of the manuscript. The authors are supported by National Institutes of Health grant NS088378 (to A.B.) and the Mathers Foundation (to A.B.). A.J.-A was supported by a postdoctorate fellowship from Canadian Institute of Health Research (CIHR).

Author Contributions

A.J., C.C and A.B are responsible for the design and content of this review. A.B. contributed to the overall organization and content of this work.

Chapter 2: A Mouse Model of Börjeson-Forssman-Lehmann Syndrome displays deficits in cognition and neural hyperexcitability

Adapted from:

Characterization of A Mouse Model of Börjeson-Forssman-Lehmann Syndrome

Cheng Cheng, Pan-yue Deng, Yoshiho Ikeuchi, Carla Yuede, Daofeng Li, Nicholas Rensing, Ju Huang, Dustin Baldridge, Susan E Maloney, Joseph D Dougherty, John Constantino, Arezu Jahani-Asl, Michael Wong, David Wozniak, Ting Wang, Vitaly Klyachko, Azad Bonni

In revision September, 2018

ABSTRACT

Mutations of the transcriptional regulator PHF6 cause the X-linked intellectual disability disorder Börjeson-Forssman-Lehmann syndrome (BFLS), characterized by cognitive impairment, developmental delay and seizures. However, the mechanisms by which mutations of *PHF6* contribute to the pathogenesis of BFLS remain poorly understood. Here, we report the first mouse model of BFLS. Using a CRISPR-Cas9 approach, we have generated mice in which Cysteine 99 within the PHD domain of PHF6 is replaced with phenylalanine (C99F). Mice harboring the patient-specific PHF6 C99F mutation display deficits in cognitive functions, emotionality, and social behavior as well as reduced threshold to seizures. Electrophysiological studies reveal that the intrinsic excitability of entorhinal cortical stellate neurons is increased, providing a cellular basis for seizure predisposition upon PHF6 deficiency. Our findings advance our understanding of the mechanisms underlying BFLS pathogenesis.

INTRODUCTION

Intellectual disability (ID) is a prevalent developmental disorder that affects 1% to 3% of the general population (Bhasin et al., 2006). With no effective treatments, ID poses enormous economic costs to society. There is thus an urgent need to better understand the pathogenesis of ID. Human genetics studies have uncovered a number of gene mutations associated with ID. However, although a few genetic causes of ID such as fragile X and Rett syndrome have been the subject of intense scrutiny (Amir et al., 1999; Verkerk et al., 1991), the functions of most ID proteins and the mechanisms by which these proteins regulate pathologically relevant biological processes remain poorly understood.

Börjeson-Forssman-Lehman syndrome (BFLS) was identified over five decades ago as an X-linked syndrome of moderate to severe impaired cognitive function associated with developmental delay, truncal obesity, and seizures (Börjeson et al., 1962; Gécz et al., 2006; Lower et al., 2002). Forty years later, mutations in the gene encoding the PHD and zinc finger domain-containing protein PHF6 were identified as the genetic cause of BFLS (Lower et al., 2002). Since then, multiple mutations in distinct regions of *PHF6* including within its two PHD domains have been identified in BFLS patients (reviewed in Jahani-Asl et al., 2016). However, how *PHF6* mutations trigger the pathogenesis of BFLS remains to be elucidated. Modeling of cognitive disorders such as fragile X and Rett syndromes in mice has helped to advance our understanding of these disorders (Guy et al., 2001; Irwin et al., 2000). However, a mouse model of BFLS using patient-specific *PHF6* mutations has yet to be established.

In this study, we report the first patient-specific PHF6 mutant mouse model of BFLS. Using a CRISPR-Cas9 approach, we have generated mice in which Cysteine 99 within the PHD domain of PHF6 is replaced with phenylalanine (C99F). Mice with the patient-specific PHF6 C99F mutation display deficits in cognitive functions, emotionality and social behaviors, and are more susceptible to seizures, suggesting that PHF6 C99F mice feature phenotypes relevant to

BFLS. In electrophysiological studies in acute slices, the intrinsic excitability of entorhinal cortical layer II stellate neurons is increased, providing a cellular basis for susceptibility of BFLS mice to seizures. Collectively, our findings broaden our understanding of the cellular underpinnings of BFLS pathogenesis.

RESULTS

Generation of patient-specific PHF6 mutant mouse model of BFLS

We reasoned that generating a patient-specific knock-in mutation of PHF6 in mice would provide a useful tool in studies of BFLS pathogenesis. We first characterized the expression of different patient-specific mutations of PHF6 in cells. Among patient-specific mutations of PHF6, three mutations led to substantial reduction of PHF6 protein levels (Figure 3a), suggesting that BFLS may result from hypomorphic PHF6 function. Among the three mutations, substitution of cysteine 99 with phenylalanine (C99F), located in the first PHD domain of PHF6, dramatically reduced the levels of PHF6 protein (Figure 3a).

We next generated C99F knock-in mice. Using a CRISPR-Cas9 method. The single nucleotide mutation nt.296G>T was successfully introduced in the mouse *PHF6* gene, confirmed with Sanger sequencing (Figure 3b, S1a). PHF6 C99F mice were backcrossed to mice with C57B6 background for more than ten generations. Screening of potential CRISPR-Cas9 off-target sites in the mouse genome predicted by COSMID (Cradick et al., 2014) and CRISPOR (Haeussler et al., 2016) revealed no mutations. Genomic sequences in the ~1kb regions flanking the C99F point mutation were also intact (Figure S1a). PHF6 C99F knock-in mice were born with Mendelian ratio, had slightly reduced body weight, length, body surface area and survived to adulthood (Figure S1d-g). Notably, morphological analyses of PHF6 C99F and control littermate mice showed little or no differences in body mass index (BMI), ear length, facial length, interocular distance and testis weight when normalized to body weight (Figure S1h-l). These data suggest that PHF6 C99F mice do not phenocopy syndromic features of BFLS patients.

Having generated the PHF6 C99F knock-in mouse, we characterized the expression of PHF6 in the cerebral cortex in these mice. As expected, immunoblotting analyses in control mice revealed PHF6 was expressed in the mouse cerebral cortex at early embryonic ages, and was

substantially downregulated postnatally (Figure 3c) (Zhang et al., 2013). In immunohistochemical analyses, PHF6 co-localized with the layer V marker Ctip2 in the cortical plate of control mice at embryonic day 14 (E14), and was expressed in all layers of the cortical plate at E18 (Figure 3d). Strikingly, the levels of PHF6 protein were substantially reduced, though not eliminated, in the cerebral cortex in PHF6 C99F mice at E14.5 and P0 (Figure 3e-g, S1c). However, the levels of PHF6 mRNA in the cerebral cortex in the C99F mice were not reduced (Figure 3f), suggesting that the stability of PHF6 protein in C99F mice may be reduced.

PHF6 C99F knock-in mice display impairments in cognition, social interaction and emotionality

We conducted behavioral analyses on PHF6 C99F mice in a battery of tests to assess locomotor activity, sensorimotor function, spatial learning/memory, fear conditioning, social interaction and startle response. In analyses of contextual fear conditioning data, PHF6 C99F mice exhibited significantly reduced freezing levels compared with control littermate animals on day 2 (Figure 4a), suggesting that learning is impaired in PHF6 C99F mice to associate the contextual cues present in the chamber with the foot shock. Importantly, no differences were observed between groups during either the baseline period or during tone-shock training on day 1 (Figure S2a). Also, the groups did not differ during the altered context baseline on day 3, although moderate performance deficits were observed in the PHF6 C99F mice during the auditory cue test on day 3 (Figure S2a). The performance difference between the groups of mice in contextual fear responses were not due to alterations in shock sensitivity of (data not shown). Defects in contextual fear memory were observed in another independent cohort of mice (Figure S3a). Mice were also subjected to a novel object-location test to evaluate recognition memory in mice. We found that control mice, but not PHF6 C99F mice spent more time investigating the moved object than the stationary object (Figure 4b). In other analyses, PHF6 C99F mice did not

exhibit performance deficits during the cued, place (Figure S2b), or probe (not shown) conditions when tested in the Morris water maze (MWM), suggesting that PHF6 C99F mice may not be impaired in spatial learning acquisition or retention. Together, our data suggest that PHF6 C99F mice have deficits in contextual fear conditioning and in some forms of spatial learning.

To characterize sociability and preference for social novelty, mice were subjected to a three-chamber social approach task. Both control and PHF6 C99F mice exhibited preference for investigating a novel stimulus mouse versus an empty withholding cage (data not shown). However, control littermate mice, but not PHF6 C99F mice, showed a preference for a novel mouse compared to a familiar (cagemate) mouse (Figure 4c, S3b). A similar preference for the novel mouse in control but not PHF6 C99F mice was observed in an independent cohort (Figure S3c, d). Together, these data suggest that PHF6 C99F mice display normal levels of sociability, but may be impaired in social recognition memory.

Ambulatory activity and exploratory behavior during a control 1-h locomotor activity test prior to the conditioned fear procedure revealed reduced activity in PHF6 C99F mice, but only in latter part of the test session (Figure 4d). Vertical rearing frequency was also significantly reduced in PHF6 C99F mice (Figure 4e). Similar effects of the PHF6 C99F mutation on ambulatory activity and vertical rearing were observed in an independent cohort (Fig. S3e-f). These results suggest that PHF6 C99F mice may show reduced levels of attention or interest toward novel environments, which may also account for reduced investigation time toward the moved object in the object location test (Figure 4b). In two independent cohorts, PHF6 C99F mice also exhibited significantly reduced acoustic startle response throughout the test session (Figure 4f, S3g), although no significant effects were observed on prepulse inhibition (PPI) (not shown). These data suggest that sensorimotor reactivity was attenuated in PHF6 C99F mice compared to littermate controls, although sensorimotor gating appeared unaffected in the mutant mice. Collectively, our data suggest that PHF6 plays critical roles in normal cognitive development as it relates to certain forms of learning and memory, emotionality and social

behaviors.

PHF6 C99F mice exhibit increased neuronal excitability and seizure susceptibility

Besides impaired cognitive functions, seizures represent an important aspect of the clinical presentation of BFLS (Jahani-Asl et al., 2016, Kasper et al., 2017). We therefore characterized the susceptibility of PHF6 C99F knock-in mice to seizures. We injected PHF6 C99F and control littermate mice intraperitoneally with pentylenetetrazol (PTZ), a GABA antagonist. PHF6 C99F mice showed reduced time to reach generalized seizures (Figure 5a). PTZ-induced seizures are rapidly progressing (Zhang and Wong, 2012). We, therefore, used the glutamate agonist kainic acid to induce slowly progressing seizures, allowing for scoring seizure stages according to the Racine scale (Racine et al., 1972). PHF6 C99F animals showed more rapid seizure progression and greater number of seizure events at higher Racine scores (Figure 5b). Together, these results suggest that PHF6 C99F mice phenocopy the predisposition of BFLS patients to seizures.

We next determined the cellular basis for seizure predisposition in PHF6 C99F mice. Alterations of neuronal excitability in diverse neuronal populations may be epipeptogenic (Scharfman, 2007). We focused our analyses on layer II stellate neurons in the entorhinal cortex, whose excessive activation triggers seizures (Vismer et al., 2015). Current-clamped stellate neurons in acute brain slices from C99F and control littermate mice were depolarized to a range of potentials from -55 mV to -44 mV with a 1-mV step via automatic current injection to induce action potential firing. We observed a large increase in the probability of action potential firing in stellate neurons in C99F mice. Nearly 40% of all neurons in brain slices of PHF6 C99F mice fired action potentials at -53 mV compared to none from control mice, and over 90% of all neurons from C99F mice fired action potentials at -50 mV in contrast with only 15% of control neurons (Figure 5c). In addition, the number of action potentials fired at -50 mV over a 20 sec

period was markedly increased in C99F mice (Figures 5d-e). In a standard ramp protocol (Deng and Klyachko, 2016; Yamada-Hanff and Bean, 2013), action potential threshold of stellate neurons in C99F mice was significantly decreased (Figure 5f-g). Together, these results suggest that entorhinal cortical stellate neurons have increased excitability in PHF6 C99F mice.

We next determined the physiological basis for increased neuronal excitability in PHF6 C99F mice. No detectable changes in the resting membrane potential were observed in stellate neurons of C99F mice (Figure 5h). However, membrane capacitance was significantly decreased (Figure 5i) and input resistance was significantly increased (Figure 5j) in PHF6 C99F mice compared to control littermate mice. Input resistance normalized to cell capacitance in each recorded cell was also significantly increased in C99F mice (Figure 5k), suggesting that alterations in input resistance occur independently of changes in capacitance. Notably, two clearly distinguishable subpopulations of stellate neurons were observed in C99F knock-in mice that stratified according to the cell capacitance (Supplementary Figure S4A; large neurons: 125.4 ± 8.2 pF, n = 8; small neurons: 55.3 ± 5.8 pF, n = 6; P = 0.00003). However, alterations in input resistance and action potential threshold in C99F knock-in neurons occurred independently of differences in capacitance (Supplementary Figures S4B-4E). Taken together, our data suggest that stellate neurons in C99F knock-in mice are hyperexcitable due to, at least in part, deminition of action potential firing threshold associated with increased input resistance and decreased cell capacitance. Because stellate neurons represent the major projection neurons to the hippocampus, our electrophysiological data suggest that hippocampal inputs from the entorhinal cortex are abnormally hyperexcitable, which may contribute to susceptibility to seizures.Taken together, our data suggest that stellate neurons in C99F mice are hyperexcitable due to at least in part diminution of action potential firing threshold associated with increased input resistance and decreased cell capacitance.

DISCUSSION

In this study, we report the first mouse model of Börjeson-Forssman-Lehmann syndrome (BFLS). Mice harboring the patient-specific PHF6 C99F mutation display deficits in cognitive functions, emotionality, and social behaviors, and are susceptible to seizures, phenocopying key clinical features of BFLS. Electrophysiological analyses reveal increased excitability of entorhinal cortical stellate neurons secondary to reduced threshold to action potential firing in PHF6 C99F mice, providing a cellular basis for seizure predisposition of the brain upon PHF6 deficiency. Gene profiling analyses in PHF6-deficient mice show that PHF6 promotes the expression of neurogenesis genes and concomitantly suppresses expression of synaptic genes. PHF6-regulated genes are overrepresented in gene signatures and modules that are deregulated in the brain of patients with autism spectrum disorder (ASD). Taken together, our findings provide novel insights into the cellular and molecular underpinnings of BFLS, and may suggest potential links of BFLS with autism spectrum disorders.

The identification of a novel mouse model of BFLS provides an excellent tool for studies of the pathogenesis of BFLS. In addition to mild to severe intellectual disability, BFLS patients display disturbances in adaptive behaviors including aggressive behavior, poor spatial awareness and short attention span (Crawford et al., 2006; Gécz et al., 2006; Mangelsdorf et al., 2009; Zweier et al., 2013b). Consistent with the diverse picture of cognitive impairment in BFLS patients, behavior analyses reveal that PHF6 C99F mice have deficits in multiple domains including some forms of learning and memory, social interactions, and emotionality.

The identification of increased seizure susceptibility in the C99F mouse sheds light on the cell types and neural circuits that might contribute to epilepsy in BFLS patients. The finding of increased excitability associated with reduced action potential and increased input resistance in entorhinal cortical layer II stellate neurons provides a cellular basis for seizures in BFLS. Because increased excitation from stellate cells to the hippocampal dentate gyrus is associated

with temporal lobe epilepsy (Janz et al., 2017), it will be interesting to determine whether BFLS patients have focal seizures of temporal lobe origin, as suggested by a case of a BFLS patient with temporal lobe spikes on EEG (Kasper et al., 2017). Notably, layer II stellate neurons project to the hippocampus via the perforant pathway, which plays a critical role in contextual fear memory and object location recognition (Kitamura et al., 2015; Tennant et al., 2018). Thus, electrophysiological abnormalities of stellate neurons may also contribute to defects in spatial recognition and contextual fear memory in PHF6 C99F knock-in mice. Beyond neurons in the entorhinal cortex, it will be important in future studies to explore the role of other populations of neurons and their networks in the pathogenesis of epilepsy in BFLS.

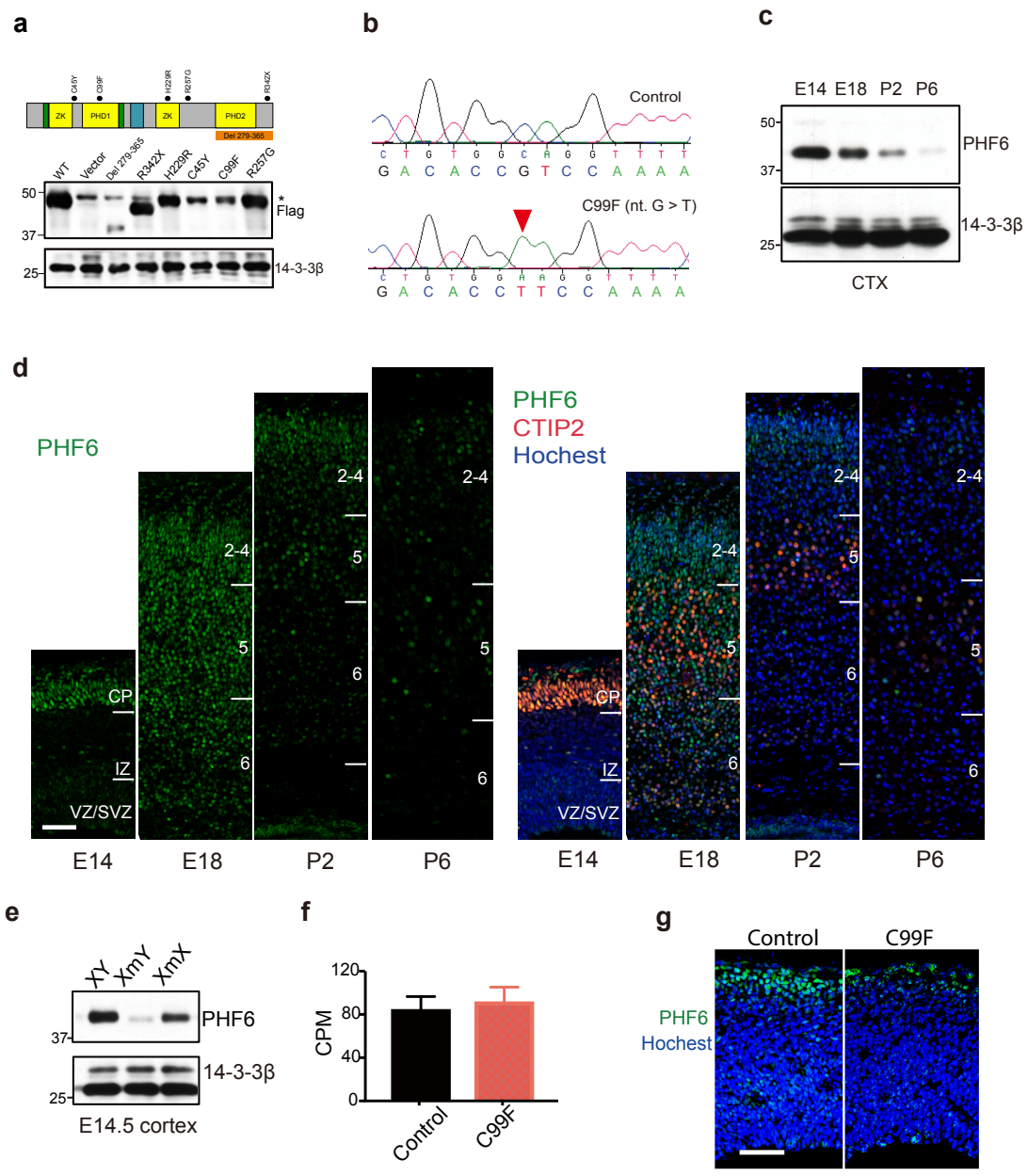

Figure 3. Generation of patient-specific PHF6 mutant mouse model of BFLS.

(a) (Top) Schematic of PHF6 is shown with patient-specific mutations in BFLS labeled with asterisks. Green indicates nuclear localization sequence; blue indicates nucleolar localization sequence. (Bottom) Lysates of 293T cells transfected with expression plasmids encoding FLAG and HA-tagged PHF6, the control vector or patient specific mutations of PHF6 were subjected to immunoblotting with the Flag antibody and an antibody to 14-3-3β, the latter serving as loading control.

(b) Sequencing traces of the wildtype and C99F PHF6 alleles.

(c) Lysates of the mouse cerebral cortex at embryonic day 14 (E14), E18, postnatal day 2 (P2) and P6 were subjected to immunoblotting with the PHF6 and 14-3-3β antibodies, the latter serving as loading control. PHF6 was highly expressed at E14 to E18, and declined postnatally.

(d) Sections of the cerebral cortex from mice at E14, E18, P2 and P6 were subjected to immunohistochemistry using the PHF6 antibody alone (left) or together with the CTIP2 antibody, which labels layer V/VI neurons, and the DNA dye bisbenzimide (Hoechst) (right). PHF6 was co-localized with CTIP2 at E14, and was ubiquitously expressed in all cortical layers at E18. Scale bar = 50 um

(e) Lysates of the cererbral cortex from control male, C99F male, and C99F heterozygote female mice were subjected to immunoblotting with the PHF6 and 14-3-3β antibodies. Levels of PHF6 protein were reduced in the cortex of male C99F mice.

(f) The levels of PHF6 mRNA in the cerebral cortex of control and C99F mice in RNA-seq analysis (n = 5) were not different. Data are presented as mean ± SEM.

(g) Sections of the cerebral cortex from E14.5 control and C99F mice were subjected to immunohistochemistry analyses using the PHF6 antibody and the DNA dye bisbenzimide (Hoechst). PHF6 expression was reduced in the cortical plate in C99F mice. Scale bar = 50 um.

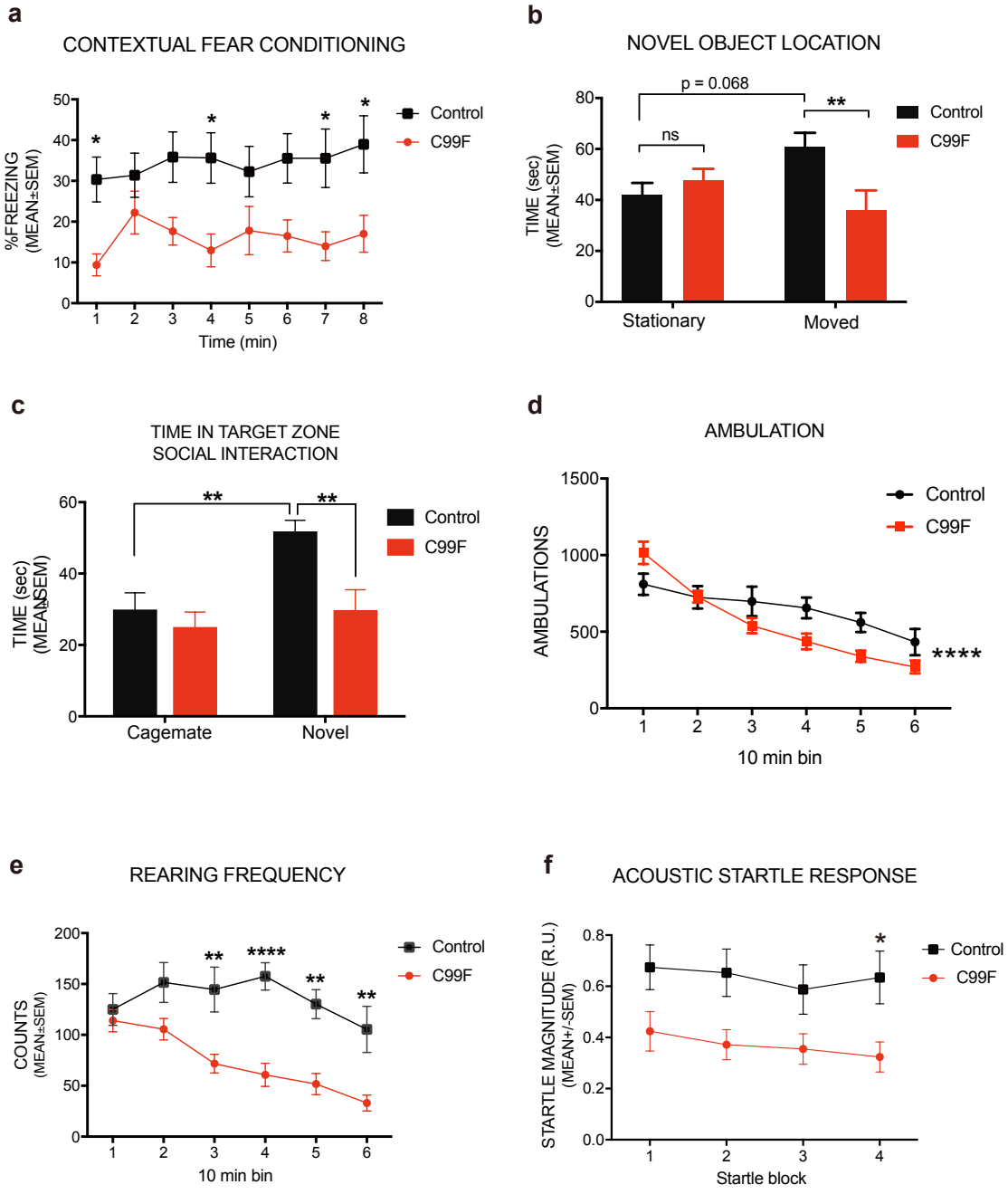

Figure 4. PHF6 C99F knock-in mice exhibit deficits in cognition, social interaction and emotionality.

(a) C99F mice (n = 12) and control littermates (n = 12) were evaluated on a contextual fear conditioning test where the C99F group exhibited significantly reduced freezing levels.

(b) Performance of control (n = 11) and PHF6 C99F knock-in mice (n = 11) was assessed on a novel object-location test. Control, but not C99F knock-in mice spent more time investigating

the object moved to a novel location.

(c) Sociability and preference for social novelty were evaluated in control (n = 12) and PHF6 C99F knock-in mice (n = 12) using the three- chambered social approach test. Control but not C99F mice spent more time investigating the novel mouse than cagemate mouse.

(d) PHF6 C99F knock-in mice (n = 12) displayed reduced ambulations compared to control (n = 12) in the 1-hour locomotor activity test.

(e) PHF6 C99F knock-in mice (n = 12) displayed reduced vertical rearing frequency compared to control (n = 12) in the 1-hour locomotor activity test.

(f) C99F knock-in mice (n = 12) displayed significantly reduced acoustic startle magnitudes compared to control littermate animals (n = 12).

*p<0.05, **p<0.01, ****p<0.0001 two-way repeated measure ANOVA, followed by pair-wise comparisons that were Bonferroni adjusted.

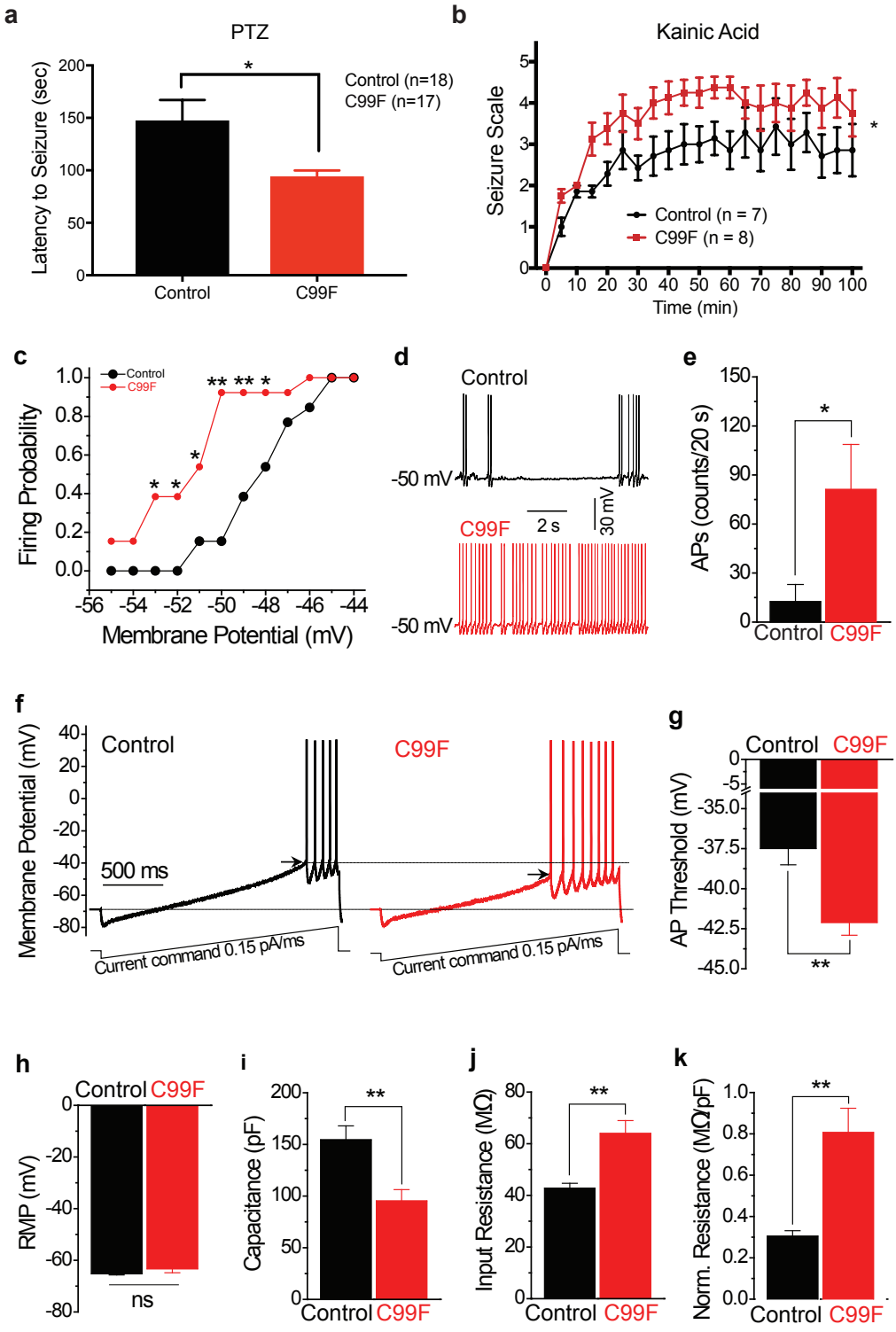

Figure 5. PHF6 C99F knock-in mice exhibit seizure susceptibility and increased neuronal excitability.

(a) Control littermate (n = 18) and PHF6 C99F knock-in mice (n = 17) were subjected to PTZ-induced seizures. Time to reach generalized seizure was recorded. PHF6 C99F knock-in mice showed reduced time to reach generalized seizure, unpaired t-test, *p<0.05.

(b) Control littermate (n = 7) and PHF6 C99F knock-in mice (n = 8) were subjected to seizure induction by kainic acid followed by Racine scale scoring of animal behavior every 5min for 100mins. PHF6 C99F knock-in mice reached higher Racine stage than control mice at earlier time points. Two-way repeated measure ANOVA, *p<0.05

(c) Current-clamped layer II stellate cells in acute slices of the entorhinal cortex were depolarized to different potentials (from -55 to -44 mV with a step of 1 mV) via automatic current injection to induce action potential (AP) firing. Stellate neurons in C99F knock-in mice had higher firing probability compared to control cells * p<0.05, ** p<0.01, Chi-square test within corresponding potentials.

(d) Sample traces of spontaneous AP firing recorded at -50 mV in control and C99F cells.

(e) AP firing rate was measured as a number of AP fired over a 20sec period. C99F cells had increased AP firing rate. *p<0.05, t-test.

(f) APs were evoked by a ramp current injection (0.15 pA/ms, lower traces). Representative AP traces are shown (upper traces). Only the first AP was used to estimate the AP threshold (arrows).

(g) Summary of the data in (f) reveated that AP threshold is decreased in C99F mice. C99F cells had reduced AP threshold. **p<0.01, t-test.

(h) Average rest membrane potential (RMP) in control and C99F cells were not different.

(i) Membrane capacitance in C99F cells were reduced compared to control cells.

(j) Input resistance in C99F cells were increased compared to control cells.

(k) Capacitance-normalized input resistance in C99F cells were increased compared to control cells.

**p<0.01, t-test. Unless specified, data are presented as mean ± SEM.

Supplemental Figures

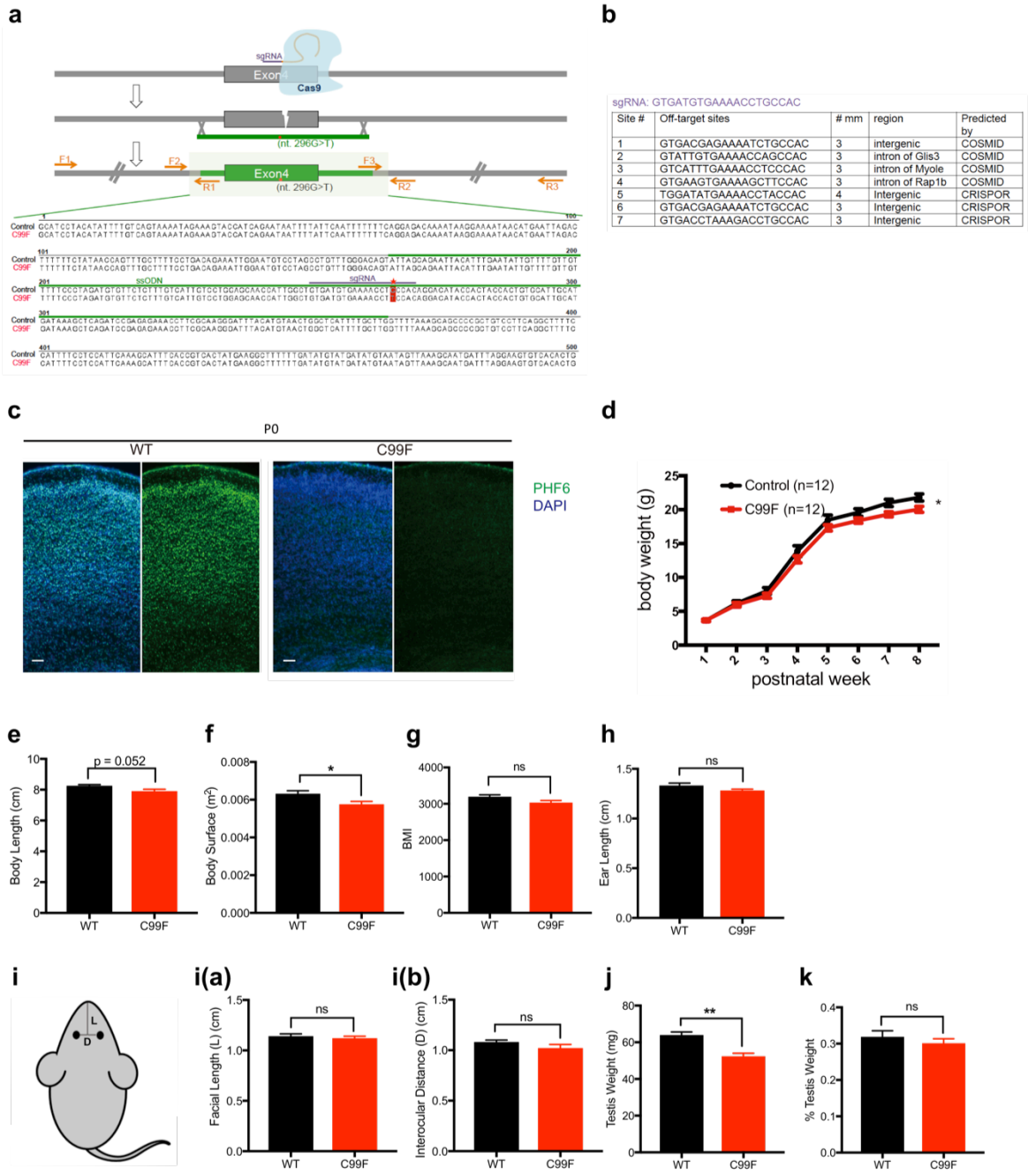

Figure S1. Validation of PHF6 C99F knock-in mice.

(a) Schematics of PHF6 C99F knock-in mouse generation using CRISPR-Cas9 technology. Primers labeled in yellow were used for Sanger sequencing to detect potential off-target mutation. No off-target mutation was detected.

(b) Potential off-target sites in the genome predicted by COSMID and CRISPROR were subjected to Sanger Sequencing and no mutations were detected.

(c) Sections of the cerebral cortex from control and C99F knock-in mice at postnatal day 0 (P0) were subjected to immunohistochemistry using PHF6 antibody and the DNA dye bisbenzimide (Hoechst). PHF6 expression was reduced in the cortical plate in C99F mice. Scale bar = 50um.

(d) Body weight of PHF6 C99F mice (n = 12) was slightly reduced compared to control littermate mice (n = 12). Data are presented as mean ± SEM. Two-way repeated measure ANOVA, *$p<0.05$.

(e-f) PHF6 C99F knock-in mice has slightly reduced body length (e) and body surface (f) compared to control.

(g-i) No differences in BMI (g), ear length (h), facial length and interocular distance (i) between C99F and control.

(j-k) No differences in normalized testicular weight between C99F and control.

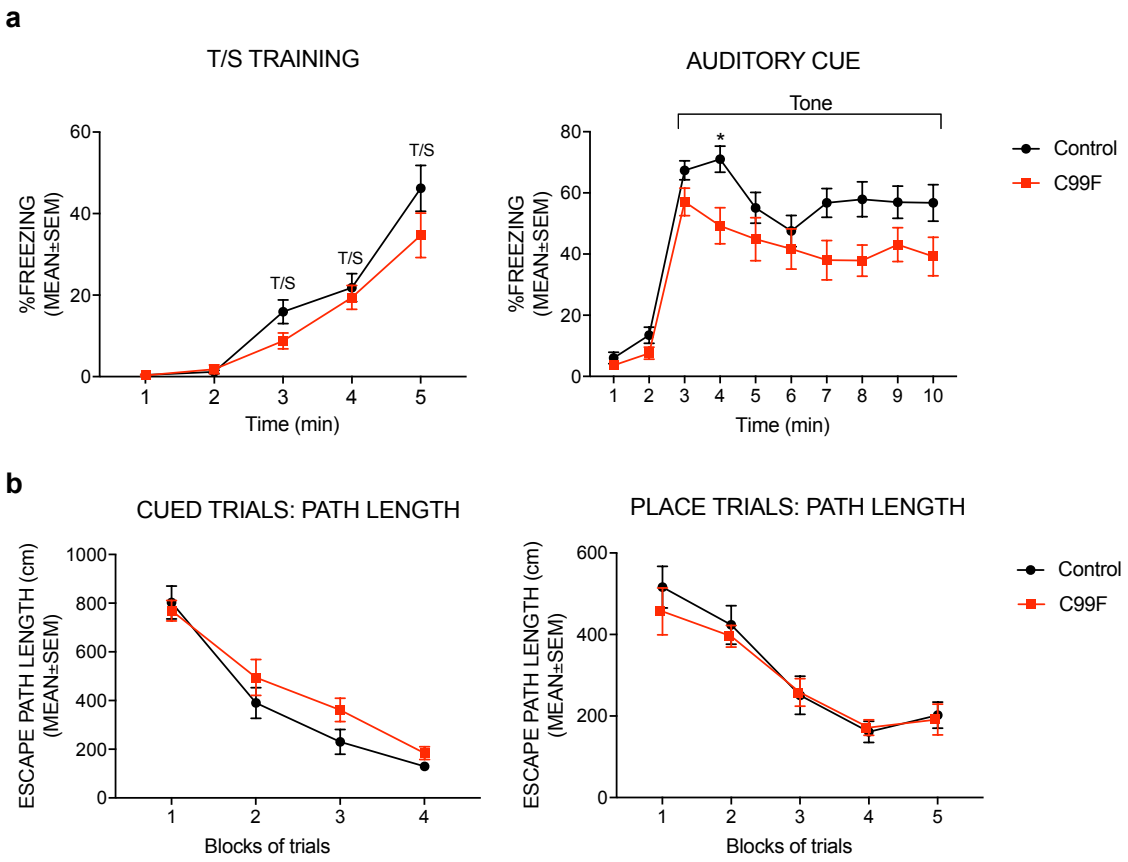

Figure S2. Behavior phenotyping of PHF6 C99F knock-in mice.

(a) Control (n = 12) and PHF6 C99F knock-in mice (n = 12) were tested on the conditioned fear procedure. (Left panel): Freezing levels were not found to be different during either the 2-min baseline period or during tone-shock (CS-US) training on day 1. (Right panel): Freezing levels were also observed to be similar during the 2-min altered context baseline on day 3, although the C99F knock-in mice displayed reduced freezing response compared to controls during the auditory cue test.

(b) No performance differences were observed between the C99F knock-in (n = 12) and control (n = 12) groups for the cued or place (spatial learning) trials in the Morris water maze.

Two way repeated measure ANOVA, followed by pair-wise comparisons that were Bonferroni adjusted. *p <0.05. Data are presented as mean ± SEM.

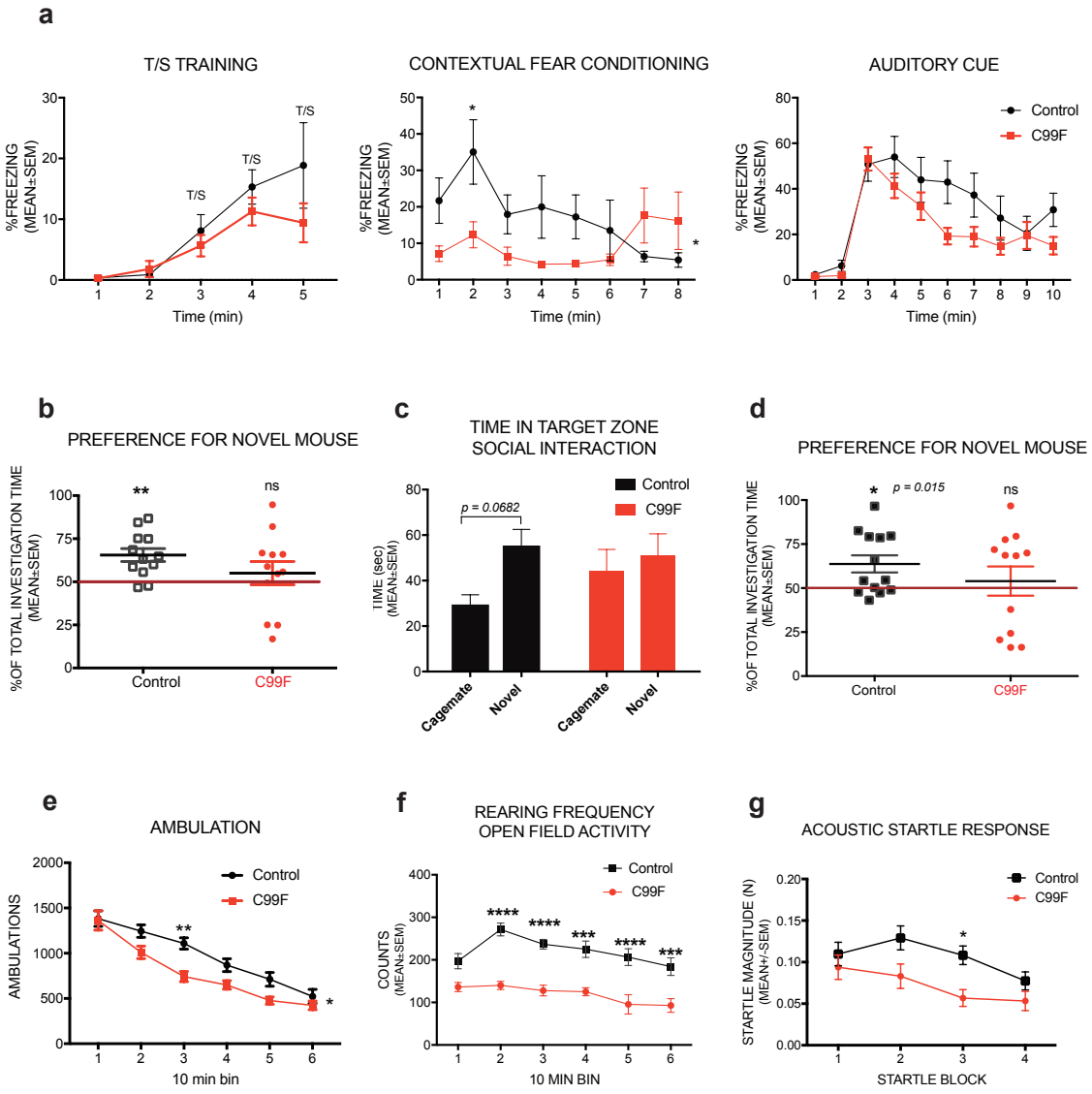

Figure S3. Additional cohort of C99F knock-in mice show deficits in cognition, social interaction and emotionality.

(a) (Left panel) Testing the control (n = 11) and PHF6 C99F knock-in mice (n = 11) on the conditioned fear procedure revealed that the two groups displayed similar freezing levels during the 2-min baseline and tone-shock training periods on day 1. (Middle panel) The C99F knock-in mice exhibited reduced freezing levels during the contextual fear test (genotype x minutes interaction: $F(7,140) = 4.34$, $p = 0.014$), particularly during the first two minutes of the test session. (Right panel) Although the C99F knock-in mice generally displayed lower freezing levels compared to controls, no significant overall effects involving genotypes were found for the auditory cue data.

(b) The percentage of time control mice, but not *PHF6* C99F knock-in mice from the first cohort, interacted with the novel mice was significantly above chance (**p<0.01, one sample t-test).

(c) Control mice (n = 13), but not C99F knock-in mice (n = 12) from the second cohort displayed a increasing trend

in time spent for investigating a novel mouse than a cagemate.

(d) The percentage of time control mice, but not *PHF6* C99F knock-in mice from the second cohort, interacted with the novel mice was significantly above chance (**p<0.01, one sample t-test).

(e) PHF6 C99F knock-in mice (n = 12) displayed reduced ambulatory activities compared to control (n = 13) in the open field test.

(f) PHF6 C99F knock-in mice (n = 12) displayed reduced rearing frequency compared to control (n = 13) in the open field test.

(g) C99F knock-in mice (n = 12) displayed reduced acoustic startle response compared to control littermate animals (n = 13).

*p<0.05, ***p<0.001, ****p<0.0001, unless specified, two-way repeated measures ANOVA, followed by pair-wise comparisons that were Bonferroni adjusted were used for statistical analysis. Data are presented as mean ± SEM.

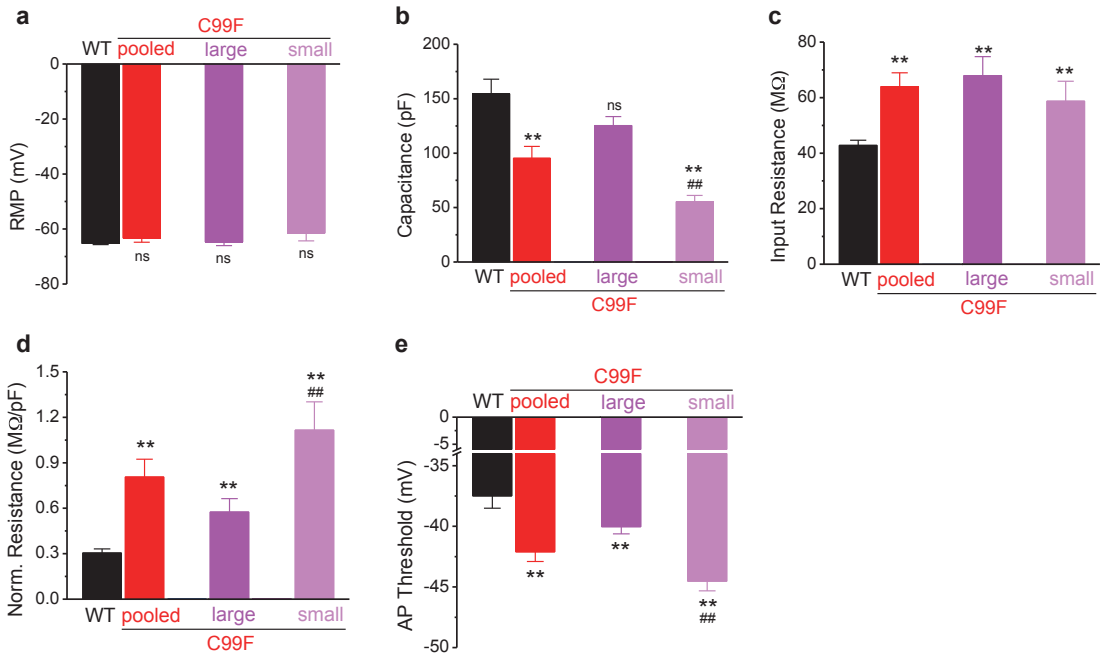

Figure S4. Altered intrinsic membrane properties and AP threshold in two subpopulations of stellate cells in C99F mice.

Stellate cells in KI mice were subdivided in two size groups according to cell capacitance (small size and large size groups).

(A-E) Altered intrinsic membrane properties cannot be attributed to changes in cell size in KI mice. No detectable changes in RMP were observed in either subgroup (A). Increased input resistance (C,D) and decreased AP threshold (E) were observed in both groups in KI mice, although a significant decrease in membrane capacitance was observed only in small size group (B). ns, not significant, ** $P<0.01$ for KI vs WT; $^{\#\#}$ $P<0.01$ for small vs large C99F groups.

Material and Methods

Plasmids

PHF6 patient mutations del 279-365, R342X, H229R, C45Y, C99F, C305X and R257G were generated using site-directed mutagenesis and subcloned into the pHAGE-NTAP vector.

Animals

Rodents were maintained under pathogen-free conditions. All animal experiments were done according to protocols approved by the Animal Committee of Washington University School of Medicine and in accordance with the National Institutes of Health guidelines.

Target specific sgRNAs (5'-GTGATGTGAAAACCTGCCAC-3') were cloned into BbsI digested plasmid pX330 (addgene # 42230) and sgRNA cleavage activity was validated in vitro by transfecting NIH3T3 cells, followed by T7E1 assay (NEB). T7 sgRNA and Cas9 templates for in vitro transcription were pcr amplified, gel purified, and in vitro transcribed with the MEGAshortscript T7 kit (sgRNA, Life Technologies) or the T7 mMessage mMachine Ultra kit (Cas9, Life technologies). After transcription, both RNAs were purified with the Megaclear kit (Life Technologies). A 200nt ssODN donor DNA with the mutation(s) centered within the oligo was synthesized by IDT as an ultramer oligo. Injection concentrations were: 50ng/ul Cas9, 25ng/ul gRNA, 100ng/ul ssODN. All animal experiments were approved by institutional IACUC protocols. B6/CBA F1 mice at 3-4 weeks of age (JAX Laboratories, Bar Harbor ME, USA) were superovulated by intraperitoneal injection of 5 IU pregnant mare serum gonadotropin, followed 48h later by intraperitoneal injection of 5 IU human chorionic gonadotropin (PMS from SIGMA, HGC from Millipore USA). Mouse zygotes were obtained by mating B6/CBA stud males with superovulated B6/CBA females at a 1:1 ratio. One-cell fertilized embryos were injected into the pronucleus and cytoplasm of each zygote. Microinjections and mouse transgenesis experiments

were performed as described previously (Behringer et al., 2014). Our founder animals that were mosaic for the nt.296G > T (p.C99F) missense mutation and nt. 298insG frameshift mutation using a pyrosequencing. Two mutation alleles were segregated in F1 generation, and their genotypes were confirmed with Sanger sequencing. Based on detailed molecular characterization, we confirmed nt. 298insG line is a null.

Antibodies

Antibodies include PHF6 (Novus biological, NB100-68262), Ctip2 (Abcam ab18465), 14-3-3β (Santa Cruz, sc-1657), Flag (Sigma f7425).

Immunohistochemistry

The brain from mice at distinct ages were fixed with 2% PFA and 4% sucrose and subjected to cryosectioning. Sections were blocked with blocking buffer (10% goat serum, 3% BSA, and 0.4% Triton-X in PBS), and subjected to immunofluorescence analyses with rabbit anti-PHF6 and/or rat anti-CTIP2. The DNA dye bisbenzimide (Hoechst 33258) was used to label cell nuclei. Confocal images were acquired with Olympus FV1200 with identical scanning configurations for all samples in the same experiment.

One-hour locomotor activity and open-field behavior test

Mice in cohorts 1 and 2 were evaluated over a 1-h period in transparent enclosures as previously described (Dougherty et al., 2013). Each cage was surrounded by a frame containing a 7 × 15 matrix of photocell pairs, the output of which was fed to an on-line computer (Kinder Scientific, LLC, Poway, CA). The system software was used to define a 33 × 11 cm central zone and a

peripheral or surrounding zone that was 5.5 cm wide with the sides of the cage being the outermost boundary. In cohort 3, ambulatory activity and exploratory behaviors of the C99F and control mice were quantified (Wozniak et al., 2013) over a 1-h period in an open-field (41×41×38.5 cm high) constructed of Plexiglas, which utilized computerized photobeam instrumentation that included a frame containing a 16×16 matrix of photocell pairs surrounding the apparatus. Total ambulations (whole body movements) and vertical rearing frequency were computed using system software (Kinder Scientific, LLC) and were analyzed for both tests.

Conditioned fear

Mice were trained and tested using two clear-plastic conditioning chambers (26×18×18 cm high) (Med-Associates, St. Albans, VT) easily distinguished by different olfactory, visual, and tactile cues present in each chamber as described (Wozniak et al., 2007). On day 1, each mouse was placed into the conditioning chamber for 5 min and freezing behavior was quantified using FreezeFrame image analysis software during a 2 min baseline period. After baseline measurements, a conditioned stimulus (CS) consisting of an 80 dB tone (white noise) was presented for 20 seconds followed by an unconditioned stimulus (US) consisting of a 1 s, 1.0 mA continuous foot shock. This tone-shock (T/S) pairing was repeated each minute over the next 2 min, and freezing was quantified after each of the three tone-shock pairings. Twenty-four hours after training, each mouse was placed back into the original conditioning chamber to test for fear conditioning to the contextual cues in the chamber. Twenty-four hours later, each mouse was placed into the other chamber containing distinct cues. Freezing was quantified during a 2 minutes "altered context" baseline period as well as over a subsequent 8 min period during which the auditory cue (CS) was presented. Shock sensitivity was evaluated following completion of the conditioned fear test, which involved determining shock levels that elicited flinching, escape-related behaviors and vocalization.

Novel object and novel location recognition

Using a previously published protocol (Brown et al., 2010), each mouse was habituated to the test chamber over two days and on the following day given two sample trials and two test trials. For novel object recognition, a sample trial consisted of placing a mouse in the familiar arena that contained two copies of the same object and allowing it to explore for 10 min, and then returning it to its home cage. A 10-min test trial was conducted following a 50-min delay, when a mouse was placed back into the test arena, where a novel object was presented along with the copy of the familiar object used during the sample trial. Fifty minutes later, another 10-min sample trial was administered in which two new novel objects were placed in opposite corners of the arena. Mice were again returned to their home cage for a 50 min delay, then placed back into the test arena where one of the objects had been moved to a novel location. The amount of time each animal spent actively investigating the objects was manually scored and the investigation times for the novel versus the familiar object (or locations) were analyzed as a measure of recognition memory.

Social Approach

Sociability and preference for novel social interactions were evaluated in a rectangular apparatus divided into three chambers each measuring 19.5cm x 39cm x 22 cm according to previously published methods (Dougherty et al., 2013). Two small stainless steel withholding cages (Galaxy Pencil/Utility Cup, Spectrum Diversified Designs, Streetsboro, OH) were used to prevent contact between test and stimulus mice with one being placed in each outer chamber. Test sessions were recorded using a digital camera connected to a PC and scored using the ANY-maze (Stoelting, Co, Wood Dale, IL) software program. Time spent, distance traveled, entries into, and latency to enter each chamber and the investigation zones around the holding cages were analyzed. Each test session contained five consecutive, 10-min trials, with the first two trials being dedicated to habituation to the apparatus without stimulus animals present followed by three test trials. After habituation, sociability exhibited toward a novel stimulus mouse versus a familiar, empty withholding cage was assessed in the first test trial by placing an unfamiliar, gender-matched

stimulus mouse in one withholding cage while the other was left empty, and the test mouse was allowed to freely explore the apparatus and investigate the novel mouse in the withholding cage. For the second test trial, a gender-matched cagemate was placed in one withholding cage while the other remained empty, and the test mouse could freely explore the apparatus and investigate the cagemate in the withholding cage. During the third test trial, the familiar cagemate remained in the withholding cage, although a new, unfamiliar gender-matched stimulus mouse was now placed in the other withholding cage, and the test mouse was allowed to explore the apparatus and investigate the two mice contained in the withholding cages. Entries, latency to enter, and time spent in each chamber and investigation zone were recorded for each mouse.

Acoustic startle response/prepulse inhibition

Sensorimotor reactivity and gating were evaluated in the mice by quantifying the magnitude of their acoustic startle (ASR) and PPI responses (Hamilton Kinder, LLC) as previously described (Yuede et al., 2010). In the first cohort, a startle response to a 120 dB auditory stimulus pulse (40 ms broadband burst) and PPI (response to a prepulse plus the startle pulse) were measured concurrently in mice. Beginning at stimulus onset, 1 ms force readings were averaged to obtain an animal's startle amplitude. A total of 20 startle trials were presented over a 20 min test period during which the first 5 min served as an acclimation period when no stimuli above the 70 dB white noise background were presented. The session began and ended by presenting 5 consecutive startle (120 db pulse alone) trials unaccompanied by other trial types. The middle 10 startle trials were interspersed with PPI trials (consisting of an additional 30 presentations of 120 dB startle stimuli preceded by pre-pulse stimuli of either 4, 12, or 20 dB above background (10 trials for each PPI trial type). A percent PPI score for each trial was calculated using the following equation: %PPI = 100*(ASRstartle pulse alone - ASRprepulse+startle pulse)/ASRstartle pulse alone Another cohort was tested using an upgraded instrumentation system (Kinder Scientific, LLC), and a slightly modified protocol. This involved evaluating startle responses to increasing sound pressure levels (80 to 110 dB), as well as the startle

response to 120 dB collected over 20 trials as described above. Pre-pulse levels tested in this cohort were 4, 8, and 16 dB above background, and PPI was calculated using the same equation.

Morris Water Maze Test

Reference memory was evaluated in the mice using the Morris Water Maze navigation test similar to previously published procedures (Wozniak et al., 2004). The protocol included cued (visible platform), place (submerged, not visible platform), and probe trials (platform removed). Testing took place in a round pool (118 cm diameter) containing water made opaque with non-toxic white tempura paint. All trials were monitored through a live video feed by computer software (Any-maze, Stoelting Co., Wood Dale, IL) which calculated swim speed, escape path length, escape latency, and time and distance spent in each of the four quadrants of the pool. The maximum score for all water maze trials was 60 s. Cued trials were conducted first to determine if nonassociative deficits (e.g., visual or sensorimotor disturbances, or alterations in motivation) were likely to affect swimming performance and confound interpretation of the acquisition data collected during the place trials. Mice received 4 cued trials per day for 2 consecutive days. Mice were placed in the quadrant directly opposite a submerged platform marked with a visible cue. The platform was moved to a different location for each trial within a day and there were very few distal cues available during this time, both of which limited spatial learning. Escape path length and latency and swimming speeds were used to evaluate performance during the cued and place conditions. Place trials were performed following the cued trials. Stationary distal cues to facilitate learning were placed around the room and mice were evaluated on their ability to learn the location of a hidden, unmarked platform. Four place trials per day were administered for 5 consecutive days during which the platform remained in the same location for all trials. The mice were released from 4 different locations each day. The daily protocol involved administering 2 sets of 2 trials each, with sets being separated by approximately 1 hr. A single probe trial was administered approximately 1 hr after completion of place trials on the fifth

day. During the probe trial, the platform was removed from the pool and the animals placed in the quadrant directly opposite the former platform location. Mice were allowed to explore for 60 s during which time various aspects of their search behaviors for the platform were quantified. The number of times a mouse passed directly over the platform location (platform crossings), the time spent in the target quadrant that had contained the platform, and spatial bias (preference for the target quadrant compared to other quadrants) were used to evaluate retention performance during the probe trial.

Seizure induction

Pentylenetetrazole (Sigma) dissolved in 0.9% saline was injected intraperitoneally (75mg/kg) into 5-7 month old mice as described (Zhang and Wong, 2012). Mice then were placed individually into cages for observation. A trained blinded observer performed the experiment. Generalized seizure was characterized by sudden loss of upright posture with diffuse tonic posturing followed by clonic shaking. The time to the generalized seizure was recorded for each mouse.

Kainic acid (Sigma) dissolved in the 0.9% saline was injected intraperitoneally (25mg/kg) into 5-7 month old mice. Mice then were placed individually in cages for observation and only two mice were simultaneously observed. Mouse genotypes were blinded from the experimenter. The Racine scale was used to score seizure progression in mice as described (Racine, 1972). A score of 1 was assigned when mice displayed absence-like immobility and oro-alimentary movements. Mice received a score of 2 for hunching with facial or manual automatisms and head bobbing. Mice scored 3 rearing with facial or manual automatisms and forelimb clonus, and achieved a score of 4 with repeated rearing with continuous forelimb clonus and falling. Score of 5 was assigned if mice displayed generalized tonic-clonic seizure with lateral recumbence or jumping. Death was also scored as 5. Mice were scored every five-minute for 100 minutes.

Electrophysiology

Animals and slice preparation

Electrophysiological recordings were conducted blind to genotype. Slices were prepared as described (Deng and Klyachko, 2016). In brief, 18-23-day-old male mice were used. After deep anesthesia with CO_2, mice were decapitated and the brain was dissected out in ice-cold saline containing (in mM): 130 NaCl, 24 $NaHCO_3$, 3.5 KCl, 1.25 NaH_2PO_4, 0.5 $CaCl_2$, 5.0 $MgCl_2$, and 10 glucose, pH 7.4 (saturated with 95% O_2 and 5% CO_2). Horizontal brain slices (350 μm) including the entorhinal cortices were cut using a vibrating microtome (Leica VT1100S). Slices were initially incubated in the above solution at 35°C for 1 h for recovery and then kept at room temperature (~23°C) until use. All animal procedures were in compliance with the US National Institutes of Health Guide for the Care and Use of Laboratory Animals, and conformed to Washington University Animal Studies Committee guidelines.

Action potential recording and threshold determination

Whole-cell patch-clamp recordings using a Multiclamp 700B amplifier (Molecular Devices) in current-clamp mode were made from stellate cells of EC superficial layers visually identified with differential interference contrast optics (Olympus BX51WI). Current-clamp recordings were made with pipette capacitance compensation and bridge-balance compensation. Stellate cells were identified according to morphology and electrophysiological properties as described (Deng et al., 2007). All recordings were conducted at near-physiological temperature (33–34°C). The recording electrodes were filled with (in mM): 130 K-gluconate, 10 KCl, 0.1 EGTA, 2 $MgCl_2$, 2 $ATPNa_2$, 0.4 GTPNa, and 10 HEPES, pH 7.3. The extracellular solution

contained (in mM): 125 NaCl, 24 $NaHCO_3$, 3.5 KCl, 1.25 NaH_2PO_4, 2 $CaCl_2$, 1 $MgCl_2$, and 10 glucose, pH 7.4 (saturated with 95% O_2 and 5% CO_2).

For neuronal excitability measurements, cell membrane potential was set to given potentials (-55 to -44 mV with 1-mV step) through automatic current injection. Action potential (AP) firing probability and the number of APs within 20s was averaged from 4-5 trials for each cell. For AP threshold determination, APs were evoked by a ramp current injection (0.15 pA/ms) (Deng and Klyachko, 2016; Yamada-Hanff and Bean, 2013) with a hyperpolarizing onset to ensure maximal Na^+ channel availability before the 1st AP. The threshold was defined as the voltage at the voltage trace turning point, corresponding to the first peak of 3rd order derivative of AP trace (Deng and Klyachko, 2016). Ramp current-evoked AP threshold was then defined as the mean threshold of the first AP in the train averaged over 5-8 trials.

Determination of resting membrane potential, capacitance and input resistance

Resting membrane potential (RMP) was measured immediately after whole-cell formation. Cell capacitance was determined by the amplifier's auto whole-cell compensation function with slight manual adjustment to optimize the measurement if needed. The obtained values then were used for input resistance normalization. In current-clamp mode, a negative current (−50 pA for 500 ms) was injected every 5 s to assess the input resistance.

Acknowledgements

The authors thank Chi Zhang for providing plasmids for the study, Anna Oldenberg for initial maintainance of the mouse line, and members of the Bonni laboratory for helpful discussions. This work was supported by the National Institutes of Health grant NS088378 (to A.B.), NS081972 (to V.A.K.), Washington University intellectual and developmental disabilities research center (IDDRC) NIH U54 HD087011, the mouse genetics core, the Hope center transgenic vectors core, Washington University center for cellular imaging (WUCCI).

Chapter 3: The Genome-Wide Function of PHF6 in regulating gene expression during cortical development

Adapted from:

Characterization of A Mouse Model of Börjeson-Forssman-Lehmann Syndrome

Cheng Cheng, Pan-yue Deng, Yoshiho Ikeuchi, Carla Yuede, Daofeng Li, Nicholas Rensing, Ju Huang, Dustin Baldridge, Susan E Maloney, Joseph D Dougherty, John Constantino, Arezu Jahani-Asl, Michael Wong, David Wozniak, Ting Wang, Vitaly Klyachko, Azad Bonni

In revision September, 2018

ABSTRACT

PHF6 is a plant homeodomain finger protein implicated in X-linked intellectual disability disorder Börjeson-Forssman-Lehmann syndrome (BFLS). PHF6 is located in the nucleus and might regulate transcription. How PHF6 functions in the nucleus and its relevance to BFLS remains unclear. We generated PHF6 knockout and C99F knock-in mice using CRISPR-Cas9 technology. We discovered the molecular function of PHF6 in regulating gene expression in the developing cortex. Transcriptomic analysis of the cerebral cortex in C99F knock-in mice and PHF6 knockout mice show that PHF6 promotes the expression of neurogenic genes and concomitantly suppresses the expression of synaptic genes, suggesting that PHF6 may maintain neurons in an immature state and knockout of PHF6 leads to precocious differentiation. Interestingly, PHF6-regulated genes are overrepresented in gene signatures and modules that are deregulated in the brain of patients with autism spectrum disorders. Our findings advance our understanding of the mechanisms underlying BFLS pathogenesis and may suggest a potential link between BFLS and autism spectrum disorders.

INTRODUCTION

PHF6, in plant homeodomin zinc finger protein (PHD) family, is a 365 amino acid protein that contains two PHD-like zinc fingers and nuclear and nucleoli localization sequences. PHD-like zinc fingers are often found in components of chromatin remodeling proteins as epigenetic readers that interact with modified histones. Therefore, PHF6 is often regarded as a transcriptional regulator.

Mutations in PHF6 have been implicated in syndromic form of X-linked intellectual disability, Börjeson-Forssman-Lehmann syndrome (BFLS). Most of the mutations identified in BFLS patients are missense mutation leading to single amino acid change (Lower et al., 2002, Gecz et al., 2006). These mutations are distributed across the PHF6 gene. Some mutations in PHF6 lead to decreased protein level, suggesting that BFLS may result from hypomorphic PHF6 function. How do these mutations regulate gene expression compared to a null allele, and what is the residual function of the mutant allele has yet to be discussed.

PHF6 protein is localized in the nucleus and interacts with the PAF1 transcription elongation factor complex, NuRD chromatin remodeling complex, and upstream binding factor UBF1 (Liu et al., 2014b; Todd et al., 2015; Zhang et al., 2013). In the leukemia biology, PHF6 regulates chromatin accessibility to lineage-specific transcription factors. PHF6 promotes genes involved in B-cell development and represses genes involved in T-cell signaling. And loss of PHF6 leads to a lymphoma with mixed-lineage in vivo (Feliciano et al., 2017)
. In the nervous system, knockdown of PHF6 in the mouse cerebral cortex impairs the migration of cortical neurons, leading to white matter heterotopias (Zhang et al., 2013), suggesting a role for PHF6 in the regulation of cortical neuron positioning. Accordingly, PHF6 is thought to regulate transcription in neurons (Zhang et al., 2013). How PHF6 regulation of gene expression, particularly at a genome-wide level, impacts BFLS pathogenesis remains incompletely understood.

In this study, we report the first patient-specific PHF6 mutant mouse model of BFLS and a whole body knockout mouse of PHF6. Genome-wide RNA-seq analyses of the cerebral cortex

in PHF6 C99F and PHF6 knockout mice show that PHF6 promotes the expression of neurogenic genes and concomitantly suppresses the expression of synaptic genes. PHF6-regulated genes are overrepresented in autism spectrum disorder (ASD) relevant gene signatures including gene modules that are misregulated in the brain of ASD patients. Consistently, we have identified an ASD patient with an underlying PHF6 missense mutation. Collectively, our findings broaden our understanding of the cellular and molecular underpinnings of BFLS pathogenesis, and may suggest a potential link between BFLS and ASD.

RESULST

PHF6 regulates neurogenic and synaptic genes during brain development

Having identified PHF6 C99F knock-in mice as a novel model of BFLS, we next characterized the mechanism by which PHF6 deficiency might contribute to BFLS pathogenesis. Due to PHF6's putative transcriptional role, we subjected the cerebral cortex from P0 PHF6 C99F mice and control littermate to RNA-seq analyses. Surprisingly, the expression of only 48 genes was altered in PHF6 C99F mice with false discovery rate (FDR)<0.05 in EdgeR analyses. Because the C99F mutation leads to substantial but incomplete downregulation of PHF6 protein (Figure 1e), the presence of residual PHF6 protein in these mice might not allow detection of robust transcriptional changes. Fortuitously, in the process of generating the C99F allele, a nucleotide insertion adjacent to the Cas9 cleavage site was also obtained, leading to a frameshift mutation and consequent knockout of PHF6 in mice (Figure S5a-b). Unlike the C99F knock-in mice, PHF6 knockout (KO) animals died perinatally. Consisent with the prediction that PHF6 KO mice might provide a more robust means for identification of PHF6-regulated genes, the expression of 193 genes was significantly altered (FDR<0.05 in EdgeR) in the cerebral cortex of PHF6 KO mice compared to control littermate animals (Figure 6a). Transcriptomic analysis using DEseq2 showed that 87.5% differentially expressed genes upon PHF6 KO overlapped with those obtained by EdgeR analyses (Figure S5d-e). Notably, alterations in gene expression in the cerebral cortex upon PHF6 KO with FDR<0.05 correlated significantly with changes in their expression in PHF6 C99F mice (Figure 6b), supporting the interpretation that the C99F mutation may act as hypomorphic allele in the regulation of gene expression. In control permutation analyses, the observed r=0.48 was highly significant compared to 10,000 random samplings of 193 gene pairs in PHF6 KO and C99F mice ($p = 8.5e-8$) (Figure 6c). Additionally, significantly downregulated and upregulated genes upon PHF6 KO (FDR<0.05) were also downregulated and upregulated, respectively, in PHF6 C99F mice (Figure 6d). We therefore focused subsequent analyses on deregulated genes in the cerebral cortex of PHF6 KO mice.

Using the dataset that contains genes enriched in major brain cell types (Zeisel et al., 2015), we found that PHF6-regulated genes were enriched in interneurons and excitatory neurons (Figure 6e) but not in glia cells, suggesting that PHF6-regulated genes are represented in neurons. In DAVID gene ontology (GO) analyses, genes encoding potassium transport, terminal bouton, and synapse proteins were found among upregulated genes, whereas genes encoding developmental, zinc finger, and cell differentiation proteins were found among downregulated genes in the cerebral cortex of PHF6 KO mice (Figure 6f). These analyses suggest that PHF6 promotes the expression of differentiation genes and concomitantly suppresses the expression of synaptic genes in the cerebral cortex.

We next characterized the developmental expression pattern of PHF6-regulated genes in the human brain, using the available developing human brain transcriptome dataset-BrainSpan (BrainSpan, 2013). PHF6 mRNA was significantly downregulated beginning at post-conceptual week 8 (pcw8) during human brain development in the ventral frontal cortex (VFC) (Figure S5c), mimicking its expression pattern in mice. In contrast, doublecortin (DCX) was upregulated from pcw8 to pcw24 and subequently downregulated (Figure S5c). Importantly, the expression of genes upregulated upon PHF6 loss steadily increased throughout human development from pcw8 to 40 years of age in the VFC, similar to the expression pattern of genes for chemical synaptic transmission (Figures 6g-i). Concomitantly, genes downregulated upon PHF6 loss had high level of expression at early time points during human brain development but steadily declined starting at pcw8, displaying a similar pattern as genes encoding neurogenesis (Figures 6g-i). Similar results were observed in other brain regions including the dorsal frontal cortex (DFC), medial frontal cortex (MFC), and primary somatosensory cortex (S1C) (Figure S5d). Similar developmental expression patterns were observed for upregulated and downregulated genes upon PHF6 loss identified using DEseq2 analyses (Figure S5d-e). Together, our data suggest that PHF6 maintains neurons in an immature state and that PHF6 loss may lead to premature downregulation of neurogenic genes and activation of synaptic genes (Figure 7).

Transcriptomic comparisons between PHF6 knockout and C99F knock-in mice

Having established that genes altered in PHF6 KO and C99F mice were mildly correlated, we further characterized the relationship between PHF6 KO and C99F based on gene expression. We reasoned that the commonly regulated genes in both PHF6 KO and C99F might represent the genes involved in the disease pathogenesis, whereas the uncorrelated genes between PHF6 KO and C99F were genes that are deregulated specifically in PHF6 knockout. We therefore separated the 193 genes misregulated genes into two groups using arbitrary log fold change cut off of Log2 = 0.2. From the genes that were significantly changed upon PHF6 knockout, we focused on the genes that were also altered by at least 1.15 fold in PHF6 C99F with the same direction of change. With this cut off, genes could be divided into two groups, KO-KI common genes, containing genes that were highly correlated between PHF6 KO and C99F ($r = 0.72$); and KO-specific genes with genes uncorrelated between PHF6 KO and C99F ($r = 0.22$) (Figure 8a-b). In the KO-KI common gene group, the downregulated genes upon PHF6 KO were dramatically downregulated in PHF6 C99F, and the upregulated genes upon PHF6 KO were largely upregulated in PHF6 C99F (Figure 8b, d). In addition, KO-specific genes represent a large proportion of genes deregulated upon PHF6 loss compared to KO-KI common genes (Figure 8c), suggesting that the majority of the genes deregulated upon PHF6 knockout were not represented in PHF6 C99F mice.

To further characterize the biological function of the KO-specific and KO-KI common genes, we performed gene ontology analysis. Interestingly, KO-specific genes shared almost the same terminologies with all deregulated genes upon PHF6 knockout (Figure 9a). We asked whether precocious differentiation phenotype discovered from 193 deregulated genes (in PHF6 KO) were also represented by KO-specific genes. The downregulated and upregulated KO-specific genes were therefore analyzed across human developing brains using Brainspan dataset. Strikingly, similar developmental pattern was found using KO-specific genes as with 193 misregulsted genes (Figure 6h, 9c). In contrast, KO-KI common genes shared terminologies

including cell spreading, signaling and cilia (Figure 9b). These genes did not recapitulate the developmental pattern observed from KO-specific genes (Figure 9c). These data suggest that precocious differentiation identified from 193 deregulated genes upon PHF6 knockout could be the characterized by the KO-specific genes alone, and thus a potential KO-specific phenotype. However, KO-KI commonly regulated genes were not involved in maturation. To strength this observation, we loosened the FDR threshold of the differentially expressed genes in PHF6 C99F by FDR<0.2, the average gene expression was also not altered (data not shown). Taken together, these data suggest that PHF6 C99F harbor hypomorphic function of PHF6. Consistent with this finding, the density of dendritic spines in layer II stellate neurons in the entorhinal cortex did not appear to increase prematurely in PHF6 C99F mice (Figure S5i-j). These data again strengthen the hypothesis that PHF6 C99F may not lead to precocious differentiation of neurons.

PHF6-regulated genes are implicated in neurodevelopmental disorder of cognition

Because *PHF6* mutations cause ID, we reasoned that differentially expressed genes in PHF6-deficient cortex might be also regulated by proteins implicated in other neurodevelopmental disorders of cognition. We therefore compared PHF6-regulated genes with targets of FMRP, which is the most common single gene cause of ID (Coffee et al., 2009; Pieretti et al., 1991). Upregulated genes upon PHF6 loss overlapped significantly with FMRP targets (Darnell et al., 2011) (Figure 6j), suggesting that PHF6 and FMRP regulate a common group of genes. In other analyses, downregulated genes upon PHF6 loss overlapped significantly with differentially expressed genes in the cerebral cortex of mice in which the histone H3K4me3 and H3K4me2 demethylase protein KDM5C was knocked out (Iwase et al., 2016) (Figure 6j), and with misregulated genes in the cerebral cortex of mice with haploinsufficiency of the chromatin remodeling protein CHD8 (Gompers et al., 2017) (Figure 6j). Together, these observations

suggest that PHF6-regulated genes overlap with targets of other proteins associated with developmental disorders of cognition.

Because PHF6-regulated genes overlap with targets of FMRP and CHD8, which are both linked to autism in addition to ID (Bassell and Warren, 2008; Bernier et al., 2014; Iossifov et al., 2012), we asked whether PHF6-regulated genes might also be relevant to autism spectrum disorder (ASD). We intersected PHF6-regulated genes with the unbiased autism gene module termed asdM12 that is misregulated in the frontal and temporal cortex in ASD patients (Voineagu et al. 2011). Remarkably, upregulated genes upon PHF6 loss overlapped significantly with the asdM12 gene module (Figure 6j), suggesting that PHF6 may regulate gene programs that are implicated in ASD.

ASD genes converge on modules that regulate synaptogenesis during human cortical development (Berg and Geschwind, 2012; Parikshak et al., 2013). We mapped PHF6-regulated genes onto available developmental modules containing gene networks co-regulated across developmental stages, generated by weighted gene coexpression network analysis (WGCNA) using BrainSpan whole-genome transcriptomic data (Parikshak et al., 2013). Downregulated genes upon PHF6 loss were over-represented in module 3 (M3), enriched for genes encoding chromatin organization, and module 8 (M8), enriched for genes encoding neuron differentiation. In addition, upregulated genes upon PHF6 loss were over-represented in module 13 (M13) and module 17 (M17) (Figure 6k), enriched for synaptic genes. The GO terms and temporal expression of over-represented gene modules were similar to misregulated genes upon PHF6 loss (Figure 6f, S5e, f). Strikingly, upregulated genes upon PHF6 loss and the autism-associated asdM12 gene module converged onto the developmental modules M13 and M17 representing synaptic terms (Figure 6k, S5e,f). These results suggest that PHF6-regulated genes and the autism-linked gene modules coalesce in developmental modules.

Mutation of PHF6 in a patient with BFLS and autism spectrum disorder

The identification of a link between PHF6-regulated gene expression in the mouse cerebral cortex and human brain gene networks deregulated in autism raised the question of whether BFLS patients might present with autism spectrum disorder (ASD). Reports of the clinical presentation of BFLS do not include ASD symptomatology (Jahani-asl et al., 2016). However, in a recent series of patients with neurodevelopmental disorders undergoing exome sequencing, we identified a patient with ASD harboring a pathogenic nonsense mutation of PHF6 at Cysteine 305 (Baldridge et al., 2017). The purpose of the series was to assess the role of the clinician in the interpretation of exome sequencing results toward diagnosis of genetic disorders (Baldridge et al., 2017). The PHF6 C305X mutation was mentioned in a table, and a few patient symptoms were briefly listed in supplementary material (Baldridge et al., 2017). Here, a summary of the case is presented. A now 20-year-old woman was born as a full-term infant with normal weight and length. Soon after birth, parents reported difficulties in feeding coordination. She did not babble as an infant, did not speak words until 4 years of age, and began to speak in sentences at age 6. At two years, she continued to show significant language delay, with no speech, but could sign 3-4 words and follow commands. The patient was diagnosed with pervasive developmental disorder at age four. Later, in addition to cognitive impairment, the patient displayed aggressive behavior. She also developed repetitive behaviors and deficits in social interaction. These clinical features, combined with clinical observation and parental and teacher evaluations on the Social Responsiveness Scale (SRS), led to diagnosis of autism spectrum disorder (ASD) at age 11. Clinical exome sequencing at age 17 revealed a *de novo* mutation (c.915_916delTGinsAA, p.C305X, NM_032458) in the *PHF6* gene (Baldridge et al., 2017). X-inactivation testing showed an X-inactivation ratio of 100:0, consistent with a highly skewed X-inactivation. The C305X mutation was not present in the Exome Aggregation Consortium (ExAC) or Genome Aggregation Database (gnomeAD) database (data not shown), suggesting that the C305X mutation is pathogenic. The C305 mutation is located in the alpha helix of the second PHD domain of PHF6, which like C99F is an evolutionarily conserved zinc-chelating cysteine (Liu et al., 2014). Like the C99F mutation, the C305X mutation led to

substantial downregulation of PHF6 protein level in cells (Figure S5g). Collectively, these data suggest that loss of function mutations in *PHF6* may cause BFLS with autism.

DISCUSSION

In this study, we report the first mouse model of Börjeson-Forssman-Lehmann syndrome (BFLS) and a mouse with knockout of PHF6. Gene profiling analyses in PHF6-deficient mice show that PHF6 promotes the expression of neurogenesis genes and concomitantly suppresses expression of synaptic genes. PHF6-regulated genes are overrepresented in gene signatures and modules that are deregulated in the brain of patients with autism spectrum disorder (ASD). Taken together, our findings provide novel insights into the cellular and molecular underpinnings of BFLS, and may suggest potential links of BFLS with autism spectrum disorders.

Our study also provides novel insights on the role of PHF6 in brain development. The findings that PHF6 promotes the expression of neurogenesis genes and downregulates synaptic gene suggest that PHF6 may control the timing of neuronal differentiation, possibly preventing premature connectivity. Thus, deregulation of temporal control of neuronal maturation may contribute to the pathogenesis of neurodevelopmental disorders of cognition.

Analyses of PHF6-regulated genes also suggest molecular convergence with gene signatures and modules of autism spectrums disorder (ASD). Notably, clinical descriptions of BFLS are focused on intellectual disability and syndromic features of the disorder (reviewed in Jahani-Asl et al., 2016). However, our analyses of PHF6-regulated genes suggest potential links between BFLS and ASD. Consistent with this interpretation, we have identified a patient with ASD harboring the pathogenic nonsense PHF6 mutation C305X (Baldridge et al., 2017). In future clinical studies, it will be interesting to explore whether ASD features are present in other BFLS patients.

In summary, we report a novel mouse model of BFLS that features cognitive impairment and predisposition to seizures. Our findings also raise the possibility that autism may represent a component of BFLS. Our study advances understanding of the cellular and molecular

underpinnings of BFLS, and lays the foundation for potential treatments for neurodevelopmental disorders of cognition.

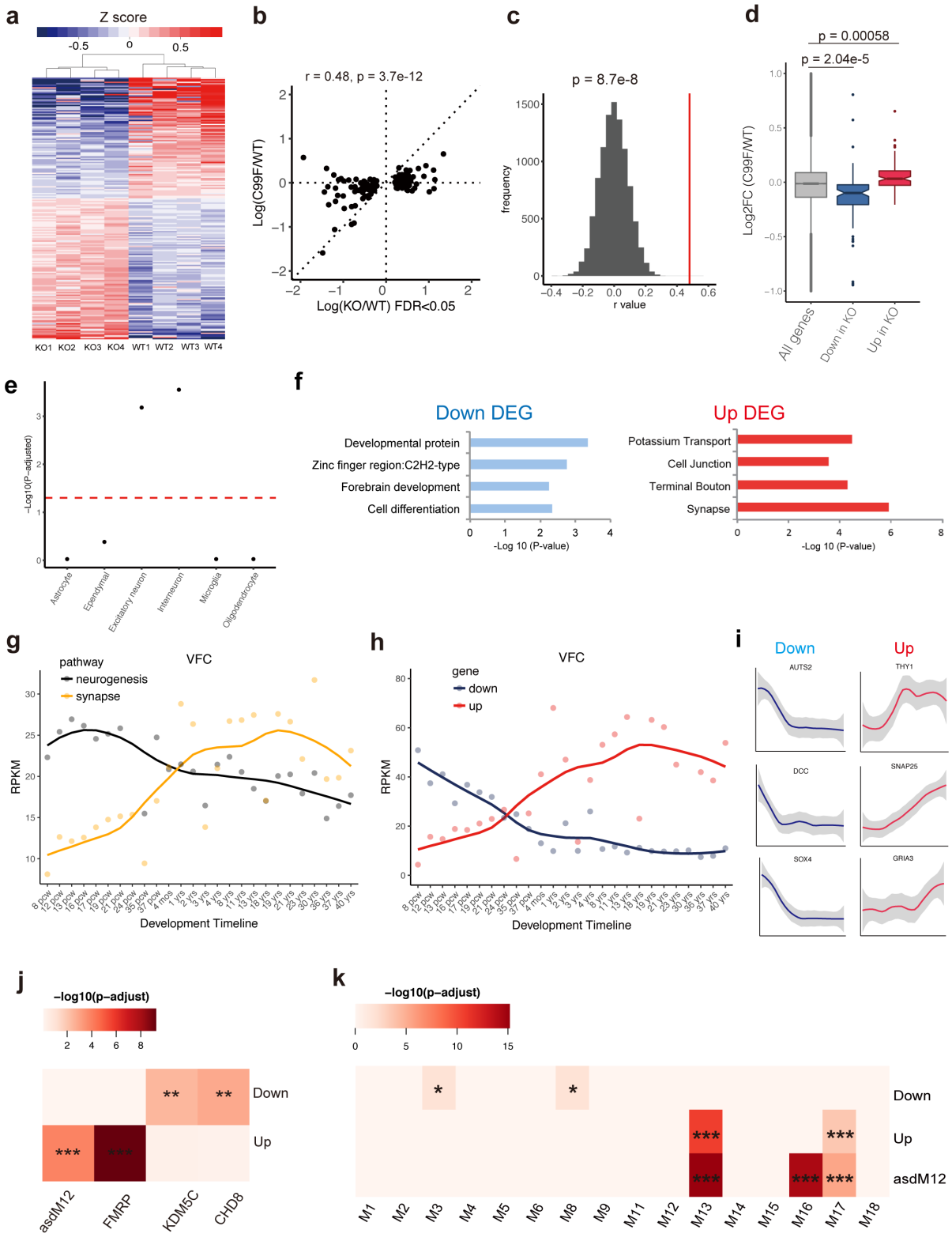

Figure 6. Transcriptional alterations in the cerebral cortex in PHF6 deficient mice.

(a) Heatmap of 193 differentially expressed genes upon PHF6 KO by RNAseq (EdgeR, FDR<0.05)

(b) Correlation analysis of alteration of gene expression in the cerebral cortex of PHF6 C99F mice that were deregulated upon PHF6 KO (193 genes; FDR<0.05).

(c) Spearman correlation rho distribution by comparing gene expression change in PHF6 KO and C99F mice calculated by random sampling of 193 genes for 10,000 times. Red line: rho=0.48 (see b). Z score statistics, p=8.7e-8.

(d) Boxplot of log fold change of up and down-regulated genes upon PHF6 KO in C99F. Wilcoxon rank-sum test, p=5.8e-4(upregulated), p=2.04e-5(downregulated).

(e) Gene enrichment analysis of major brain cell types. Dotted red line: p-adjusted=0.05.

(f) Gene ontology analysis by DAVID for downregulated and upregulated genes upon PHF6 KO.

(g) Average expression for neurogenic (GO:0050769) and synaptic (GO:0007268) genes across developmental time in VFC based on BrainSpan dataset.

(h) Average expression of downregulated and upregulated genes upon PHF6 KO across developmental time in the VFC based on BrainSpan dataset.

(i) Example of individual gene expression across development time.

(j) Enrichment analysis of up- and down-regulated genes upon PHF6 KO with gene targets of FMRP, KDM5C, CHD8 and the autism module asdM12, containing misregulated genes in the frontal and tempora l cerebral cortex in postmortem ASD patient brains.

(k) Enrichment analysis of misregulated genes upon PHF6 KO and the asdM12 gene module with previously described developmental gene coexpression network modules.

Enrichment analysis was tested by hypergeometric-test, followed by Benjamini-Hochberg multiple testing corrections. *p.adjusted <0.05, **p.adjusted <0.01, ***p.adjusted <0.001.

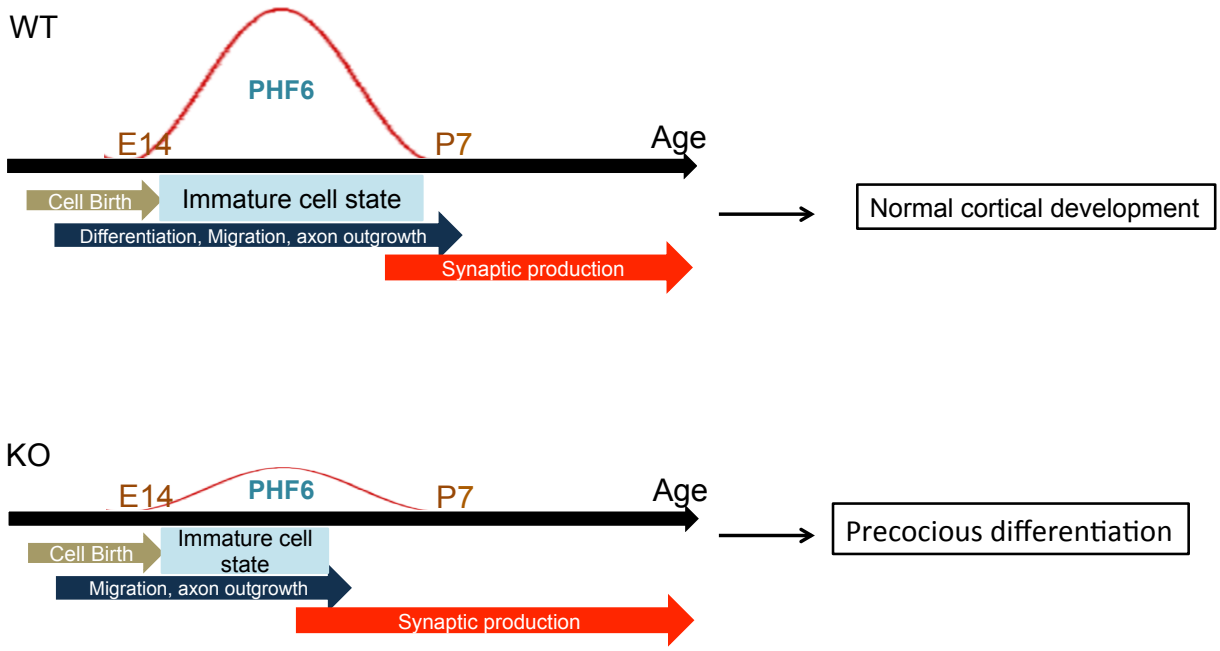

Figure 7. Working model of PHF6 maintaining neurons in an immature state.

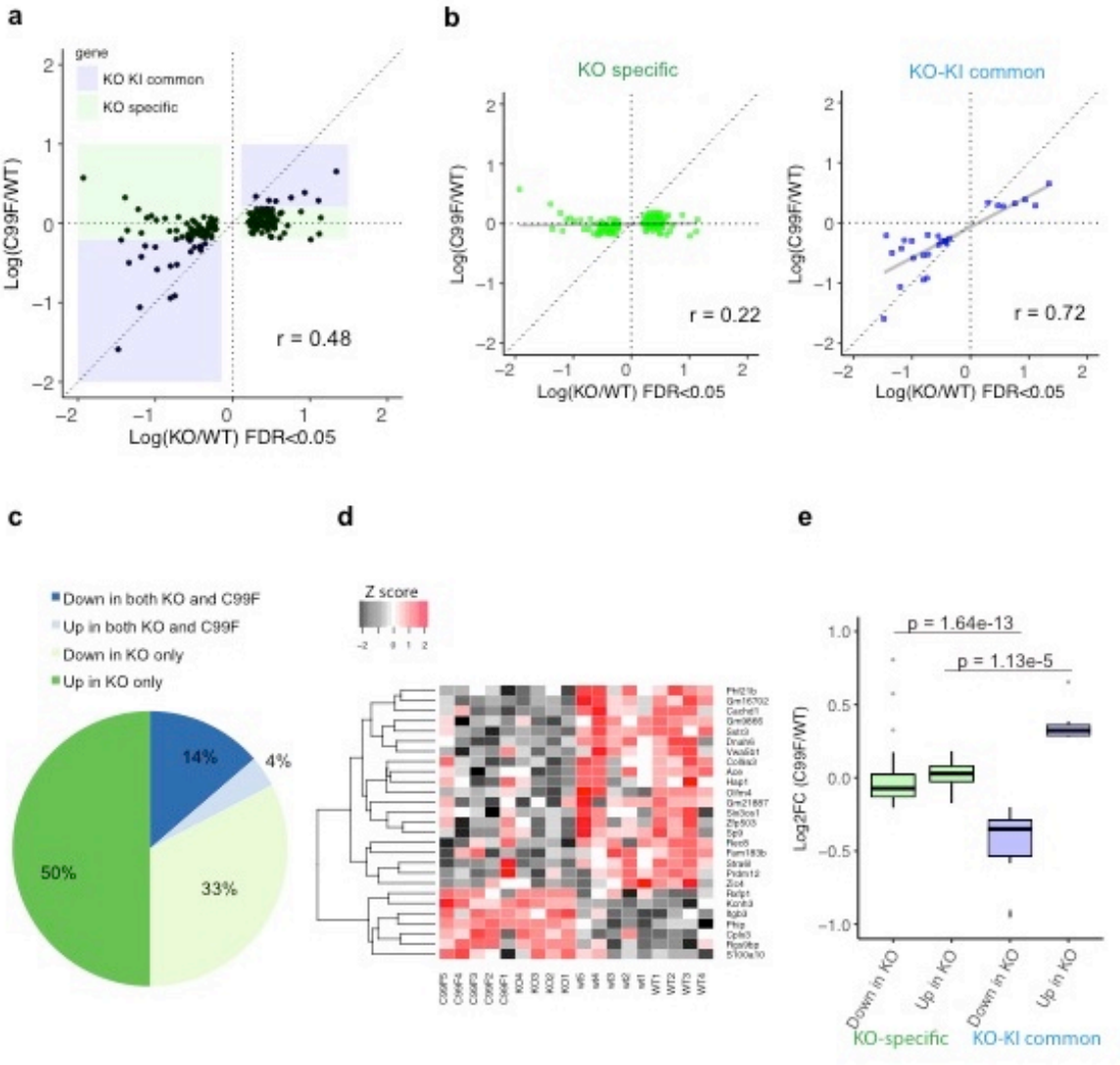

Figure 8. Bioinformatic dissection of KO-specific and KO-KI commonly regulated genes.

(a) Using Log2 Fold change of 0.2, the 193 deregulated genes upon PHF6 knockout were classified into two groups, KO-specific genes in green shade and KO-KI common genes in blue shade.

(b) (Left) Comparison between KO and C99F transcriptome for KO-specific genes showed a low correlation, Spearman, r=0.22. （Right) Comparison between KO and C99F for KO-KI commonly regulated genes showed a high correlation, Spearman, r=0.72.

(c) The percentage of KO-specific genes (green) and KO-KI common genes (blue).

(d) Heatmaps of KO-KI common genes.

(e) Boxplot of log fold change of up and down-regulated genes upon PHF6 KO and C99F for KO-specific and KO-KI common genes.

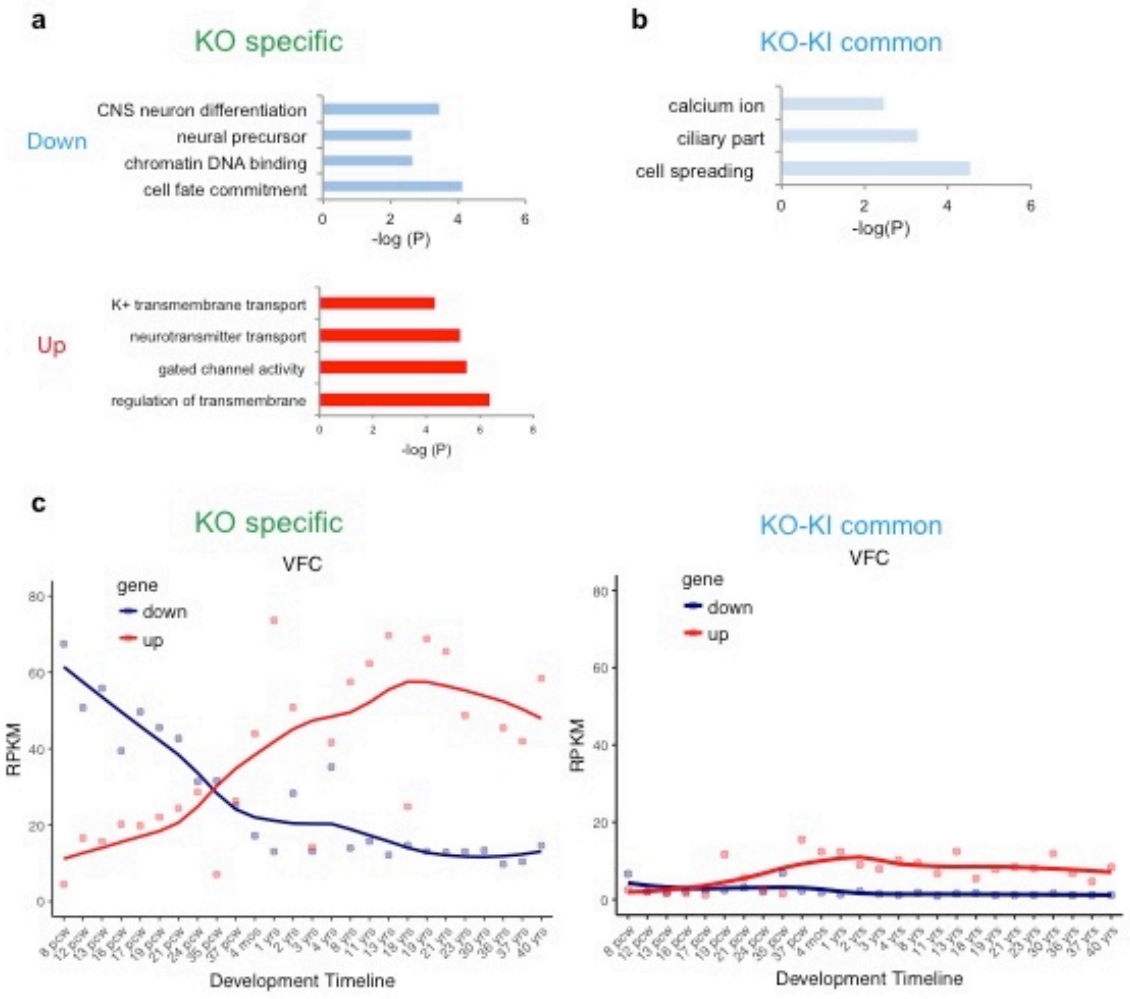

Figure 9. Functional characterization of deregulated genes upon PHF6 knockout.
(a) Gene ontology of KO-specific genes.

(b) Gene ontology of KO-KI common genes.

(c) Average expression of downregulated and upregulated genes for KO-specific group (left) and KO-KI common group (right) across developmental time in the ventral frontal cortex (VFC) based on BrainSpan dataset.

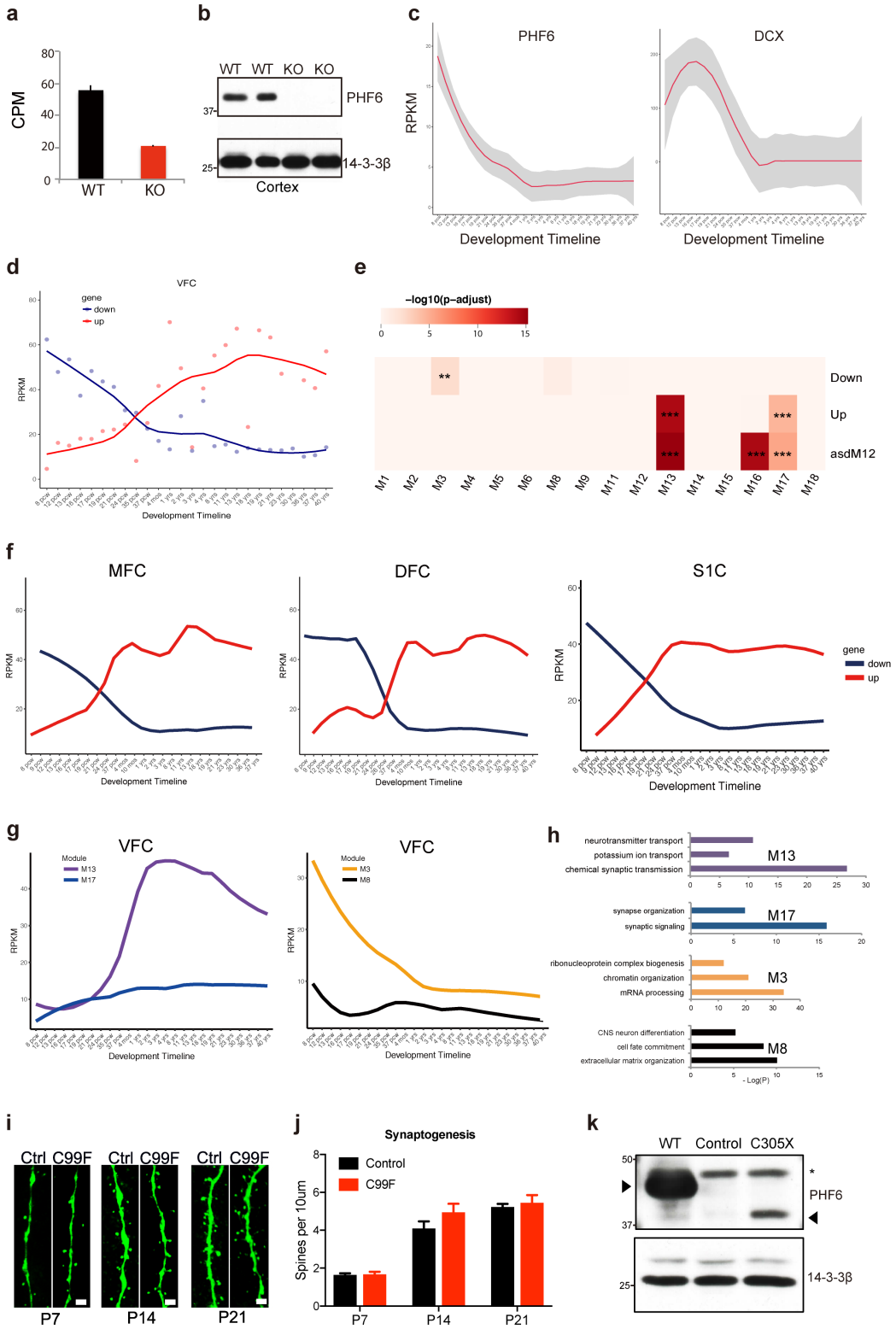

Figure S5. Gene expression in the PHF6 knockout mouse.

(a) The level of PHF6 mRNA in the cerebral cortex of PHF6 knockout mice in RNA-seq analysis (n = 4) was reduced compared to control mice (n = 4). Data are presented as mean ± SEM.

(b) Lysates of the cerebral cortex at P0 from control male and PHF6 knockout male mice were subjected to immunoblotting with the PHF6 and 14-3-3β antibodies. Levels of PHF6 protein were diminished in the cortex of PHF6 knockout mice.

(c) Expression of PHF6 (left) and DCX (right) during development in ventral frontal cortex (VFC) using BrainSpan dataset. PHF6 was developmentally downregulated, and DCX was transiently expressed from post conceptual week 8 (pcw8) to pcw24.

(d) Average expression of downregulated and upregulated genes upon PHF6 knockout discovered by DEseq2 was plotted across developmental time in the VFC based on human BrainSpan data. Downregulated genes upon PHF6 loss were also developmentally downregulated, whereas upregulated genes upon PHF6 loss were developmentally upregulated.

(e) Enrichment analysis of misregulated genes upon PHF6 knockout discovered by DEseq2 and the asdM12 gene module with previously described developmental gene coexpression network modules (Parikshak et al., 2013). Upregulated genes upon PHF6 knockout coalesced with autism gene modules. Enrichment analysis was tested by hypergeometric-test, followed by Benjamini-Hochberg multiple testing corrections. **p.adjusted <0.01, ***p.adjusted <0.001.

(f) Average expression of up- and down-regulated genes upon PHF6 knockout in medial frontal cortex (MFC), dorsal frontal cortex (DFC) and primary somatosensory cortex (S1C). Downregulated genes upon PHF6 knockout were developmentally downregulated, and upregulated genes upon PHF6 knockout were upregulated throughout development in these brain regions.

(g) Average expression of genes in developmental modules M3, M8, M13 and M17 was plotted across developmental time in the VFC based on human BrainSpan dataset.

(h) Genes from developmental modules including modules M3, M8, M13 and M17 were subjected to gene ontology analysis using Metascape.

(i) Layer II stellate neurons in entorhinal cortex were subjected to biocytin injection. Spine density from P7-9, P14-16 and P21-25 were analyzed. C99F neurons had little or no effect in synaptogenesis. Scale bar = 2um.

(j) Quantification of spine density at P7-9, P14-16 and P21-25 from C99F and control stellate neurons.

(k) Lysates of 293T cells transfected with the expression plasmids encoding FLAG-HA-tagged PHF6, the control vector or patient specific PHF6 mutation C305X were subjected to immunoblotting with the Flag and 14-3-3β antibodies, the latter serving as loading control.

C305X led to reduced PHF6 protein level. Asterisk indicates non-specific immunoreactive band. Arrowhead indicates FLAG-tagged PHF6.

Material and Methods

RNA-seq

For control and PHF6 knockout (KO) experiment, four pairs of animals were harvested from two litters. For control and PHF6 C99F knock-in experiment, five pairs were harvested from three litters. Animals were harvested at postnatal day 0 (p0). The cerebral cortex was dissected and subjected to RNA extraction using Trizol (Invitrogen). RNA from control/KO experiment was sequenced on an Illumina HiSeq 2500, and RNA from control/C99F experiment was sequenced on Illumina HiSeq 2500. EdgeR was used to analyze the differentially expressed genes. The Benjamini-Hochberg false discovery rate (FDR) was calculated for all genes.

Permutation testing

Permutation testing was performed to assess the correlation between gene expression alteration in the cerebral cortex of PHF6 knockout and C99F knock-in mice by comparing the observed correlation value with expected correlation value. Observed valued was calculated by Spearman correlation (rho) between log fold change (logFC) KO/control and C99F/control of 193 differentially expressed genes upon PHF6 KO, whereas the expected correlation distribution was generated via iterative sampling of random sets of 193 genes and calculating the logFC correlation between KO and C99F. Random sampling was repeated 10,000 times, allowing us to estimate the mean and standard deviation of the expected rho distribution. Empirical z-scores and p value were calculated for the observed rho value based on the expected rho distribution. A custom R script was used for the analysis.

Gene enrichment analyses

For cell type enrichment, we used cell marker gene set previously described ((Zeisel et al., 2015). We used the expressed genes in the postnatal day 0 (P0) mouse cortex averaging the

RPKM (mean>0.1) across control samples, and overlapping with all the expressed genes in the single cell RNA-seq dataset (Zeisel et al., 2015) as our background list.

For gene enrichment analysis with developmental modules and other ID proteins, all gene symbols were converted into human orthologs using web based HUGO multi-symbol checker. Expressed protein-coding genes in the P0 mouse cortex (RPKM > 0.1) were used as background for KDM5C and CHD8 enrichment analysis. Protein-coding genes that had probes called in Voineagu et al. 2013 were used as background for asdM12 enrichment analysis. For FMRP enrichment analysis, all protein-coding genes detected in HITS-CLIP (Darnell et al., 2011) were used as the background list, and FMRP enriched genes (765) were used as FMRP-target. Expressed genes in the P0 mouse cortex (RPKM>0.1) that had human orthologs were used as background for developmental module enrichment analysis.

All gene enrichment analyses were performed using one-sided hypergeometric test calculated according to the R function phyper(). Each p-value was adjusted by Benjamini-Hochberg correction.

BrainSpan developmental analyses

Normalized RPKM values of RNAseq data were obtained from Allen Brain Atlas BrainSpan dataset (http://www.brainspan.org/). Datasets from four brain regions, including the ventral frontal cortex (VFC), medial frontal cortex (MFC), dorsal frontal cortex (DFC) and primary somatosensory cortex (S1C) were used for developmental expression analysis. Genes from GO:0050769 and GO: 0007268, representing neurogenesis and synaptic genes respectively were first extracted from the Brainspan dataset and the average RPKM value in VFC was calculated and plotted across developmental time. Differentially expressed genes (DEGs) upon PHF6 KO were divided into up-regulated and down-regulated genes. These genes were extracted from BrainSpan data for each brain region, and the average RPKM was calculated and analyzed across the developmental time. A custom R script was used for analyses.

Biocytin injection and post-hoc staining

Biocytin labeling was performed as described (Huang et al., 2010). Intracellular recording solution containing 1% biocytin was loaded into layer II stellate neurons in the entorhinal cortex from P7-9 (C99F: n=8; control: n=7), P14-16 (C99F: n=6; control: n=7) and P21-25 (C99F: n=7; control: n=7) animals through recording electrode. Slices were fixed in 4% PFA for 2 hours. Slices were subjected to histochemical analyses with Alexa-Fluor 488-conjugated Avidin (1:1000) for 4^0C overnight.

Statistical analyses

Statistical analyses were performed using GraphPad Prism 6.0, and SPSS (v2.5)/Systat statistical software packages. Independent t-tests, one-sample t-tests, factorial ANOVAs, including repeated measures (rm) ANOVAs were used where appropriate. The Huynh-Feldt correction was applied to all within-subjects effects containing more than two levels to protect against violations of sphericity/compound symmetry assumptions underlying rmANOVA models. Specific planned comparisons were conducted to provide further clarification of significant interactions between main factors. Simple main effects were calculated for significant main effects of factors, and Bonferroni corrections were used for multiple comparisons. Probability value for statistical significance for all analyses was $P < 0.05$.

Acknowledgements

The authors thank the members of the Bonni laboratory for helpful discussions. This work was supported by the National Institutes of Health grant NS088378 (to A.B.), R01HG007175 (to T.W.), MH117070-01 (to J.D.D.) and Genome technology access center (GTAC) at Washington University School of Medicine.

Chapter 4:

Conclusions and Future Directions

Significance

In this study, we report our discoveries on pathogenic mechanisms underlying Börjeson-Forssman-Lehmann syndrome (BFLS), a well-known cause of X-linked intellectual disability. Although mutations of the transcriptional regulator PHF6 are known to cause BFLS, the pathogenic mechanisms underlying BFLS have remained to be elucidated. Using CRISPR-Cas9 technology, we have generated the first mouse model of BFLS, harboring the patient mutation that replaces Cysteine 99 within the PHD domain of PHF6 with phenylalanine (C99F). PHF6 C99F knock-in mice display deficits in cognitive functions as well as reduced threshold to seizures. In electrophysiological studies, the intrinsic excitability of entorhinal cortical stellate neurons is increased, providing a mechanistic basis for seizure predisposition upon PHF6 deficiency. Transcriptomic analysis of the cerebral cortex in PHF6 C99F knock-in and PHF6 knockout mice show that PHF6 promotes the expression of neurogenesis genes and concomitantly suppresses the expression of synaptic genes. Remarkably, PHF6-regulated genes are overrepresented in gene signatures and modules that are deregulated in the brain of patients with autism spectrum disorders. Our findings advance our understanding of the mechanisms underlying BFLS pathogenesis and offer new links between BFLS and autism spectrum disorders.

Intellectual disability (ID) is a prevalent developmental disorder that affects 1% to 3% of the general population. With no effective treatments, these disorders pose enormous economic costs to society. There is thus an urgent need to better understand the pathogenesis of ID. BFLS was identified over five decades ago as a syndrome of X-linked ID that also features epilepsy. Although rare, BFLS now represents a widely known cause of ID. The generation of the first mouse model provides unprecedented opportunities for understanding the pathogenesis of ID as demonstrated in our study in behavior, electrophysiological, transcriptomics, and bioinformatics analyses. In addition, these mice provide the opportunity for the field to identify novel therapies for neurodevelopmental disorders of cognition.

One of the most exciting aspects of our study is that bioinformatics analyses of the alterations of gene expression in the cerebral cortex has revealed that PHF6-regulated genes are overrepresented in gene signatures and modules that are deregulated in the brain of patients with autism spectrum disorders. Strikingly, we have recently identified a patient with autism spectrum disorder that harbors a nonsense mutation of Cysteine 305 within the second PHD domain of PHF6. Our findings suggest that autism may represent an underappreciated component of BFLS. In summary, our study advances understanding of the cellular and molecular underpinnings of BFLS, and lays the foundation for potential treatments for neurodevelopmental disorders of cognition. Here I highlighted a few exciting new questions this study has opened up.

Future Directions

The biological consequences of PHF6 in regulating neural maturation

Transcriptomic analyses of PHF6 knockout and control mice have revealed potential molecular mechanisms through which PHF6 regulates cell state. In particular, we found that PHF6 activates neurogenic genes and represses synaptic genes, by which maintaining neurons at an immature state. Upon PHF6 loss, the developmentally upregulated genes including synaptic genes were unregulated at an earlier time point. Concomitantly, the developmentally downregulated genes including neurogenic and cell differentiation-related genes were downregulated in advance.

To determine the biological consequences of the precocious differentiation in PHF6 knockout mice, two biological events including neural differentiation and synaptogenesis could be tested. Interestingly, the dendritic spine development did not seem to be advanced in the entorhincal cortex layer II stellate neurons in the C99F mice, even with the moderate correlation between C99F and PHF6 knockout transcriptome. Because the bioinformatics analyses were primarily based on differentially regulated genes upon PHF6 knockout, it is important to determine the biological consequence of precocious differentiation in the PHF6 knockout mice. With the impossibility of testing synaptogenesis in the developing PHF6 knockout mice *in vivo*,

due to perinatal lethality, it is also important to determine whether the neurons *in vitro* undergo advanced synaptogenesis.

When neurons first exist mitotic cycle, they immediately start expressing doublecortin (DCX). DCX is subsequently downregulated once the neurons become mature (Donato et al., 2017). Therefore, to test whether the differentiation process is advanced in the PHF6 knockout neurons, DCX could be used as an immature neuron marker. For future study it will be interesting to test the necessity and sufficiency of PHF6 in preventing neuronal premature differentiation by label the neurons with the same birthdate and follow through their development and analyzed the expression of DCX in the synchronized neural population to assess neural maturation in the context of PHF6 knockout or overexpression.

What is the molecular mechanisms underlying BFLS pathogenesis?

The gene expression changes upon PHF6 knockout provide clues for studying the function of PHF6, whereas the gene expression alterations in PHF6 C99F give insights on the molecular mechanisms underlying BFLS. Through bioinformatics analyses, we discovered that the transcriptomic changes in PHF6 knockout and C99F were moderately correlated. In other analyses, we identified that the genes specifically altered in the PHF6 knockout were involved in mechanism in maintaining immature cell state, whereas the genes that were highly correlated in the two genotypes occupy only a small fraction and were involved in other mechanisms such as cell signaling and cilia. Up until now, what goes awry molecularly in PHF6 C99F and the molecular mechanisms underlying BFLS pathogenesis remains unclear.

In the bulk RNAseq experiments, we did not identify many differentially expressed genes in the PHF6 C99F mice. Notably, when we used DEseq2, a more stringent way for differential gene expression analysis, only one gene, *PHIP*, was detected (data not shown). Since PHF6 C99F significantly altered the neural excitability and later on fear learning, some developmental changes due to PHF6 C99F knock-in must have happened. The small number of differentially expressed genes detected through bulk RNAseq could be due to the dilution effect from tissue

heterogeneity. Interestingly, the neural excitability was increased in entorhinal cortex layer II stellate neurons, while remained same in layer II/III pyramidal neurons of the somatosensory cortex in PHF6 C99F mice compared to WT, suggesting that PHF6 regulate biological function in a cell type and brain region specific manner. It is therefore critical to determine whether the gene expression of PHF6 is also regulated in a cell-type specific manner.

The discovery of the altered intrinsic excitability in the entorhincal cortex layer II stellate neurons specifically has provided important clue on which cell types to perform transcriptomic analyses. In future studies, it would be essential to understand the gene expression changes and potential epigenetic alterations in an enriched cell type, such as entorhincal cortex stellate neurons in the PHF6 C99F mice. These systematic profiling of C99F mice could shed light on the molecular pathogenesis of BFLS in a cell-type specific manner.

Epigenetic regulation of transcription by PHF6

PHF6 contains two PHD-like zinc finger domains, which gives potential for PHF6 to bind to DNA or modified histones. Studies have shown that PHF6 interacts with transcriptional elongation complex, PAF1 and nucleosome remodeling complex, NuRD. Recent studies have provided insights on how PHF6 regulate gene expression along with chromatin accessibility in B-cell leukemia. Particularly, loss of PHF6 led to downregulation of B-cell developmental genes, and activation of T-cell signaling genes, by which gave rise to lymphoma with mixed lineages (Feliciano et al., 2017). The expression alteration of B-cell and T-cell lineage was correlated with chromatin accessibility. Similarly, in our study, upon PHF6 loss, differentiation genes were downregulated and synaptic genes were upregulated, leading to precocious differentiation, suggesting PHF6 can act both as a transcriptional activator as well as repressor. However, how PHF6 regulates gene expression, perhaps through epigenetic mechanisms and the direct targets of PHF6 in mouse cortex remains unknown. For future studies, it is critical to understand the biochemical function of PHF6 in the developing cortex. Important specific questions include:

1. Where does PHF6 bind in the genome in the developing cortex?

In the preliminary studies, we performed PHF6 ChIP-seq experiments to investigate its genome occupancy. Using two biological replicates, we identified over 2000 PHF6 binding sites; the majority of them were at promoters. PHF6 binding is positively correlated with gene expression and active histone markers (See Appendix Figure S9), suggesting that PHF6 mainly binds to active promoters. One caveat of the experiment was that instead of using the PHF6 KO or IgG as negative control, we used PHF6 C99F as a negative control because of dramatic reduction in PHF6 protein level *in vivo*. Even though, we were able to identify PHF6 signals across the genomes, those peaks were identified with less confidence due to improper negative control. In future studies, it is critical to use PHF6 WT and KO cortex to perform PHF6 ChIP-seq experiments to understand the genome occupancy of PHF6. Our prediction though, is still the same that PHF6 binds to active gene promoters.

2. Through what epigenetic mechanisms does PHF6 regulate transcription?

Previously, PHF6 has been shown to interact with NuRD complex, which contains histone deacetylase proteins. We also observed endogenous interaction of PHF6 with NuRD complex subunits (See appendix Figure S6). Therefore, we hypothesize that PHF6 can regulate gene expression through epigenetic mechanisms. To test that hypothesis, PHF6 control and KO cortex could be used to profile for DNA hypersensitivity, chromatin opening and histone modifications. In fact, in our preliminary work profiling histone modifications ChIP-seq using H3K27ac, H3K4me3 and H3K9/14ac antibodies in three pairs of PHF6 control and C99F cortex, we found there was little or no changes in histone peaks or histone density at PHF6-regulated genes (identified upon PHF6 knockout) (Figure S9). This observation was somewhat expected because histone modification is correlated with gene expression and there was not many genes altered in the C99F cortex from bulk RNAseq. It is possible that PHF6 functions downstream of histone modification in regulating gene expression. However, we could not rule out the potential effect of PHF6 on histone modification under PHF6 knockout condition. We reason that understanding chromatin opening, histone modification and DNA hypersensitity sites in PHF6 knockout cortex can help understand where PHF6 functions in the regulation of transcription.

Is entorhinal cortex-hippocampal pathway disrupted in mouse model of BFLS?

The discovery of entorhincal cortex (EC) layer II stellate neuron (L2) hyperexcitability in the PHF6 C99F mice shed light on the potential circuit that might be disrupted in the mouse model of BFLS. The circuit connecting EC and hippocampus (HPC) has been studied for decades. Medial entorhinal cortex layer II stellate neurons (MEC-L2) projects to dentate gyrus (DG) of hippocampus, which then projects to CA3, followed by CA1, lateral entorhinal cortex layer V pyramidal neurons (LEC-L5) and LEC layer II pyramidal neurons (LEC-L2). This circuit is implicated in multiple behavior paradigm as well as seizures (Janz et al., 2017, Kitamura et al., 2015). Since many of the behavioral impairments observed in our PHF6 C99F are pointing to this circuit malfunction, it will be important to understand whether stellate neurons alone or the EC-HPC circuit is implicated in the BFLS. First of all, detailed electrophysiological and circuit-mapping analyses could be performed to understand major effect of stellate neuron hyperexcitability on downstream target cells such as DG granule neurons. Another aspect to analyze the circuit is measuring circuit maturation (Donato et al., 2017). Previous studies have suggested that the excitability of MEC-L2 stellate neurons drive the maturation of EC-HPC circuit (Donato et al., 2017). Silencing of the MEC-L2 stellate neurons disrupts the maturation of EC-HPC circuit. In our mouse model of BFLS, entorhinal cortex layer II stellate neurons display increased intrinsic excitability. Therefore, EC-HPC circuit maturation could be disrupted/advanced in the PHF6 C99F mice as a result of stellate neuron hyperexcitability.

How do entorhinal cortex layer II stellate neurons function during contextual fear learning?

In our study, we found that PHF6 C99F mice displayed impaired contextual fear memory. This impairment was reproducibly observed in two independent cohorts of mice. During contextual fear conditioning, the animals need to first encode a representation of the context (context encoding), associate the context representation with unconditioned stimulus

(US) (in this case, foot shock); then both context memory and context-US association undergo memory consolidation (Maren et al., 2013). The step of memory encoding is necessary for memory consolidation. In our study, it is difficult to understand whether the impaired contextual fear was because of lack of memory encoding or consolidation. Therefore, in the future studies, it is important to understand which part of contextual fear memory is disrupted, context encoding or memory consolidation? Using more detailed behavior paradigm such as context discrimination assay can help dissect out the fear memory impairment.

Also, studies have suggested that memory encoding and consolidation could happen in different brain regions. The context information is presented in the entorhincal cortex stellate neurons before reaching the granule cells in the DG, whereas the memory consolidation mainly occurs in the hippocampus. Interestingly, MEC layer II stellate neurons, projecting to DG granule cells, are involved in context-specific encoding, activation of CA3 pyramidal cells and contextual fear memory. In particularly, MEC layer II stellate neurons show context-specific calcium activity, and are critical for Discriminatory Encoding in CA3 regions, which then facilitates contextual fear memory. With the intrinsic hyperexcitability observed in the PHF6 C99F EC layer II stellate neurons, it will be interesting to analyze whether these cells have abnormal neural coding through analysis of their Ca2+ responses, which in turn affects neural coding.

Altered neuronal and circuits excitability in BFLS

The discovery of hyperexcitability in the EC layer II stellate neurons associated with increased input resistance and reduced cell capacitance has opened a new area of investigation on what ion channel(s) might be involved. Importantly, in the preliminary experiment, we did not find increased EPSPs in the stellate neurons, suggesting the increased excitability is not due to the elevation of the excitatory input from upstream neurons (data not shown). Instead, the increased excitability is likely due to cell intrinsic alteration of the channel activities. In the field of neural excitability, multiple factors could be contributing to alteration of the action potential.

For example, the noninactivating persistent sodium current is increased in the EC layer III pyramidal neurons of FMRP KO mice, leading to the reduced action potential threshold and neural hyperexcitability (Deng and Klyachko, 2016). Additionally, reduction in Kv4.2 (Gross et al., 2011), and altered HCN channel expression (Brager et al., 2012) have also been linked to abnormal excitability in the FMRP KO mouse model. In our case, the decreased the action potential threshold could be resulting from increased sodium current, or decreased potassium current. A defect in the action potential rising phase indicates sodium channelopathy, whereas the repolarization phase disruption could be due to defected potassium channel, and abnormal action potential duration could be due to voltage-gated potassium channels. Therefore, a detailed investigation of action potential waveform is critical for identification of the channelopathy in PHF6 C99F stellate neurons.

Due to heterogeneity of the cell types in the cortex, neurons response differently upon constitutive genetic mutation. This is most evident in the field of electrophysiological research in FMRP knockout mice (Contractor et al., 2015; Deng and Klyachko, 2016; Deng et al., 2013; Lee and Jan, 2012). For example, studying of somatosensory cortex layer V principle cells in the FMRP model have suggested that pyramidal tract (PT) neurons show altered HCN channel, while HCN current remains intact in intratelecephalic tract (IT) neurons upon FMRP knockout. EC layer III pyramidal neurons exhibit reduced action potential threshold caused by increased persistent sodium current, whereas EC layer II stellate neurons display normal excitability in the FMRP KO mice (Deng and Klyachko, 2016). Therefore, neural excitability in these XLID models is affected in a brain region and cell type specific manner. For future investigation, it will be interesting to understand the affect of PHF6 loss on neural excitability in different brain regions and cell types, possibly combining the molecular tools such as translating-ribosome-affinity-purification-seq (TRAP-seq) or INTACT for in-depth molecular mechanisms.

The link between BFLS and ASD

The mouse model of BFLS has behavioral impairments in the social interaction; in particular, the PHF6 C99F mice displayed normal social motivation, but reduced social recognition. Interestingly, PHF6 C99F mice also displayed reduced ambulatory activity and vertical rearing frequency in the open field tests. These data suggest that PHF6 C99F mice could also be lack of interest/curiosity, which is displayed in other autism spectrum disorder (ASD) mouse models. However, we did not identify behavioral defects in the ultrasonic vocalization or marble burying (data not shown), which measure communication and stereotypic movements in the mouse. In our PHF6 C99F mouse model, we did not identify major autistic-like phenotypes. However, the identification of ASD patient harboring C305X mutation and the gene enrichment analyses on PHF6-regulated genes with ASD relevant genes have raised the question whether ASD is presented in BFLS in an underappreciated rate. Here, we raised the possibility of linking BFLS and ASD both at a clinical setting and in basic research setting. In the future studies, it would be interesting to test whether the newly generated BFLS mouse models (with different patient mutations) harbor autistic-like behaviors.

Another important aspect of the BFLS is the disease diagnosis in the female patients. Interestingly, BFLS has been diagnosed in the female patients only in recent years after combining exome sequencing. This is because female patients of BFLS display a more diverse picture of syndromic and behavioral features compared to male patients. Also, it seems that female patients of BFLS harbor mutations that might be more deleterious, ranging from whole region deletion to duplication of exon 4 and 5 (Jahani-Asl et al., 2016). The C305X mutation case linking BFLS and ASD is also found in a female patient. Therefore, in the impossibility of testing the autistic-like phenotype in our PHF6 KO mice, it will be worthwhile to characterize the heterozygous PHF6 KO female mice, since the heterozygous PHF6 KO female could represent another BFLS disease model to study the disease from a sexual dimorphism perspective.

Appendix

PHF6-NuRD complex interaction

INTRODUCTION

The nucleosome remodeling and deacetylase (NuRD) complex is a major chromatin remodeling complex found in mammalian cells. The NuRD complex comprises at least seven proteins: the histone deacetylases Hdac1 and Hdac2, two histone-binding proteins RbAp46/48, CHD3/4 proteins that have ATP-dependent nucleosome-remodeling activity, mta1/2, MBD3, as well as P66. NuRD complex has been widely studied in cancer and embryonic stem cells (ESC) (Lai and Wade, 2011). NuRD complex aberrantly regulate gene repression through deposition of epigenetic repressive marks in acute promyelocytic leukemia (APL) (Morey et al., 2008). Also, balanced targeting of NuRD by lineage-specific transcription factors facilitates lymphocyte development and prevents leukemogenesis (Zhang et al., 2012). In ES cells, NuRD complex subunits MBD3 has been shown to facilitate ESC differentiation and inhibits ESC self-renewal in a Lif-independent manner (Kaji et al., 2006). Recently, two *de novo* mutations in NuRD subunit-p66alpha were found in patients with severe intellectual disability (Willemsen et al., 2013). As it turns out, NuRD complex also plays a role in neural development and controls circadian rhythm by regulating gene expression (Kim et al., 2014; Sparmann et al., 2013; Yamada et al., 2014). NuRD complex is known to specifically repress genes essential for synaptogenesis in cerebellar granule neurons (Yamada et al., 2014). During cortical development, NuRD can recruit Polycomb repressor complex 2 (PRC2) to regulate the neurogenic to astrogenic switch (Sparmann et al., 2013).

In the previous studies, PHF6 has been shown to interact with NuRD complex subunits in the 293T cells (Todd et al., 2015). This interaction was further predicted by the crystal structure analyses of second PHD domain of PHF6 (Liu et al., 2014). However, in B-cells, PHF6-NuRD interaction was not observed (Feliciano et al., 2017), suggesting that PHF6-NuRD interaction could be cell type specific. Additionally, in our RNA-seq analyses upon PHF6 knockout, about 50% genes were upregulated and another 50% were downregulated, indicating that PHF6 might

regulate gene expression both through transcriptional activation and repression. Previous study by Zhang et al. demonstrated endogenous interaction of PHF6 with PAF1 elongation complex, giving a potential activation mechanism of PHF6 in regulating transcription. However, whether PHF6 interact with NuRD complex in neurons, potentially by which to repress gene expression remains unknown.

RESULTS

To test whether PHF6 and NuRD complex interact, we first performed co-immunoprecipitation (co-IP) experiments analyzing PHF6 interaction with NuRD complex subunits in the 293T cells and in cortex. As expected, overexpression of FLAG-tagged PHF6 plasmid was able to pull down endogenous NuRD complex subunits (data not shown). Similarly, in the reciprocal co-IP by immunoprecipitating FLAG-tagged MTA1 and CHD4, PHF6 was also co-immunoprecipitated (data not shown). Additionally, to investigate the interaction of PHF6 and NuRD complex under more physiological condition, we performed immunoprecipitation of endogenous PHF6 in E18 cortex, and immunoblotted with NuRD complex subunits. Interestingly, we observed similar PHF6-NuRD interaction endogenously (Figure S6a). In the reciprocal co-IP experiments by either RBAP48 or CHD4, PHF6 was also co-immunoprecipitated (Figure S6b). These data suggested that PHF6 could interact with NuRD complex subunits in the developing cortex. We next asked whether the PHF6 was part of the NuRD complex in the developing cortex. Additional co-IP experiments were performed by immunoprecipitating RBAP48, followed by stringent washing conditions. The NuRD complex interaction was present after high salt wash, whereas the PHF6-NuRD complex interaction was abolished (Figure S6c), suggesting that PHF6 was not part of the NuRD complex in the developing cortex.

To characterize which domain of PHF6 was important for the interaction with the NuRD complex subunits, we overexpressed the FLAG-tagged PHF6 with different domain deletions of PHF6 proteins in 293T cells, and performed co-IP experiments looking at endogenous NuRD

complex subunits interaction. Notably, all the truncated PHF6 protein that we tested showed interaction with NuRD (Figure S6d-e). Interestingly, by deleting the regions containing the first or second PHD domain resulted in an increase in the interaction with NuRD complex subunits including MTA1/2, HDAC1 and CHD4, suggesting that the two PHD domains might be competing with each other in NuRD interaction.

The discovery of interaction of PHF6-NuRD complex in cortex has shed light upon the potential mechanism through which PHF6 regulates transcription through gene repression. In future studies, it would be important to first determine the effect of the subunits of NuRD complex also in neural development, such as cortical neuronal migration, and to understand how transcription can be regulated through the PHF6-NuRD interaction.

METHODS

Co-immunoprecipitation

Tissues or cells were lysed in a lysis buffer containing 150 mM NaCl, 20 mM Tris-HCl (pH 7.5), 1% Triton-X, and protease inhibitor cocktail (Sigma-Aldrich). For immunoprecipitation of Flag-tagged proteins, lysates were incubated with anti-Flag M2 agarose beads (Sigma-Aldrich) for 3 hr at 4°C and washed five times with lysis buffer. For immunoprecipitation of endogenous proteins, lysates were incubated with the appropriate primary antibody overnight at 4°C. The antibody-protein complexes were purified with protein G Sepharose 4 Fast Flow beads (GE Healthcare) for 2 hr at 4°C and washed five times with lysis buffer. The immunoprecipitated protein complexes were then analyzed by SDS-PAGE and transferred to a nitrocellulose membrane for immunoblotting analyses with the appropriate primary antibodies and horseradish peroxidase-conjugated secondary antibodies (Jackson ImmunoResearch).

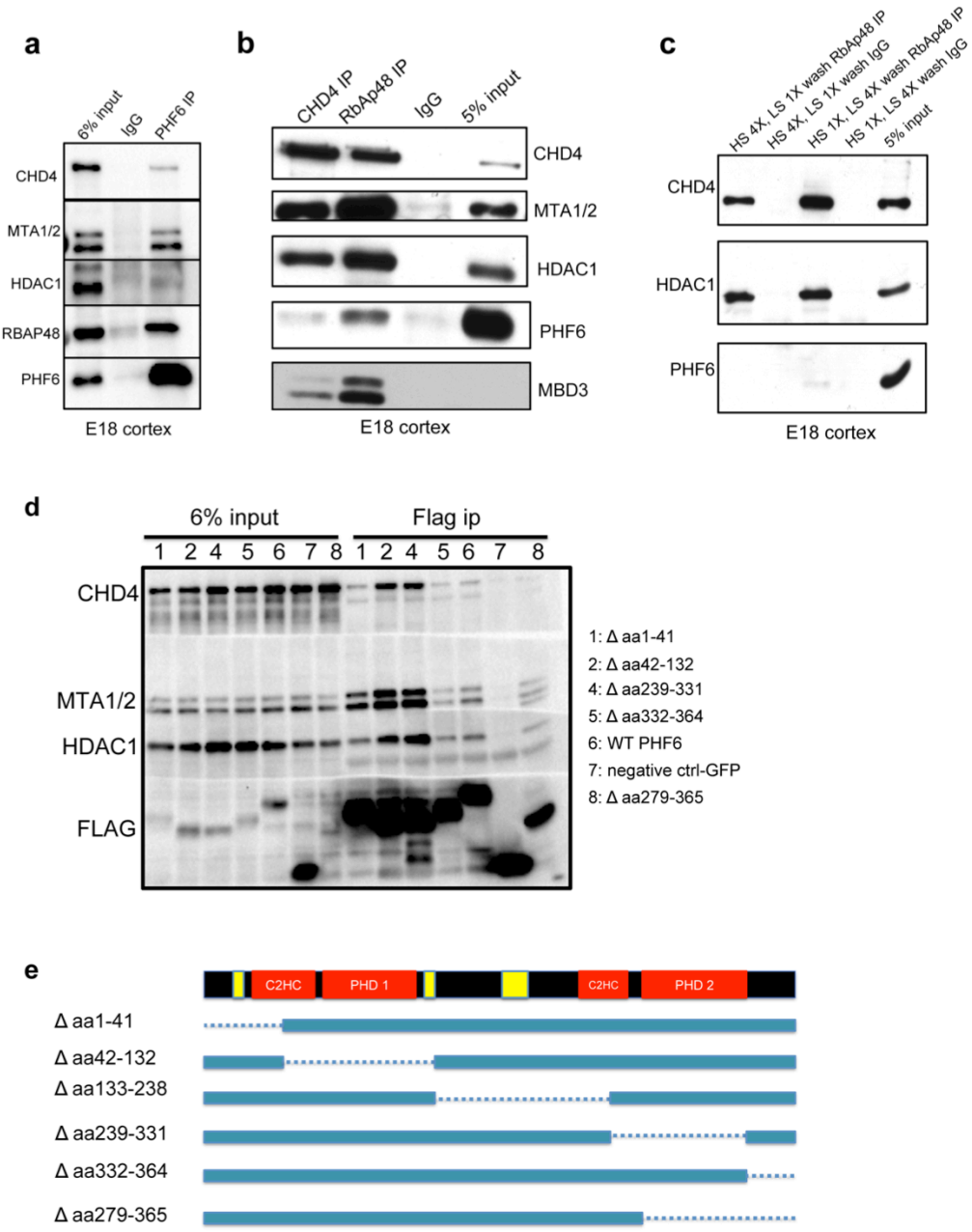

Figure S6. The interaction of PHF6 and NuRD complex.

(a) PHF6 was immunoprecipited from lysate of E18 cortex and unveiled in Western blot using antibodies against CHD4, MTA1/2, HDAC1, RBAP48 and PHF6. IgG was used as a negative control. PHF6 interacts with NuRD complex subunits.

(b) CHD4 or RBAP48 was immunoprecipitated from lysate of E18 cortex and unveiled in Western blot using antibodies against CHD4, MTA1/2, HDAC1, PHF6 and MBD3. IgG was used as negative control. In the reciprocal IP, PHF6 interacts with NuRD complex.

(c) RBAP48 was immunoprecipitated from lysate of E18 cortex, followed by combined high salt (HS) and low salt (LS) wash, and unveiled in Western blot using antibodies against CHD4, HDAC1 and PHF6. IgG was used as negative control. PHF6 interaction with NuRD complex is abolished upon high salt wash.

(d) FLAG-tagged PHF6 with different truncations expressed in 293T cells was immunoprecipitated with anti-FLAG antibody. Samples were unveiled in Western blot using antibodies against CHD4, MTA1/2, HDAC1 and FLAG. Truncated PHF6 remains interactions with NuRD complex.

(e) Schematic of PHF6 protein structure with different truncations. Yellow box: nuclear/nucleolar localization sequences. Dot line: PHF6 truncated region.

PHF6 knockout mouse displays excitatory/inhibitory imbalance

In the process of backcrossing the PHF6 knockout mice with C57BL6 mice, we noticed that the mice started to die around birth. We therefore also kept the PHF6 knockout line in the hybrid background of C57BL6 and CBA mice. To our surprise, PHF6 knockout mice kept in C57BL6/CBA background were born with expected Mendelian ratio, able to survive into adulthood and were smaller than the control mice. More interestingly, PHF6 knockout mice develop spontaneous seizure around 8 month old. Following this observation, we asked whether the neural circuit in the PHF6 knockout mice was hyperactive. To test the hypothesis, we performed whole-cell patch clamp and measured the evoked inhibitory postsynaptic current (IPSC) and excitatory postsynaptic current (EPSC) in CA1 pyramidal neurons in the hippocampus of PHF6 knockout and control mice. Interestingly, with the same amplitude of EPSCs evoked, the control CA1 neurons were able to recruit IPSCs with larger amplitude compared to PHF6 knockout neurons (Figure S7a,b). When we quantified the inhibitory-excitatory balance by calculating the ratio of IPSC to EPSC amplitude (I/E), we found the PHF6 knockout neurons displayed reduced I/E ratio (Figure S7c-e). These data suggest that the ability of inhibitory input recruitment was reduced in the PHF6 knockout CA1 neurons. Additionally, no differences were observed in the spontaneous EPSC frequencies, whereas spontaneous IPSC (sIPSC) frequencies were largely reduced in the PHF6 knockout CA1 neurons, while the amplitudes were unchanged (Figure S7f-g).

These data have raised important questions for future investigation, what aspects of the presynaptic defects led to the reduction in sIPSC frequency in the PHF6 knockout neurons? Does PHF6 have specific roles in interneurons and excitatory neurons?

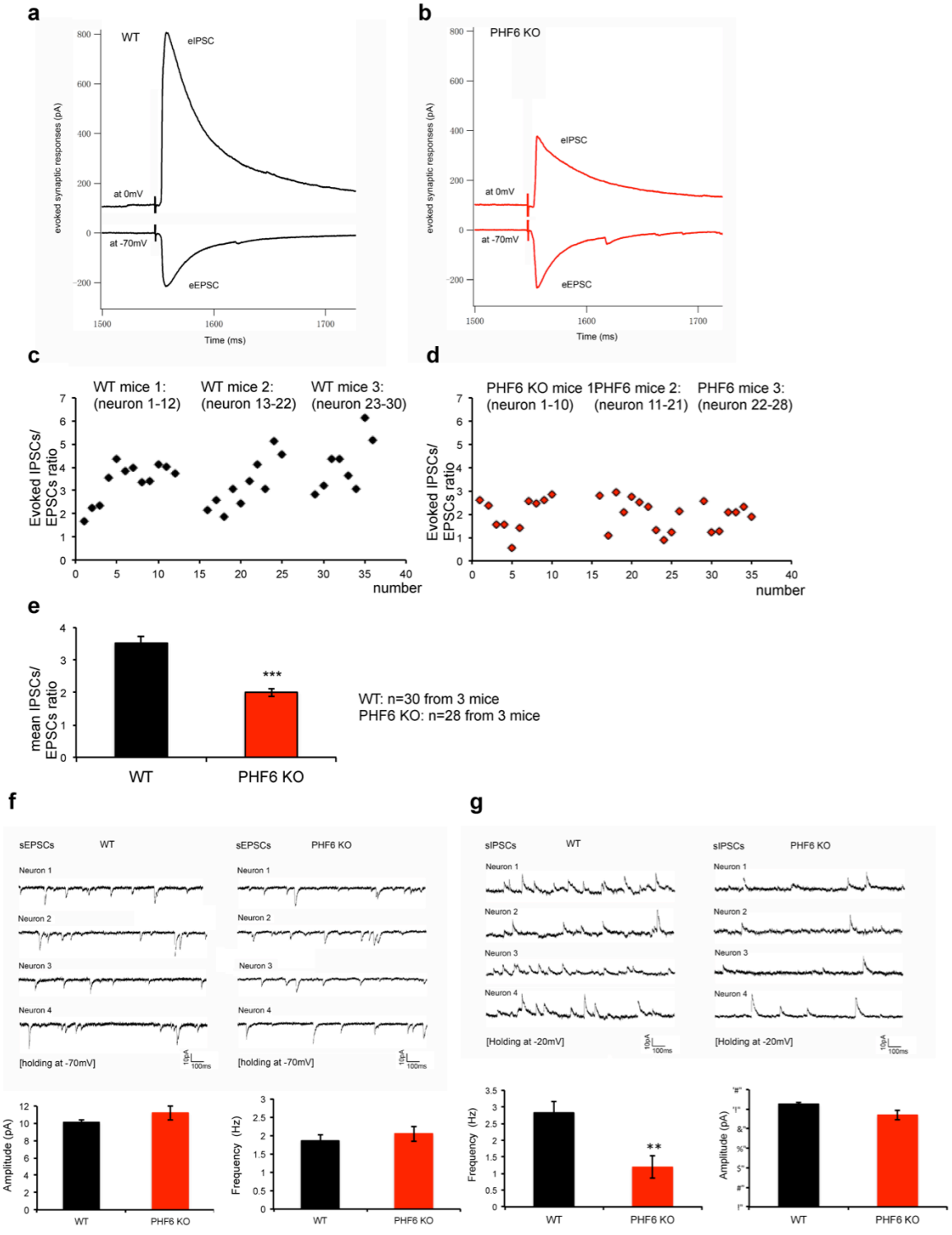

Figure S7. Excitatory/inhibitory imbalance in PHF6 knockout mice.

(a-b) Whole cell patch clamp of CA1 pyramidal neurons. Sample trace of evoked EPSC and IPSC in WT (a) and PHF6 KO (b) cells.

(c) The ratio of IPSC to EPSC amplitude (I/E) was calculated for each cell. PHF6 KO cells display reduced I/E ratio.

(e) Quantification of I/E ratio in WT and PHF6 KO cells.

(f-g) spontaneous EPSCs (f) by holding at -70mV and IPSCs (g) by holding at -20mV in the CA1 pyramidal neurons in WT and PHF6 KO mice. PHF6 KO cells have similar EPSC amplitude and frequencies, but reduced IPSC frequencies.

Cellular characterization of mouse model of PHF6 deficiency

Because PHF6 is highly expressed during early cortical development (Figure 1), prior to the detailed behavioral characterization, we first performed a series of cellular phenotyping covering early biological events of cortical development in the PHF6 C99F knock-in mice. We first performed BrdU labeling at E17 brain. Little or no differences were detected comparing control and PHF6 C99F cortices (Figure S8a). We next used the superficial layer marker, Cux1 and deep layer marker, Ctip2 to characterize whether cortical layering was affected. Notably, no obvious differences were detected (Figure S8b). In other analysis, we used electrophysiology to characterize the intrinsic electrical properties of layer II/III pyramidal neurons in the somatosensory cortex. There were little or no differences in resting membrane potential, intrinsic excitability, membrane capacitance in PHF6 C99F cells (data not shown). Biocytin injection in the layer II/III pyramidal neurons at P17-21 also showed similar cell morphology (Figure S8c) and spine density (data not shown) with the control cells. Altogether these data suggest that PHF6 C99F knock-in mice did not exhibit gross morphological defects in the brain.

Notably, in the characterization of PHF6 knockout brains, we noticed a consistent enlargement of lateral ventricle in the PHF6 knockout mice at P0 (Figure S8d). This enlargement of lateral ventricle was not observed at E18 (data not shown), suggesting that the increased in lateral ventricle did not occur until the mice were born. Enlarged ventricle has also been shown in the patient of BFLS (Berland et al., 2011; Zweier et al., 2013). Anecdotally, we have observed many “cilia” related genes decreased upon PHF6 knockout. In fact, the correlated genes between KO and KI cortex (KO-KI common) are enriched for GO terms including “cilia”. These evidence pointing towards to the ependymal cells defects. However, the mechanisms and cell type underlying the enlarged ventricle remains to be discovered.

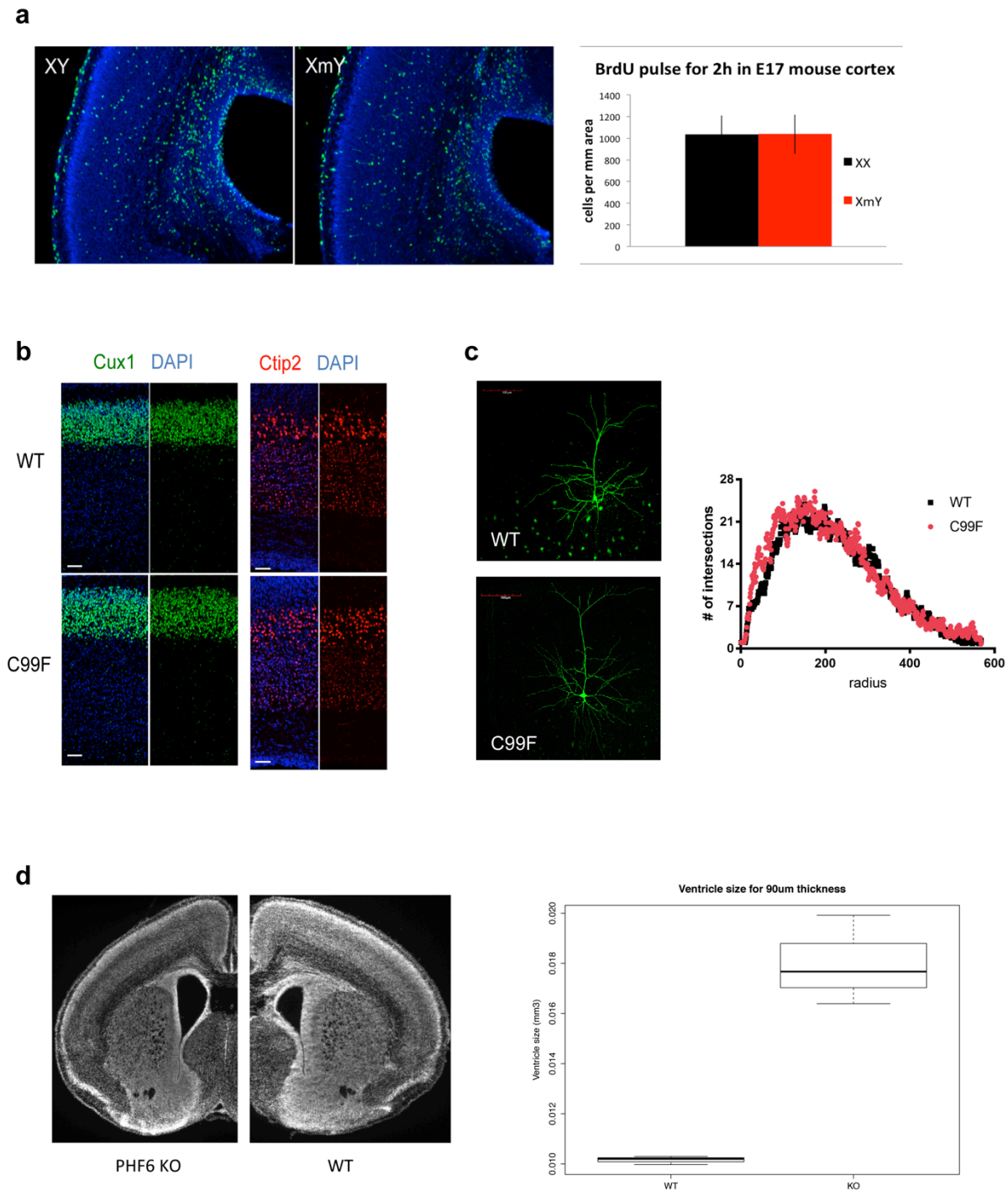

Figure S8. Cellular characterization of PHF6 KO and C99F knock-in mice.

(a) E17 pregnant female were pulsed with BrdU for 2 hours. Brains from E17 embryos were collected, sectioned and subjected to immunohistochemistry analyses using antibodies against BrdU. Hoechst was used as counter staining. Little or no differences in BrdU+ cells between PHF6 C99F knock-in and WT mice.

(b) Brain sections of P2 mice were subjected to immunohistochemistry analyses using antibodies against Cux1 and Ctip2. Cortical layering seems similar in WT and PHF6 C99F knock-in mice.

(c) P17-21 pyramidal cells from somatosensory cortex were injected with biocytin, followed by post-hoc staining with Avidin-488. Dendrite arborizations were subjected to Sholl analysis. WT and PHF6 C99F cells have similar dendrite arborization.

(d) Brain sections from P0 mice were subjected to immunohistochemistry analyses using Hoechst. Ventricle size was measured in PHF6 KO and WT mice. PHF6 KO mice display enlarged ventricle compared to WT mice.

PHF6 binds to active gene promoters

In our study, we described how PHF6 regulates gene expression at the genome-wide level. However, detailed mechanisms on PHF6 regulation of transcription remain unexplored. Here, in our preliminary work, we characterized the PHF6 genome occupancy in the P0 mouse cortex by performing ChIP-seq experiments of PHF6. Interestingly, in PHF6 ChIP-seq experiments, we identified approximately 2000 peaks of PHF6 from two biological replicates. The PHF6 peaks were found in mainly at the promoter regions (Figure S9a). Therefore, we focused on the PHF6 occupancy at the active promoters by intersecting all the promoters with H3K4me3 peaks in the P0 cortex. We found that PHF6 density was enriched at the active promoters, and this enrichment was depleted in the PHF6 C99F mice. When we grouped the expressed genes in the P0 cortex by gene expression, we found that PHF6 density was positively associated with increase in gene expression (Figure S9c). In other analyses, most of PHF6 peaks were also enriched for H3K27ac and H3K4me3 markers labeling active transcribed gene promoters in the genome (Figure S9d). These data suggest that PHF6 binds to active promoter, and its occupancy is positively correlated with gene expression. Notably, PHF6 peaks were enriched for GO terms including zinc finger, transcription factors and abnormal nervous system, suggesting that these peaks were specific for the nervous system.

To understand the relationship between PHF6 binding and gene expression, we compared the PHF6 ChIP signals with misregulated genes upon PHF6 knockout. Interestingly, for both downregulated and upregulated genes upon PHF6 loss, similar density of PHF6 signal was observed at those gene promoters (Figure S9f), suggesting that PHF6 could bind to gene promoters to regulate gene expression. Our preliminary studies have suggested that PHF6 can interact with NuRD complex in the developing cortex (Figure S6a). NuRD complex contains histone deacetylase proteins HDAC1/2 to regulate H3K27ac and H3K9/14ac, through which repress transcription (Yamada et al., 2014). Therefore, we asked whether PHF6 could regulate histone modifications, perhaps through which regulates gene expression. We therefore performed H3K27ac, H3K4me3 and H3K9/14ac ChIP-seq in both WT and C99F cortex. Interestingly, the

density of H3K27ac did not changed in for all the expressed genes in the genome, or for the downregulated and upregulated genes upon PHF6 knockout, suggesting that PHF6 could regulate gene expression through histone-independent mechanisms.

One caveat of the experiment was that instead of using the PHF6 KO or IgG as negative control, we used PHF6 C99F as a negative control because of dramatic reduction in PHF6 protein level *in vivo*. Even though, we were able to identify PHF6 signals across the genomes, those peaks were identified with less confidence due to improper negative control. In future studies, it is critical to use PHF6 WT and KO cortex to perform PHF6 ChIP-seq experiments to understand the genome occupancy of PHF6. Our prediction is still that PHF6 is localized at active gene promoters.

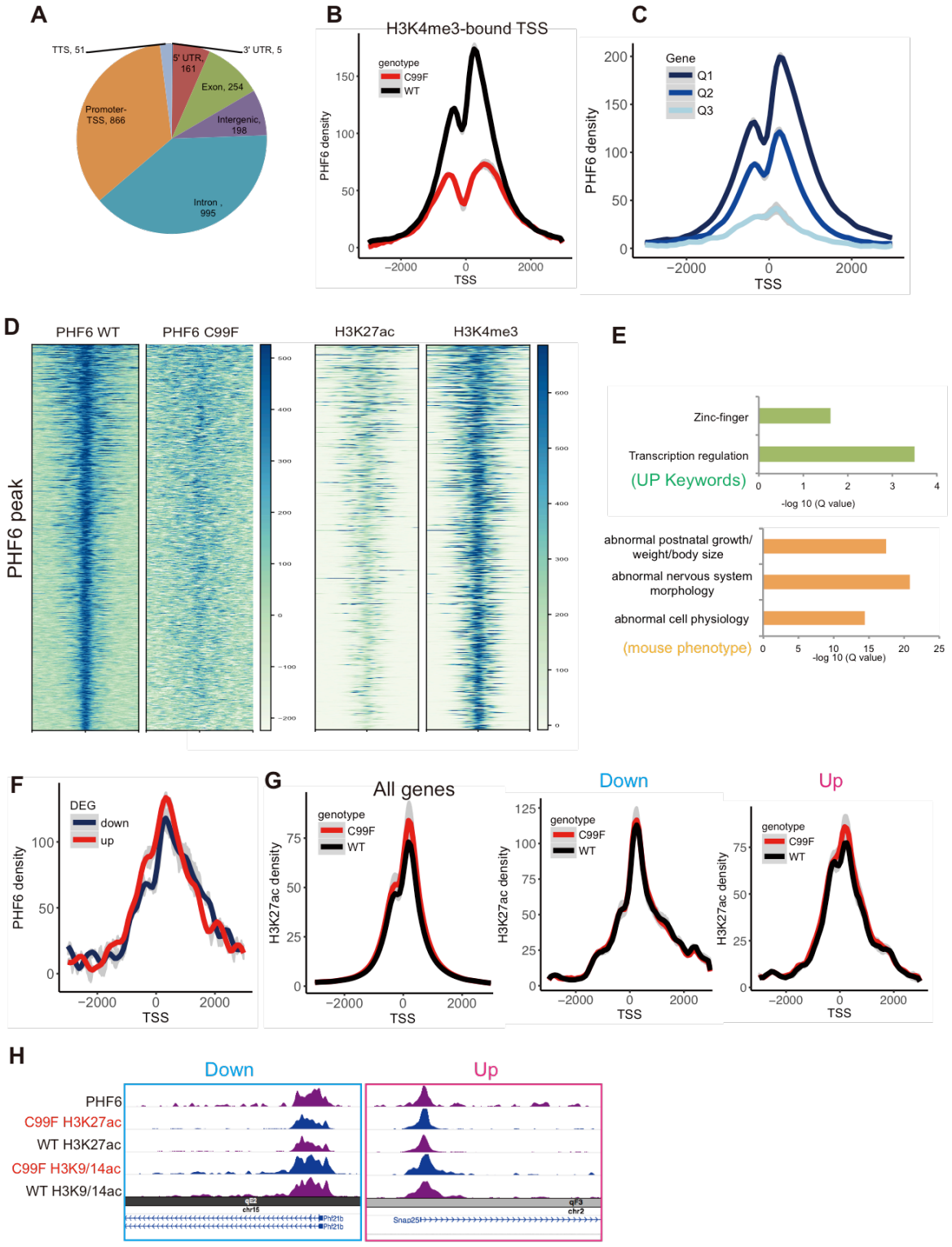

Figure S9. PHF6 binds to active promoters.

(A) The distribution of PHF6 peaks across the genome.

(B) PHF6 density at H3K4me3-bound promoters in WT and C99F cortex.

(C) PHF6 density at gene promoters of genes with low (Q3), medium (Q2) and high (Q1) expression.

(D) (Left) heatmap of PHF6 peaks in PHF6 WT and C99F cortex. (Right) H3K27ac and H3K4me3 density in all PHF6 peaks.

(E) GO terms for PHF6 peaks analyzed by GREAT.

(F) PHF6 density in upregulated and downregulated genes upon PHF6 knockout.

(G) H3K27ac density of WT and C99F cortex in all genes (left), downregulated (middle) and upregulated (right) genes upon PHF6 knockout.

(H) Examples of epigenome browser shot of PHF6 and H3K27ac peaks.

References

Aasland, R., Gibson, T.J., and Stewart, a. F. (1995). The PHD finger: Implications for chromatin-mediated transcriptional regulation. Trends Biochem. Sci. *20*, 56–59.

Ackman, J.B., Aniksztejn, L., Crepel, V., Becq, H., Pellegrino, C., Cardoso, C., Ben-Ari, Y., and Represa, A. (2009). Abnormal Network Activity in a Targeted Genetic Model of Human Double Cortex. J. Neurosci. *29*, 313–327.

Aghakhani, Y., Kinay, D., Gotman, J., Soualmi, L., Andermann, F., Olivier, A., and Dubeau, F. (2005). The role of periventricular nodular heterotopia in epileptogenesis. Brain *128*, 641–651.

Amir, R.E., Van den Veyver, I.B., Wan, M., Tran, C.Q., Francke, U., and Zoghbi, H.Y. (1999). Rett syndrome is caused by mutations in X-linked MECP2, encoding methyl-CpG-binding protein 2. Nat. Genet. *23*, 185–188.

Anton, E.S., Marchionni, M. a, Lee, K.F., and Rakic, P. (1997). Role of GGF/neuregulin signaling in interactions between migrating neurons and radial glia in the developing cerebral cortex. Development *124*, 3501–3510.

Ayala, R., Shu, T., and Tsai, L.H. (2007). Trekking across the Brain: The Journey of Neuronal Migration. Cell *128*, 29–43.

Baldridge, D., Heeley, J., Vineyard, M., Manwaring, L., Toler, T.L., Fassi, E., Fiala, E., Brown, S., Goss, C.W., Willing, M., et al. (2017). The exome clinic and the role of medical genetics expertise in interpretation of exome sequencing results. *19*, 1040–1048.

Ballas, N., Lioy, D.T., Grunseich, C., and Mandel, G. (2009). Non-cell autonomous influence of MeCP2-deficient glia on neuronal dendritic morphology. Nat. Neurosci. *12*, 311–317.

Bassell, G.J., and Warren, S.T. (2008). Fragile X Syndrome: Loss of Local mRNA Regulation Alters Synaptic Development and Function. Neuron *60*, 201–214.

Baumstark, A., Lower, K.M., Sinkus, A., Andriuskeviciute, I., Jurkeniene, L., Gecz, J., and Just, W. (2003). Novel Phf6 mutation p.D333del causes Börjeson-Forssman-Lehmann syndrome. J. Med. Genet. *40*.

Behringer, R., Gertsenstein, M., Nagy, K., and Nagy, A. (2014). Manuipulating the mouse embryo: a laboratory manual. (Cold Spring Harbor Laboratory Press).

Berg, J.M., and Geschwind, D.H. (2012). Autism genetics: searching for specificity and convergence. Genome Biol. *13*, 247.

Berland, S., Alme, K., Brendehaug, a, Houge, G., and Hovland, R. (2011a). PHF6 Deletions May Cause Borjeson-Forssman-Lehmann Syndrome in Females. Mol. Syndromol. *1*, 294–300.

Berland, S., Alme, K., Brendehaug, a, Houge, G., and Hovland, R. (2011b). PHF6 Deletions May Cause Borjeson-Forssman-Lehmann Syndrome in Females. Mol. Syndromol. *1*, 294–300.

Bernier, R., Golzio, C., Xiong, B., Stessman, H.A., Coe, B.P., Penn, O., Witherspoon, K., Gerdts, J., Baker, C., Vulto-Van Silfhout, A.T., et al. (2014). Disruptive CHD8 mutations define a subtype of autism early in development. Cell *158*, 263–276.

Bhakar, A.L., Dölen, G., and Bear, M.F. (2012). The pathophysiology of fragile X (and what it teaches us about synapses). Annu. Rev. Neurosci. *35*, 417–443.

Bhasin, T., Brocksen, S., Avchen, R., and Van Naarden Braun, K. (2006). Morbidity and Mortality Weekly Report: Prevalence of four developmental disabilities among children aged 8 Years — Metropolitan Atlanta Developmental Disabilities Surveillance Program , 1996 and 2000. *55*.

van Bokhoven, H., and Kramer, J.M. (2010). Disruption of the epigenetic code: an emerging mechanism in mental retardation. Neurobiol. Dis. *39*, 3–12.

Börjeson, M., Forssman, H., and Lehmann, O. (1962). An X-linked, Recessively Inherited Syndrome Characterized by Grave Mental Deficiency, Epilepsy, and Endocrine Disorder. Acta Med. Scand. *171*, 13–22.

Brager, D.H., Akhavan, A.R., and Johnston, D. (2012). Impaired Dendritic Expression and Plasticity of h-Channels in the fmr1-/yMouse Model of Fragile X Syndrome. Cell Rep. *1*, 225–233.

BrainSpan (2013). http://www.brainspan.org/.

Brandt, N., Franke, K., Rasin, M.-R., Baumgart, J., Vogt, J., Khrulev, S., Hassel, B., Pohl, E.E., Sestan, N., Nitsch, R., et al. (2007). The neural EGF family member CALEB/NGC mediates dendritic tree and spine complexity. EMBO J. *26*, 2371–2386.

Brown, J.A., Emnett, R.J., White, C.R., Yuede, C.M., Conyers, S.B., O'Malley, K.L., Wozniak, D.F., and Gutmann, D.H. (2010). Reduced striatal dopamine underlies the attention system dysfunction in neurofibromatosis-1 mutant mice. Hum. Mol. Genet. *19*, 4515–4528.

Brun, A., Borjeson, M., and Forssman, H. (1974). An inherited syndrome with mental deficiency and endocrine disorder. A patho-anatomical study. J. Intellect. Disabil. Res. *18*, 317–325.

Carter, M.T., Picketts, D.J., Hunter, A.G., and Graham, G.E. (2009). Further clinical delineation of the Börjeson-Forssman-Lehmann syndrome in patients with PHF6 mutations. Am. J. Med. Genet. A *149A*, 246–250.

Chao, M.M., Todd, M. a, Kontny, U., Neas, K., Sullivan, M.J., Hunter, A.G., Picketts, D.J., and Kratz, C.P. (2010). T-cell acute lymphoblastic leukemia in association with Börjeson-Forssman-Lehmann syndrome due to a mutation in PHF6. Pediatr. Blood Cancer *55*, 722–724.

Chen, F.X., Woodfin, A.R., Gardini, A., Rickels, R.A., Marshall, S.A., Smith, E.R., Shiekhattar, R., and Shilatifard, A. (2015). PAF1, a Molecular Regulator of Promoter-Proximal Pausing by RNA Polymerase II. Cell *162*, 1003–1015.

Chen, Y., Yamaguchi, Y., Tsugeno, Y., Yamamoto, J., Yamada, T., Nakamura, M., Hisatake, K., and Handa, H. (2009). DSIF, the Paf1 complex, and Tat-SF1 have nonredundant, cooperative roles in RNA polymerase II elongation. Genes Dev. *23*, 2765–2777.

Coffee, B., Ikeda, M., Budimirovic, D.B., Hjelm, L.N., Kaufmann, W.E., and Warren, S.T. (2008). Mosaic FMR1 deletion causes fragile X syndrome and can lead to molecular misdiagnosis: a case report and review of the literature. Am. J. Med. Genet. A *146A*, 1358–1367.

Coffee, B., Keith, K., Albizua, I., Malone, T., Mowrey, J., Sherman, S.L., and Warren, S.T. (2009). Incidence of Fragile X Syndrome by Newborn Screening for Methylated FMR1 DNA. Am. J. Hum. Genet. *85*, 503–514.

Comery, T. a, Harris, J.B., Willems, P.J., Oostra, B. a, Irwin, S. a, Weiler, I.J., and Greenough, W.T. (1997). Abnormal dendritic spines in fragile X knockout mice. Proc. Natl. Acad. Sci. U. S. A. *94*, 5401–5404.

Contractor, A., Klyachko, V.A., and Portera-Cailliau, C. (2015). Altered Neuronal and Circuit Excitability in Fragile X Syndrome. Neuron *87*, 699–715.

Cradick, T.J., Qiu, P., Lee, C.M., Fine, E.J., and Bao, G. (2014). COSMID: A web-based tool for identifying and validating CRISPR/Cas off-target sites. Mol. Ther. - Nucleic Acids *3*, e214.

Crawford, J., Lower, K.M., Hennekam, R.C.M., Van Esch, H., Mégarbané, a, Lynch, S. a, Turner, G., and Gécz, J. (2006). Mutation screening in Borjeson-Forssman-Lehmann syndrome: identification of a novel de novo PHF6 mutation in a female patient. J. Med. Genet. *43*, 238–243.

Darnell, J.C., Van Driesche, S.J., Zhang, C., Hung, K.Y.S., Mele, A., Fraser, C.E., Stone, E.F., Chen, C., Fak, J.J., Chi, S.W., et al. (2011). FMRP stalls ribosomal translocation on mRNAs linked to synaptic function and autism. Cell *146*, 247–261.

Deng, P.Y., and Klyachko, V.A. (2016). Increased Persistent Sodium Current Causes Neuronal Hyperexcitability in the Entorhinal Cortex of Fmr1 Knockout Mice. Cell Rep. *16*, 3157–3166.

Deng, P.-Y., Poudel, S.K.S., Rojanathammanee, L., Porter, J.E., and Lei, S. (2007). Serotonin inhibits neuronal excitability by activating two-pore domain k+ channels in the entorhinal cortex. Mol. Pharmacol. *72*, 208–218.

Deng, P.Y., Rotman, Z., Blundon, J.A., Cho, Y., Cui, J., Cavalli, V., Zakharenko, S.S., and Klyachko, V.A. (2013). FMRP Regulates Neurotransmitter Release and Synaptic Information Transmission by Modulating Action Potential Duration via BK Channels. Neuron *77*, 696–711.

Donato, F., Jacobsen, R.I., Moser, M.B., and Moser, E.I. (2017). Stellate cells drive maturation of the entorhinal-hippocampal circuit. Science (80-.). *355*.

Di Donato, N., Isidor, B., Lopez Cazaux, S., Le Caignec, C., Klink, B., Kraus, C., Schrock, E., and Hackmann, K. (2014a). Distinct phenotype of PHF6 deletions in females. Eur. J. Med. Genet. *57*, 85–89.

Di Donato, N., Isidor, B., Lopez Cazaux, S., Le Caignec, C., Klink, B., Kraus, C., Schrock, E., and Hackmann, K. (2014b). Distinct phenotype of PHF6 deletions in females. Eur. J. Med. Genet. *57*, 85–89.

Dougherty, J.D., Maloney, S.E., Wozniak, D.F., Rieger, M.A., Sonnenblick, L., Coppola, G., Mahieu, N.G., Zhang, J., Cai, J., Patti, G.J., et al. (2013). The Disruption of Celf6, a Gene Identified by Translational Profiling of Serotonergic Neurons, Results in Autism-Related Behaviors. J. Neurosci. *33*, 2732–2753.

Eberhart, D.E., Malter, H.E., Feng, Y., and Warren, S.T. (1996). The fragile X mental retardation protein is a ribonucleoprotein containing both nuclear localization and nuclear export signals. Hum. Mol. Genet. *5*, 1083–1091.

Feliciano, Y.M.S., Bartlebaugh, J.M.E., Liu, Y., Rivera, F.J.S., Bhutkar, A., Weintraub, A.S., Buenrostro, J.D., Cheng, C.S., Regev, A., Jacks, T.E., et al. (2017). PHF6 regulates phenotypic plasticity through chromatin organization within lineage-specific genes. Genes Dev. *31*, 973–989.

Franzoni, E., Booker, S.A., Parthasarathy, S., Rehfeld, F., Grosser, S., Srivatsa, S., Fuchs, H., Tarabykin, V., Vida, I., and Wulczyn, F.G. (2015). miR-128 regulates neuronal migration, outgrowth and intrinsic excitability via the intellectual disability gene Phf6. Elife *2015*, 1–23.

Gabel, H.W., Kinde, B., Stroud, H., Gilbert, C.S., Harmin, D.A., Kastan, N.R., Hemberg, M., Ebert, D.H., and Greenberg, M.E. (2015). Disruption of DNA-methylation-dependent long gene repression in Rett syndrome. Nature *522*, 89–93.

Gécz, J., Turner, G., Nelson, J., and Partington, M. (2006). The Börjeson-Forssman-Lehman syndrome (BFLS, MIM #301900). Eur. J. Hum. Genet. *14*, 1233–1237.

Gompers, A.L., Su-Feher, L., Ellegood, J., Copping, N.A., Riyadh, M.A., Stradleigh, T.W., Pride, M.C., Schaffler, M.D., Wade, A.A., Catta-Preta, R., et al. (2017). Germline Chd8 haploinsufficiency alters brain development in mouse. Nat. Neurosci. *20*, 1062–1073.

Greig, L.C., Woodworth, M.B., Galazo, M.J., Padmanabhan, H., and Macklis, J.D. (2013). Molecular logic of neocortical projection neuron specification, development and diversity. Nat. Rev. Neurosci. *14*, 755–769.

Gross, C., Yao, X., Pong, D.L., Jeromin, A., and Bassell, G.J. (2011). Fragile X Mental Retardation Protein Regulates Protein Expression and mRNA Translation of the Potassium Channel Kv4.2. J. Neurosci. *31*, 5693–5698.

Guenther, M.G., Levine, S.S., Boyer, L.A., Jaenisch, R., and Young, R.A. (2007). A Chromatin Landmark and Transcription Initiation at Most Promoters in Human Cells. Cell *130*, 77–88.

Guy, J., Hendrich, B., Holmes, M., Martin, J.E., and Bird, a (2001). A mouse Mecp2-null mutation causes neurological symptoms that mimic Rett syndrome. Nat. Genet. *27*, 322–326.

Haeussler, M., Schönig, K., Eckert, H., Eschstruth, A., Mianné, J., Renaud, J.B., Schneider-

Maunoury, S., Shkumatava, A., Teboul, L., Kent, J., et al. (2016). Evaluation of off-target and on-target scoring algorithms and integration into the guide RNA selection tool CRISPOR. Genome Biol. *17*, 1–12.

Huang, J., Zhang, W., Qiao, W., Hu, A., and Wang, Z. (2010). Functional connectivity and selective odor responses of excitatory local interneurons in drosophila antennal lobe. Neuron *67*, 1021–1033.

Huber, K.M., Gallagher, S.M., Warren, S.T., and Bear, M.F. (2002). Altered synaptic plasticity in a mouse model of fragile X mental retardation. Proc. Natl. Acad. Sci. U. S. A. *99*, 7746–7750.

Impagnatiello, F., Guidotti, A.R., Pesold, C., Dwivedi, Y., Caruncho, H., Pisu, M.G., Uzunov, D.P., Smalheiser, N.R., Davis, J.M., Pandey, G.N., et al. (1998). A decrease of reelin expression as a putative vulnerability factor in schizophrenia. Proc. Natl. Acad. Sci. U. S. A. *95*, 15718–15723.

Iossifov, I., Ronemus, M., Levy, D., Wang, Z., Hakker, I., Rosenbaum, J., Yamrom, B., Lee, Y. ha, Narzisi, G., Leotta, A., et al. (2012). De Novo Gene Disruptions in Children on the Autistic Spectrum. Neuron *74*, 285–299.

Irwin, S. a, Galvez, R., and Greenough, W.T. (2000). Dendritic spine structural anomalies in fragile-X mental retardation syndrome. Cereb. Cortex *10*, 1038–1044.

Iwase, S., Brookes, E., Agarwal, S., Badeaux, A.I., Ito, H., Vallianatos, C.N., Tomassy, G.S., Kasza, T., Lin, G., Thompson, A., et al. (2016). A Mouse Model of X-linked Intellectual Disability Associated with Impaired Removal of Histone Methylation. Cell Rep. *14*, 1000–1009.

Jaehning, J.A. (2010). The Paf1 complex: Platform or player in RNA polymerase II transcription? Biochim. Biophys. Acta - Gene Regul. Mech. *1799*, 379–388.

Janz, P., Savanthrapadian, S., Häussler, U., Kilias, A., Nestel, S., Kretz, O., Kirsch, M., Bartos, M., Egert, U., and Haas, C.A. (2017). Synaptic Remodeling of Entorhinal Input Contributes to an Aberrant Hippocampal Network in Temporal Lobe Epilepsy. Cereb. Cortex *27*, 2348–2364.

Jin, P., and Warren, S.T. (2000). Understanding the molecular basis of fragile X syndrome. Hum. Mol. Genet. *9*, 901–908.

Kaji, K., Caballero, I.M., MacLeod, R., Nichols, J., Wilson, V. a, and Hendrich, B. (2006). The NuRD component Mbd3 is required for pluripotency of embryonic stem cells. Nat. Cell Biol. *8*, 285–292.

Kasper, B.S., Dörfler, A., Di Donato, N., Kasper, E.M., Wieczorek, D., Hoyer, J., and Zweier, C. (2017). Central nervous system anomalies in two females with Borjeson-Forssman-Lehmann syndrome. Epilepsy Behav. *69*, 104–109.

Kaufmann, W.E., and Moser, H.W. (2000). Dendritic anomalies in disorders associated with mental retardation. Cereb. Cortex *10*, 981–991.

Khan, M.A., Rafiq, M.A., Noor, A., Hussain, S., Flores, J. V., Rupp, V., Vincent, A.K., Malli, R., Ali, G., Khan, F.S., et al. (2012). Mutation in NSUN2, which encodes an RNA methyltransferase, causes autosomal-recessive intellectual disability. Am. J. Hum. Genet. *90*, 856–863.

Kim, J.Y., Kwak, P.B., and Weitz, C.J. (2014). Specificity in Circadian Clock Feedback from Targeted Reconstitution of the NuRD Corepressor. Mol. Cell 1–11.

Kinugasa, Y., Ishiguro, H., Tokita, Y., Oohira, A., Ohmoto, H., and Higashiyama, S. (2004). Neuroglycan C, a novel member of the neuregulin family. Biochem. Biophys. Res. Commun. *321*, 1045–1049.

Kitamura, T., Sun, C., Martin, J., Kitch, L.J., Schnitzer, M.J., and Tonegawa, S. (2015). Entorhinal Cortical Ocean Cells Encode Specific Contexts and Drive Context-Specific Fear Memory. Neuron *87*, 1317–1331.

Kleine-Kohlbrecher, D., Christensen, J., Vandamme, J., Abarrategui, I., Bak, M., Tommerup, N., Shi, X., Gozani, O., Rappsilber, J., Salcini, A.E., et al. (2010). A functional link between the histone demethylase PHF8 and the transcription factor ZNF711 in X-linked mental retardation. Mol. Cell *38*, 165–178.

Kothare, S. V, VanLandingham, K., Armon, C., Luther, J.S., Friedman, A., and Radtke, R.A. (1998). Seizure onset from periventricular nodular heterotopias: depth-electrode study. Neurology *51*, 1723–1727.

Kriegstein, A.R., and Noctor, S.C. (2004). Patterns of neuronal migration in the embryonic cortex. Trends Neurosci. *27*, 392–399.

Krogan, N.J., Kim, M., Ahn, S.H., Zhong, G., Kobor, M.S., Cagney, G., Emili, A., Shilatifard, A., Buratowski, S., and Greenblatt, J.F. (2002). RNA Polymerase II Elongation Factors of Saccharomyces cerevisiae : a Targeted Proteomics Approach. Society *22*, 6979–6992.

Krogan, N.J., Dover, J., Wood, A., Schneider, J., Heidt, J., Boateng, M.A., Dean, K., Ryan, O.W., Golshani, A., Johnston, M., et al. (2003). The Paf1 complex is required for histone H3 methylation by COMPASS and Dot1p: Linking transcriptional elongation to histone methylation. Mol. Cell *11*, 721–729.

Krumm, A., Hickey, L.B., and Groudine, M. (1995). Promoter-proximal pausing of RNA polymerase II defines a general rate-limiting step after transcription initiation. Genes Dev. *9*, 559–572.

Lai, A.Y., and Wade, P. a (2011). Cancer biology and NuRD: a multifaceted chromatin remodelling complex. Nat. Rev. Cancer *11*, 588–596.

Larson, S.., K., C.L., L., A., N., K., J.H., L., and D., A. (2001). Prevalence of mental retardation and developmental disabilities: Estimates from the 1994/1995 National Health Interview Survey Disability Supplements. Am. J. Ment. Retard. *106*, 231–295.

Lee, H.Y., and Jan, L.Y. (2012). Fragile X syndrome: Mechanistic insights and therapeutic avenues regarding the role of potassium channels. Curr. Opin. Neurobiol. *22*, 887–894.

Lee, S.C.S., Cowgill, E.J., Al-Nabulsi, A., Quinn, E.J., Evans, S.M., and Reese, B.E. (2011). Homotypic regulation of neuronal morphology and connectivity in the mouse retina. J. Neurosci. *31*, 14126–14133.

Leigh, M.J., and Hagerman, R.J. (2013). Fragile X Clinical Features and Neurobiology (Elsevier Inc.).

Li, J., Pelletier, M.R., Perez Velazquez, J.-L., and Carlen, P.L. (2002). Reduced cortical synaptic plasticity and GluR1 expression associated with fragile X mental retardation protein deficiency. Mol. Cell. Neurosci. *19*, 138–151.

Liu, Z., Li, F., Ruan, K., Zhang, J., Mei, Y., Wu, J., and Shi, Y. (2014a). Structural and functional insights into the human Börjeson-Forssman-Lehmann syndrome-associated protein PHF6. J. Biol. Chem. *289*, 10069–10083.

Liu, Z., Li, F., Ruan, K., Zhang, J., Mei, Y., Wu, J., and Shi, Y. (2014b). Structural and Functional Insights into the Human Börjeson-Forssman-Lehmann Syndrome-associated Protein PHF6. J. Biol. Chem. *289*, 10069–10083.

Lower, K.M., Turner, G., Kerr, B. a, Mathews, K.D., Shaw, M. a, Gedeon, A.K., Schelley, S., Hoyme, H.E., White, S.M., Delatycki, M.B., et al. (2002). Mutations in PHF6 are associated with Börjeson-Forssman-Lehmann syndrome. Nat. Genet. *32*, 661–665.

Lower, K.M., Solders, G., Bondeson, M.-L., Nelson, J., Brun, A., Crawford, J., Malm, G., Börjeson, M., Turner, G., Partington, M., et al. (2004). 1024C> T (R342X) is a recurrent PHF6 mutation also found in the original Börjeson-Forssman-Lehmann syndrome family. Eur. J. Hum. Genet. *12*, 787–789.

Manent, J.-B., Wang, Y., Chang, Y., Paramasivam, M., and LoTurco, J.J. (2009). Dcx reexpression reduces subcortical band heterotopia and seizure threshold in an animal model of neuronal migration disorder. Nat. Med. *15*, 84–90.

Mangelsdorf, M., Chevrier, E., Mustonen, A., and Picketts, D.J. (2009). Börjeson-Forssman-Lehmann Syndrome due to a novel plant homeodomain zinc finger mutation in the PHF6 gene. J. Child Neurol. *24*, 610–614.

Marchetto, M.C.N., Carromeu, C., Acab, A., Yu, D., Yeo, G., Mu, Y., Chen, G., Gage, F.H., and Alysson R. Muotri (2010). A model for neural development and treatment of Rett Syndrome using human induced pluripotent stem cells. Cell *143*, 527–539.

Maren, S., Phan, K.L., and Liberzon, I. (2013). The contextual brain: implications for fear conditioning, extinction and psychopathology. Nat. Rev. Neurosci. *14*, 417–428.

Marton, H.A., and Desiderio, S. (2008). The Paf1 complex promotes displacement of histones upon rapid induction of transcription by RNA polymerase II. BMC Mol. Biol. *9*, 4.

Morey, L., Brenner, C., Fazi, F., Villa, R., Gutierrez, A., Buschbeck, M., Nervi, C., Minucci, S., Fuks, F., and Di Croce, L. (2008). MBD3, a component of the NuRD complex, facilitates chromatin alteration and deposition of epigenetic marks. Mol. Cell. Biol. *28*, 5912–5923.

Morgan-Smith, M., Wu, Y., Zhu, X., Pringle, J., and Snider, W.D. (2014). GSK-3 signaling in developing cortical neurons is essential for radial migration and dendritic orientation. Elife *3*, e02663.

Muse, G.W., Gilchrist, D.A., Nechaev, S., Shah, R., Parker, J.S., Grissom, S.F., Zeitlinger, J., and Adelman, K. (2007). RNA polymerase is poised for activation across the genome. Nat. Genet. *39*, 1507–1511.

Nadarajah, B., and Parnavelas, J.G. (2002). Modes of neuronal migration in the developing cerebral cortex. Nat. Rev. Neurosci. *3*, 423–432.

Nan, X., Campoy, F.J., and Bird, A. (1997). MeCP2 is a transcriptional repressor with abundant binding sites in genomic chromatin. Cell *88*, 471–481.

Nan, X., Ng, H.H., Johnson, C.A., Laherty, C.D., Turner, B.M., Eisenman, R.N., and Bird, A. (1998). Transcriptional repression by the methyl-CpG-binding protein MeCP2 involves a histone deacetylase complex. Nature *393*, 386–389.

Nechaev, S., and Adelman, K. (2012). Transcription Initiation Into Productive Elongation. *1809*, 34–45.

Nemeth, A., and Langst, G. (2011). Genome organization in and around the nucleolus. Trends Genet. *27*, 149–156.

Paradee, W., Melikian, H.E., Rasmussen, D.L., Kenneson, A., Conn, P.J., and Warren, S.T. (1999). Fragile X mouse: Strain effects of knockout phenotype and evidence suggesting deficient amygdala function. Neuroscience *94*, 185–192.

Parikshak, N.N., Luo, R., Zhang, A., Won, H., Lowe, J.K., Chandran, V., Horvath, S., and Geschwind, D.H. (2013). XIntegrative functional genomic analyses implicate specific molecular pathways and circuits in autism. Cell *155*, 1008–1021.

Pieretti, M., Zhang, F., Fu, Y.H., Warren, S.T., Oostra, B.A., Caskey, C.T., and Nelson, D.L. (1991). Absence of expression of the FMR-1 gene in fragile X syndrome. Cell *66*, 817–822.

Racine, R., Okujava, V., and Chipashvili, S. (1972). Modification of seizure activity by electrical stimulation. 2. Motor Seizure. Electroencephalogr. Clin. Neurophysiol. *32*, 295–299.

Rais, Y., Zviran, A., Geula, S., Gafni, O., Chomsky, E., Viukov, S., Mansour, A.A., Caspi, I., Krupalnik, V., Zerbib, M., et al. (2013). Deterministic direct reprogramming of somatic cells to pluripotency. Nature *502*, 65–70.

Reiss, A.L., Faruque, F., Naidu, S., Abrams, M., Beaty, T., Bryan, R.N., and Moser, H. (1993). Neuroanatomy of Rett Syndrome : A VolumetIric Imagmg Study. 227–234.

Rio, C., Rieff, H.I., Qi, P., Khurana, T.S., and Corfas, G. (1997). Neuregulin and erbB receptors play a critical role in neuronal migration. Neuron *19*, 39–50.

Robinson, L.K., Jones, K.L., Culler, F., Nyhan, W.L., Sakati, N., and Jones, K.L. (1983). The Borjeson-Forssman-Lehmann Syndrome. *468*, 457–468.

Rondon, A., Gallardo, M., Garcia-Rubio, M., and Aguilera, A. (2004). Molecular evidence indicating that the yeast PAF complex is required for transcription elongation. EMBO Rep *5*, 47–53.

Ropers, H.H. (2010). Genetics of early onset cognitive impairment. Annu. Rev. Genomics Hum. Genet. *11*, 161–187.

Roussel, P., André, C., Comai, L., and Hernandez-Verdun, D. (1996). The rDNA transcription machinery is assembled during mitosis in active NORs and absent in inactive NORs. J. Cell Biol. *133*, 235–246.

Samaco, R.C., and Neul, J.L. (2011). Complexities of Rett Syndrome and MeCP2. J. Neurosci. *31*, 7951–7959.

Sanchez, R., and Zhou, M.M. (2011). The PHD finger: A versatile epigenome reader. Trends Biochem. Sci. *36*, 364–372.

Scharfman, H.E. (2007). The neurobiology of epilepsy. Curr. Neurol. Neurosci. Rep. *7*, 348–354.

Skene, P.J., Illingworth, R.S., Webb, S., Kerr, A.R.W., James, K.D., Turner, D.J., Andrews, R., and Bird, A.P. (2010). Neuronal MeCP2 Is Expressed at Near Histone-Octamer Levels and Globally Alters the Chromatin State. Mol. Cell *37*, 457–468.

So, H.C., Fong, P.Y., Chen, R.Y.L., Hui, T.C.K., Ng, M.Y.M., Cherny, S.S., Mak, W.W.M., Cheung, E.F.C., Chan, R.C.K., Chen, E.Y.H., et al. (2010). Identification of neuroglycan C and interacting partners as potential susceptibility genes for schizophrenia in a Southern Chinese population. Am. J. Med. Genet. Part B Neuropsychiatr. Genet. *153*, 103–113.

Sparmann, A., Xie, Y., Verhoeven, E., Vermeulen, M., Lancini, C., Gargiulo, G., Hulsman, D., Mann, M., Knoblich, J. a, and van Lohuizen, M. (2013). The chromodomain helicase Chd4 is required for Polycomb-mediated inhibition of astroglial differentiation. EMBO J. *32*, 1598–1612.

Squazzo, S.L., Costa, P.J., Lindstrom, D.L., Kumer, K.E., Simic, R., Jennings, J.L., Link, A.J., Arndt, K.M., and Hartzog, G.A. (2002). The Paf1 complex physically and functionally associates with transcription elongation factors in vivo. EMBO J. *21*, 1764–1774.

Tennant, S.A., Fischer, L., Garden, D.L.F., Gerlei, K.Z., Martinez-Gonzalez, C., McClure, C., Wood, E.R., and Nolan, M.F. (2018). Stellate Cells in the Medial Entorhinal Cortex Are Required for Spatial Learning. Cell Rep. *22*, 1313–1324.

Todd, M. a M., and Picketts, D.J. (2012). PHF6 interacts with the nucleosome remodeling and deacetylation (NuRD) complex. J. Proteome Res. *11*, 4326–4337.

Todd, M.A.M., Ivanochko, D., and Picketts, D.J. (2015). Phf6 degrees of separation: The multifaceted roles of a chromatin adaptor protein. Genes (Basel). *6*, 6.

Tomita, K., Kubo, K. ichiro, Ishii, K., and Nakajima, K. (2011). Disrupted-in-schizophrenia-1 (Disc1) is necessary for migration of the pyramidal neurons during mouse hippocampal development. Hum. Mol. Genet. *20*, 2834–2845.

Tomson, B.N., and Arndt, K.M. (2013). The many roles of the conserved eukaryotic Paf1 complex in regulating transcription, histone modifications, and disease states. Biochim. Biophys. Acta - Gene Regul. Mech. *1829*, 166–126.

Turner, G., Lower, K.M., White, S.M., Delatycki, M., Lampe, a K., Wright, M., Smith, J.C., Kerr, B., Schelley, S., Hoyme, H.E., et al. (2004). The clinical picture of the Börjeson-Forssman-Lehmann syndrome in males and heterozygous females with PHF6 mutations. Clin. Genet. *65*, 226–232.

Vaillend, C., Poirier, R., and Laroche, S. (2008). Genes, plasticity and mental retardation. Behav. Brain Res. *192*, 88–105.

Vallée, D., Chevrier, E., Graham, G.E., Lazzaro, M. a, Lavigne, P. a, Hunter, a G., and Picketts, D.J. (2004). A novel PHF6 mutation results in enhanced exon skipping and mild Börjeson-Forssman-Lehmann syndrome. J. Med. Genet. *41*, 778–783.

Verkerk, A.J.. M.., Pieretti, M., Sutcliffe, J.S., Fu, Y., Kuhl, D.P.A., Pixxuti, A., Refner, O., Richards, S., Victoria, M.F., Zhang, F., et al. (1991). Identification of a Gene (FMR-1) Containing a CGG Repeat Coincident with a Breakpoint Cluster Region Exhibiting length Variation in Fragile X Syndrome. *65*, 905–914.

Vismer, M.S., Forcelli, P.A., Skopin, M.D., Gale, K., and Koubeissi, M.Z. (2015). The piriform, perirhinal, and entorhinal cortex in seizure generation. Front. Neural Circuits *9*, 1–14.

Voineagu, I., Wang, X., Johnston, P., Lowe, J.K., Tian, Y., Mill, J., Cantor, R., Blencowe, B.J., and Daniel, H. (2013). Transcriptomic analysis of autistic brain reveals convergent molecular pathology. Nature *474*, 380–384.

Voss, A.K., Gamble, R., Collin, C., Shoubridge, C., Corbett, M., Gécz, J., and Thomas, T. (2007). Protein and gene expression analysis of Phf6, the gene mutated in the Börjeson-Forssman-Lehmann Syndrome of intellectual disability and obesity. Gene Expr. Patterns *7*, 858–871.

Wang, J., Leung, J.W., Gong, Z., Feng, L., Shi, X., and Chen, J. (2013). PHF6 regulates cell cycle progression by suppressing ribosomal RNA synthesis. J. Biol. Chem. *288*, 3174–3183.

Wieczorek, D., Bögershausen, N., Beleggia, F., Steiner-Haldenstätt, S., Pohl, E., Li, Y., Milz, E., Martin, M., Thiele, H., Altmüller, J., et al. (2013). A comprehensive molecular study on Coffin-Siris and Nicolaides-Baraitser syndromes identifies a broad molecular and clinical spectrum converging on altered chromatin remodeling. Hum. Mol. Genet. *22*, 5121–5135.

Willemsen, M.H., Nijhof, B., Fenckova, M., Nillesen, W.M., Bongers, E.M.H.F., Castells-Nobau, A., Asztalos, L., Viragh, E., van Bon, B.W.M., Tezel, E., et al. (2013). GATAD2B loss-of-function mutations cause a recognisable syndrome with intellectual disability and are associated with learning deficits and synaptic undergrowth in Drosophila. J. Med. Genet. *50*, 507–514.

de Winter, C.F., van Dijk, F., Stolker, J.J., and Hennekam, R.C.M. (2009). Behavioural phenotype in Börjeson-Forssman-Lehmann syndrome. J. Intellect. Disabil. Res. *53*, 319–328.

Wood, A., Schneider, J., Dover, J., Johnston, M., and Shilatifard, A. (2003). The Paf1 complex is essential for histone monoubiquitination by the Rad6-Bre1 complex, which signals for histone methylation by COMPASS and Dot1p. J. Biol. Chem. *278*, 34739–34742.

Wozniak, D.F., Hartman, R.E., Boyle, M.P., Vogt, S.K., Brooks, A.R., Tenkova, T., Young, C., Olney, J.W., and Muglia, L.J. (2004). Apoptotic neurodegeneration induced by ethanol in neonatal mice is associated with profound learning/memory deficits in juveniles followed by progressive functional recovery in adults. Neurobiol. Dis. *17*, 403–414.

Wozniak, D.F., Xiao, M., Xu, L., Yamada, K.A., and Ornitz, D.M. (2007). Impaired spatial learning and defective theta burst induced LTP in mice lacking fibroblast growth factor 14. Neurobiol. Dis. *26*, 14–26.

Wozniak, D.F., Diggs-Andrews, K.A., Conyers, S., Yuede, C.M., Dearborn, J.T., Brown, J.A., Tokuda, K., Izumi, Y., Zorumski, C.F., and Gutmann, D.H. (2013). Motivational Disturbances and Effects of L-dopa Administration in Neurofibromatosis-1 Model Mice. PLoS One *8*.

Wysocka, J., Swigut, T., Xiao, H., Milne, T.A., Kwon, S.Y., Landry, J., Kauer, M., Tackett, A.J., Chait, B.T., Badenhorst, P., et al. (2006). A PHD finger of NURF couples histone H3 lysine 4 trimethylation with chromatin remodelling. Nature *442*, 86–90.

Yamada-Hanff, J., and Bean, B.P. (2013). Persistent Sodium Current Drives Conditional Pacemaking in CA1 Pyramidal Neurons under Muscarinic Stimulation. J. Neurosci. *33*, 15011–15021.

Yamada, T., Yang, Y., Hemberg, M., Yoshida, T., Cho, H.Y., Murphy, J.P., Fioravante, D., Regehr, W.G., Gygi, S.P., Georgopoulos, K., et al. (2014). Promoter decommissioning by the NuRD chromatin remodeling complex triggers synaptic connectivity in the mammalian brain. Neuron *83*, 122–134.

Yu, A.S., Pritchard, M., Kremer, E., Lynch, M., Nancarrow, J., Baker, E., Holman, K., Warren, S.T., Schlessinger, D., Sutherland, G.R., et al. (1991). Fragile X Genotype Characterized by an Unstable Region of DNA. *252*, 1179–1181.

Yuede, C.M., Wozniak, D.F., Creeley, C.E., Taylor, G.T., Olney, J.W., and Farber, N.B. (2010). Behavioral consequences of NMDA antagonist-induced neuroapoptosis in the infant mouse brain. PLoS One *5*.

Zalfa, F., Eleuteri, B., Dickson, K.S., Mercaldo, V., De Rubeis, S., di Penta, A., Tabolacci, E.,

Chiurazzi, P., Neri, G., Grant, S.G.N., et al. (2007). A new function for the fragile X mental retardation protein in regulation of PSD-95 mRNA stability. Nat. Neurosci. *10*, 578–587.

Zeisel, A., Muñoz-Manchado, A.B., Codeluppi, S., Lönnerberg, P., Manno, G. La, Juréus, A., Marques, S., Munguba, H., He, L., Betsholtz, C., et al. (2015). Cell types in the mouse cortex and hippocampus revealed by single-cell RNA-seq. Science (80-.). *347*, 1138–1142.

Zhang, B., and Wong, M. (2012). Pentylenetetrazole-induced seizures cause acute, but not chronic, mTOR pathway activation in rat. Epilepsia *53*, 506–511.

Zhang, C., Mejia, L.A., Huang, J., Valnegri, P., and Bennett, E.J. Supplemental Information The X - Linked Intellectual Disability Protein PHF6 Associates with the PAF1 Complex and Regulates Neuronal Migration in the Mammalian Brain. *78*, 1–15.

Zhang, C., Mejia, L. a, Huang, J., Valnegri, P., Bennett, E.J., Anckar, J., Jahani-Asl, A., Gallardo, G., Ikeuchi, Y., Yamada, T., et al. (2013). The X-linked intellectual disability protein PHF6 associates with the PAF1 complex and regulates neuronal migration in the mammalian brain. Neuron *78*, 986–993.

Zhang, J., Jackson, A.F., Naito, T., Dose, M., Seavitt, J., Liu, F., Heller, E.J., Kashiwagi, M., Yoshida, T., Gounari, F., et al. (2012). Harnessing of the nucleosome-remodeling-deacetylase complex controls lymphocyte development and prevents leukemogenesis. Nat. Immunol. *13*, 86–94.

Zhang, Y., LeRoy, G., Seelig, H.-P., Lane, W.S., and Reinberg, D. (1998). The Dermatomyositis-Specific Autoantigen Mi2 Is a Component of a Complex Containing Histone Deacetylase and Nucleosome Remodeling Activities. Cell *95*, 279–289.

Zhang, Y., Ng, H., Erdjument-bromage, H., Tempst, P., Bird, A., and Reinberg, D. (1999). Analysis of the NuRD subunits reveals a histone deacetylase core complex and a connection with DNA methylation. 1924–1935.

Zhu, B., Mandal, S.S., Pham, A.D., Zheng, Y., Erdjument-Bromage, H., Batra, S.K., Tempst, P., and Reinberg, D. (2005). The human PAF complex coordinates transcription with events downstream of RNA synthesis. Genes Dev. *19*, 1668–1673.

Zweier, C., Kraus, C., Brueton, L., Cole, T., Degenhardt, F., Engels, H., Gillessen-Kaesbach, G., Graul-Neumann, L., Horn, D., Hoyer, J., et al. (2013a). A new face of Borjeson-Forssman-Lehmann syndrome? De novo mutations in PHF6 in seven females with a distinct phenotype. J. Med. Genet. *50*, 838–847.

Zweier, C., Kraus, C., Brueton, L., Cole, T., Degenhardt, F., Engels, H., Gillessen-Kaesbach, G., Graul-Neumann, L., Horn, D., Hoyer, J., et al. (2013b). A new face of Borjeson-Forssman-Lehmann syndrome? De novo mutations in PHF6 in seven females with a distinct phenotype. J. Med. Genet. *50*, 838–847.